1-1-2008

CFD Investigation Of Mixing Of Yield-Pseudoplastic Fluid With Anchor Impeller

Poonam Prajapati
Ryerson University

CFD INVESTIGATION OF MIXING OF YIELD-PSEUDOPLASTIC FLUID WITH ANCHOR IMPELLER

by

Poonam Prajapati

Bachelor of Chemical Engineering, Gujarat University,
Ahmedabad, Gujarat, India, 1992

A thesis
presented to Ryerson University
in partial fulfillment of the
requirements for the degree of
Master of Applied Science
in the program of Chemical Engineering

Toronto, Ontario, Canada, 2008

AUTHOR'S DECLARATION

I hereby declare that I am the sole author of this thesis. I authorize Ryerson University to lend this thesis to other institutions or individuals for the purpose of scholarly research.

Poonam Prajapati

I further authorize Ryerson University to reproduce this thesis by photocopying or by other means, in total or in part, at the request of their institutions or individuals for the purpose of scholarly research.

Poonam Prajapati

ABSTRACT

CFD INVESTIGATION OF MIXING OF YIELD-PSEUDOPLASTIC FLUID WITH ANCHOR IMPELLER

Poonam Prajapati
Master of Applied Science, Department of Chemical Engineering, 2008
Ryerson University, Toronto, Canada

The Anchor impeller, which is a close clearance impeller, produces high shear near the vessel wall and is recommended for the mixing of highly viscous fluids. A thorough search of the literature suggests that few publications have been devoted to the computational fluid dynamics (CFD) modeling of mixing of non-Newtonian fluids with the anchor impeller. Thus, the objectives of this study are (i) to generate a 3-D flow field for mixing of yield-pseudoplastic fluid in a flat bottom cylindrical tank equipped with two- and four-blade anchor impellers using CFD modeling technique, (ii) to evaluate the effects of fluid rheology, agitator speed, number of blades, vessel clearance and impeller blade width on power consumption, mixing time and flow patterns, and (iii) to determine the optimum value of clearance to diameter ratio and impeller blade width to diameter ratio on the basis of minimum mixing time.

The study was carried out for a yield-stress pseudoplastic fluid, using a CFD package (Fluent), to simulate the 3-D flow domain generated in a cylindrical tank equipped with two- and four-blade anchor impellers. The multiple reference frame (MRF) technique was employed to model the rotation of impellers. The rheology of the fluid was approximated using the Herschel-Bulkley model. To validate the model, CFD results for the power were compared to experimental data. After the flow fields were calculated, the simulations for tracer homogenization was performed to simulate the mixing time. The effect of impeller speed, fluid rheology, and number of impellers on power consumption, mixing time, and flow pattern were explored. The optimum values of c/D (clearance to diameter) and w/D (impeller blade width to diameter) ratios were determined on the basis of minimum mixing time.

ACKNOWLEDGEMENT

Foremost, I would like to appreciate from my heart to my supervisor Dr. Farhad Ein-Mozaffari for giving me an opportunity to work on this project and for his support, encouragement and precious comments to accomplish this thesis. His incessant motivation would be memorable in my life.

I am thankful to my thesis oral examination chair and committee members Dr. Huu Doan, Dr. Simant Upreti and Dr. Jiangning Wu.

I would like to thank Mr. Ali Hemmati, Mr. Peter Sharping, Mr. Tondar Tajrobehkar and all staff in Chemical Engineering Department at Ryerson University for assistance provided to conduct this research.

I extent my sincere thanks to all my friends in Fluid Mixing Technology Laboratory and Chemical Engineering Department at Ryerson University for their essential help.

Financial support from Natural Sciences and Engineering Research Council of Canada (NSERC) is gratefully acknowledged for conducting this study.

I would also like to express my gratitude and love to my parents, wife, son and daughter for their love, support and encouragement.

Dedicated to
my wife Charu,
kids Chintan & Tithi
and parents for their
love and support

TABLE OF CONTENTS

LIST OF FIGURES

LIST OF TABLES

1. INTRODUCTION

Fluids exhibit a wide variety of rheological behaviour ranging from Newtonian to viscoelastic (Rao, 1999). While Newtonian agitation is well understood, understanding non-Newtonian mixing still remains difficult. Yield-stress fluids, which can be found frequently in food, paint, cosmetic, waste water treatment, pulp & paper and pharmaceutical industry, are a common class of non-Newtonian fluids. These fluids start flowing when the imposed shear stress is more than a particular threshold value due to structured networks that build up at low shear rates and break down at high shear rates (Lobe and White, 1979). These fluids have high apparent viscosity at low shear rates, which affects the mixing performance. The fluid motion ceases completely beyond a well-mixed zone (known as cavern) near the impeller (Solomon et al., 1981; Eklund and Teirfolk, 1981). The stagnant region gives rise to poor mass and heat transfer (Amanullah et al., 1997). It is desirable to eliminate these stagnant regions by properly designing the agitation systems.

Mixing of high viscosity fluid is still a difficult operation and is considered as key step in the chemical process. For example in food industries poor mixing results in the formation of dead zones, concentration gradients and temperature gradients which lead to poor quality end products. Close clearance impellers are highly recommended for mixing of high viscosity fluids in laminar regime, especially pseudoplastic fluids (Nomura et al., 1996), due to their ability to keep the entire vessel contents circulating (Tatterson, 1986). In polymerization reactors it is desirable to ensure efficient mixing to prevent phenomena like hot spots (which leads to reactor runaway or product degradation), to control the molecular weight distribution of the final product and to avoid dead zones. Close clearance impellers are recommended for such polymerization applications (Hayes et al., 1998). It is believed that large diameter close clearance impellers such as anchors and helical ribbons, which are commonly used in the agitation of viscoplastic fluids, give rise to good mixing in the entire mixing vessels (Pedrosa and Nunhez, 2000).

The evaluation of stirred vessels has been done over the years through experimental investigation for different impellers, vessel geometries and fluid rheology. Such an approach is usually costly and sometimes is not an easy task. On the other hand, the empirical correlations are often not suitable for all systems as they are commonly found for a specific system and therefore can only give an overall view of the mixing performance. Using computational fluid dynamics (CFD), the various parameters contributing to the process can be examined in shorter time and with less expense, a task otherwise difficult in experimental techniques. However, this approach is limited by a relative lack of sufficiently detailed measurements for validation and corroboration. One advantage of CFD is that once a validated solution is obtained, it can provide valuable information that would be not easy to obtain experimentally.

The thorough investigation of the published literature suggests that, in a case of pseudoplastic fluids with yield stress agitated with an anchor impeller, the 3-D CFD modeling works using finite volume method are very limited. Few research articles have been published regarding the work on power consumption and velocity profiles. However, it is obvious from the literature review that among all the work done to predict the behaviour of different aspects of mixing in non-Newtonian fluids with anchor, the work done in evaluation of mixing time, optimum blade width and clearance, especially with CFD, has not been significant.

The objectives of present study are (1) To generate a 3-D flow field for mixing of yield-pseudoplastic fluid in a flat bottom cylindrical tank equipped with two- and four-blade anchor impellers using CFD modeling technique (2) To evaluate the effects of fluid rheology, agitator speed, number of blades, vessel clearance and impeller blade width on power consumption, mixing time and flow patterns (3) To determine the optimum value of clearance to diameter ratio and impeller blade width to diameter ratio on the basis of minimum mixing time.

Chapter two gives a brief review of the literature to present the fundamentals in non-Newtonian mixing such as fluid behaviour, power consumption, impellers type, flow

pattern and mixing time. At the end, some CFD applications in the mixing process are presented.

Chapter three is concerned with the design, specification, structure, and operation of the anchor impeller vessel. Fluid rheology, experimental setup and experimental procedures are described.

Chapter four is organized in two sections: first section reviews the general information about CFD such as governing equations, numerical methods, discretization methods, grid generation and other relevant information, and the second section of the chapter is devoted to the current CFD model development.

Chapter five provides the experimental and CFD results with discussions. Results concerning power consumption, flow patterns, mixing time, optimum vessel clearance and blade width are discussed in this chapter.

Finally, Chapter six summarizes the overall conclusions of this study and gives recommendations for future work.

2. LITERATURE REVIEW

The term 'mixing' is applied to operations which have a propensity to lower the non-uniformities or gradient in composition, properties or temperature of material in bulk (Uhl and Gray, 1966). Mixing is a common unit process operation used in chemical, pharmaceutical, waste water, pulp & paper and food industries. The efficiency of the mixing operation has a noteworthy effect on the product quality and yield (Tatterson, 1994). Therefore, it is essential to achieve a detailed knowledge of mixing in stirred vessels. Among other important process parameters, power consumption and mixing time are some of the parameters that should be determined. These parameters are dependent on the impeller flow patterns which themselves are influenced by the fluid rheology.

In this chapter mechanisms of mixing and the types of mixers used in industries are discussed. The literature survey regarding anchor impeller for power consumption, mixing time, flow patterns and numerical studies is presented here.

2.1 Mixing Mechanism

The mixing process fundamentally involves the mechanical movement of an agitator and as a result the deformation and flow produces. The mixing process can be summarized as:

(i) Diffusion
(ii) Convection
(iii) Bulk movement

2.1.1 Diffusion

Diffusion occurs in mixing processes due to a velocity gradient within the fluid. When low velocity stream of fluid comes in contact with high velocity streams fluid, the low velocity fluid entrains in the high velocity streams.

2.1.2 Convection

In convection, inertial forces play a crucial role to impart motion to some portion of fluid. For example an agitator in a vessel imparts motion in the fluid some distance from the agitator. This motion is due to the convective flow and the inertial effects of the agitator. The viscosity of the fluid plays a major role in the convection process. When the viscosity is substantial, the viscous forces control the inertial forces and the fluid is convected only a short distance away from the stirrer. So if convection is to be used to enhance the fluid motion, then it is desirable to have large inertial forces to overcome the viscous forces in order to increase fluid movement in entire region of the stirred tank.

2.1.3 Bulk Movement of Fluid

The fluid intersperse and mixing in the fluid occurs as a result of bulk movement, the division and recombination of portions of materials, i.e. cutting, dividing and separating in solids mixing (Sweeney, 1978). The highly viscous fluids require large amount of power to promote turbulence or event convection, and so mixing occurs mainly by bulk movement.

2.2 Types of Impellers

Impellers can be broadly divided into two classes, axial flow and radial flow impellers. Some impellers also possess both characteristics. Impellers may also be classified as paddles, turbines or propellers. Figure 2.1 shows the various types of impellers used in mixing operations.

Axial flow impellers are those impellers whose blades make an angle of less than 90^{o} to the plane of rotation, so prompting axial top to bottom motion. Pitched-blade paddles, turbines and propellers are in this group. Radial-flow impellers have blades, which are parallel to the vertical axis of the drive shaft and vessel. Flat-blade turbines and curved-blade turbines generate radial flow.

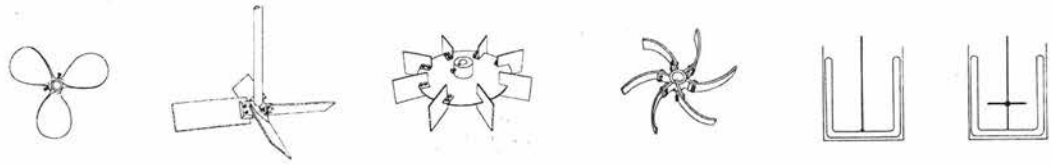

(a) (b) (c) (d) (e) (f)

Figure 2.1 Types of impellers: (a) marine type mixing propeller (b) pitched-blade Turbine (c) Flat-blade turbine (d) Curved-blade turbine (e) Anchor agitator (f) Anchor agitator with counter-rotating impeller

Anchor is a close-clearance paddle designed to conform to the shape of the vessel. It produces high shear near the wall and may scrape the surface or pass with a very small clearance. Anchor agitators are useful for preventing deposits on the vessel wall and for promoting heat transfer (Nagata, 1975). They very often operate in conjunction with higher speed paddles or other impellers, usually counter rotating. If breaker bars are put into an anchor it becomes a close-clearance gate. High shear agitators are primarily used in liquid mixing system where a particle size reduction or breaking of agglomerate solids is required. These agitators operate with a high shear and a minimum of flow. They tend to have small blade areas and operate at high speeds (Sweeney, 1978).

2.3 Laminar Mixing in Mechanically Stirred Vessels

A laminar-mixing regime occurs when the impeller Reynolds number falls below 10 for mixing high viscosity fluid. If turbine impellers are used with highly viscous fluid, flow velocities rapidly decay to low values away from the impeller. This results in the formation of a cavern around the impeller. Mixing can be good inside the cavern and poor outside (Solomon et al., 1981). The stagnant region leads to poor mass and heat transfer (Amanullah et al., 1997). For these conditions close-clearance impellers like anchor are commonly used instead of turbine impellers. There are varieties of viscous material that are mixed in the laminar regime including polymer solutions, pastes, gums, and semisolids. The mechanism of laminar mixing involves reorientation and redistribution of the viscous materials. Cutting, dicing chopping and then restacking the sectioned material will achieve this. The stacked material is then sheared or normally

elongated and then redistributed by folding for further reorientation. As the number of reorientations and redistributions increases, the interfacial area also increases. The large interfacial area eventually allows diffusion to homogenize the material. The power draw can be very high in laminar mixing compared to turbulent mixing. In addition mixers are operated at low speeds and the torque on the shaft can be extremely high.

2.4 Classification of non-Newtonian Fluids

A fluid is called Newtonian if its behavior, when subjected to a shear force, follows a simple Newton's law of viscosity.

$$\tau = \mu\dot{\gamma} \tag{2.1}$$

Here, τ is shear stress, $\dot{\gamma}$ is shear rate and μ is the viscosity of fluid. Figure 2.2 shows the rheogram of Newtonian and non-Newtonian fluids. In the rheogram curve the relationship between shear stress and shear rate is a straight line passing through the origin and the slope is the viscosity of the fluid. For Newtonian fluid the viscosity is independent of imposed rate of shear (Holland and Chapman, 1966). Some of the examples of Newtonian fluids are water, alcohol, oil, and all gases.

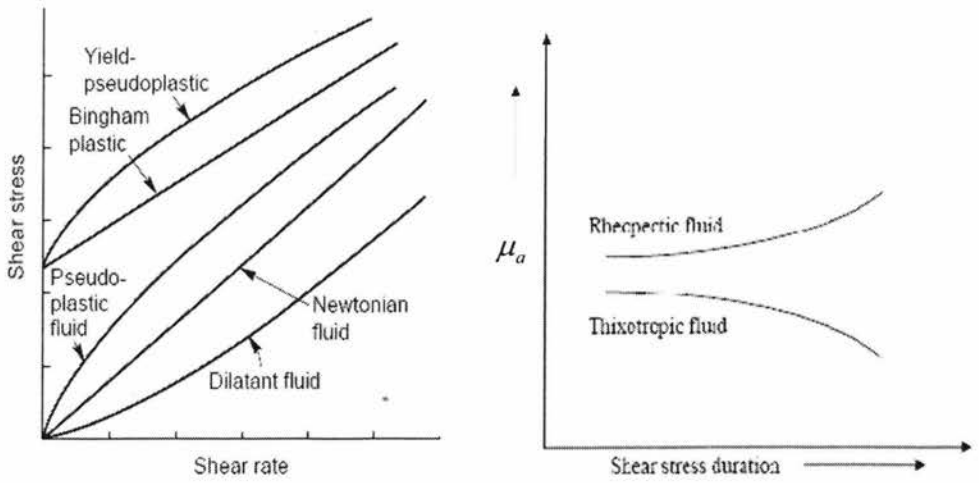

Figure 2.2 Rheograms of various kinds of Newtonian and non-Newtonian properties

Any fluid that does not obey Newton's law of viscosity is called a non-Newtonian fluid. These fluids are usually polymer melts, polymer solutions, and any Newtonian or non-Newtonian fluid with dissolved molecules.

Non-Newtonian fluids can be classified as following:

- Time-independent fluids
- Time-dependent fluids
- Viscoelastic fluids

2.4.1 Time-Independent Fluids

Time-independent fluids are the fluids in which the shear stress is a unique function of shear rate and independent of the time of shearing. So the material responds instantaneously to changes in shear rate. These fluids are further classified into three categories:

- Pseudoplastic or shear thinning
- Dilatant or shear thickening
- Viscoplastic

Figure 2.3 show the relationship of shear rate and viscosity for pseudoplastic, dilatant and Newtonian fluids. For Newtonian fluids the viscosity remains constant and independent of shear rate.

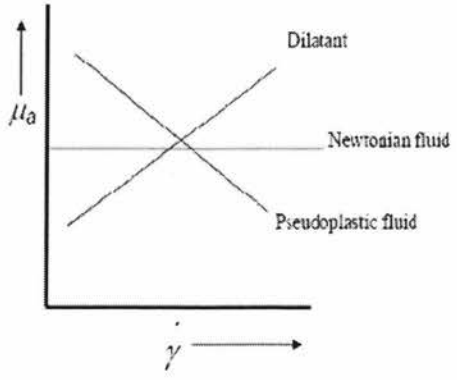

Figure 2.3 Apparent viscosity versus shear rate plot

2.4.1.1 Pseudoplastic or Shear Thinning Fluids

For pseudoplastic fluids, viscosity decreases with increasing shear rate (Harnby et al., 1997). So with high speed rotating mixers, the viscosity remains low near to the impeller even though it is high elsewhere. An extremely wide range of material in the food, biological and polymer industries exhibit this property. An apparent viscosity is defined as:

$$\mu_a = \tau / \dot{\gamma} \tag{2.2}$$

Here, τ is shear stress, $\dot{\gamma}$ is shear rate and μ_a is the apparent viscosity of fluid. The rheogram curve starts at the origin in the shear stress versus shear rate plot and is concave downward (Figure 2.2). For such a case, good mixing may occur in the impeller region with almost stagnant region in the remainder of the vessel.

2.4.1.2 Dilatant or Shear Thickening Fluids

Dilatant fluids are the fluids in which the viscosity increases with an increase in the shear rate. This property is not very common but does occur with some concentrated suspensions like china clay. The rheogram curve (Figure 2.2) starts at the origin in the shear stress versus shear rate plot but is concave upward (Rao, 1999). Apparent viscosity in a region close to the impeller increases as compared to the remainder of the vessel and velocities are very low but much the same throughout the vessel (Elson, 1990). Power required to drive the agitator also increases (Nienow and Elson, 1988).

2.4.1.3 Viscoplastic Fluids

Viscoplastic fluids are characterized by yield stress. It is found that a stress is required to break down the internal structure sufficiently before any movement will occur in fluid (Chhabra and Richardson, 1999). The rheogram curve may be either linear or non-linear and does not pass through the origin. In this case, the well-mixed region close to the

impeller which has been called a cavern, may be accompanied by a totally stagnant fluid elsewhere (Solomon et al., 1981). Plastic fluids can be classified into two groups:

- Bingham plastic
- Yield-pseudoplastic

2.4.1.3.1 Bingham Plastic Fluids

Bingham fluids are characterized by constant plastic viscosity and yield stress. The shear stress increases at constant slope with increase in shear rate as seen in the rheogram curve (Figure 2.2) and yield stress.

2.4.1.3.2 Yield-Pseudoplastic Fluids

Yield-pseudoplastic fluids possess yield stress and have a non-linear rheogram curve. These fluids are considered as a particular class of shear–thinning behavior fluids. Xanthan gum and Carbopol solutions are examples of yield-pseudoplastic fluids.

2.4.2 Time-Dependent Fluids

Time-dependent fluids exhibit considerable changes in rheology as the shearing time increases. Thus, fluid rheology depends upon both shear rate and shearing time. Two types of behaviour are possible for these fluids:

- Thixotropic Fluids
- Rheopectic Fluids

2.4.2.1 Thixotropic Fluids

For thixotropic fluids the viscosity decreases with time when the fluid is sheared at a constant shear rate (Figure 2.2). After a large time of shearing, an equilibrium viscosity is reached. Following this, if the shearing is stopped the viscosity slowly increases. Paints, tomato ketchup, and salad cream are examples of thixotropic liquids.

2.4.2.2 Rheopectic Fluids

In rheopectic fluids the apparent viscosity slowly increases with time as the liquid is sheared (Harnby et al., 1992). Concentrated suspensions of bentonite, vanadium pentoxide and gypsum have been observed as rheopectic. Rheopexy may be associated with pseudoplastic or dilatant fluids (Silvester, 1985).

2.4.3 Viscoelastic Fluids

Viscoelastic fluids behave like both viscous liquids and elastic solids (Harnby et al., 1997). These fluids start to flow when shear stress is imposed, and when the stress is removed the deformation is recovered slowly (Macosko, 1994). Bitumen and flour dough are examples of viscoelastic materials. Amongst the flow phenomena produced by viscoelasticity is the "Weissenberg effect", in which the fluid will tend to climb up a shaft rotating within it. Viscoelastic fluids are also called memory fluids because they tend to return to their original unstressed form after the deforming stress has ceased (Morrison, 2001). In the laminar flow region, viscoelasticity of the fluids increases the power consumption of the agitator (Nienow et al., 1983).

2.5 Rheological Models

Several rheological models have been developed so far to describe the rheological properties of fluids. Although pseudoplastic and dilatant refer in general to any shear-thinning or shear-thickening effect, they are often interpreted to specify proportionality between the shear stress and some power of the shear rate (Ostwald-de-waele law):

$$\tau = m\dot{\gamma}^{n} \tag{2.3}$$

The coefficient, m known as the consistency index, is the analogue to Newtonian viscosity, whereas the flow behaviour index n is simply the ratio of shear stress to strain rate at any given point. If $n < 1$ the fluid is pseudoplastic; if $n = 1$, it is Newtonian and $m = \mu$; if $n > 1$, the fluid is dilatant.

For plastic fluids that have a yield stress the following models are commonly used. One simple model, which is commonly used, is a Hershel-Bulkley model:

$$\tau = \tau_y + m\dot{\gamma}^n \tag{2.4}$$

where τ_y is the yield stress and $\dot{\gamma}$ is shear rate of fluid. Another is a Casson model:

$$\tau^{0.5} = \tau_y^{0.5} + m\dot{\gamma}^{0.5} \tag{2.5}$$

Where m is the consistency index and n is the flow behaviour index. (Ulbrecht and Patterson, 1985)

A two-parameter version of the above equation, in which n =1 and m = μ_p, is known as the Bingham model:

$$\tau = \tau_y + \mu_p\dot{\gamma} \tag{2.6}$$

Here μ_p is a viscosity. Most polymer materials will show a finite viscosity when the shear rate approaches zero rather than an infinitely high viscosity. The viscosity of these materials can be well modeled by the Carreau formula:

$$\frac{\eta - \eta_\infty}{\eta_o - \eta_\infty} = \left[1 + \left(\lambda_c \dot{\gamma}\right)^2\right]^{(n-1)/2} \tag{2.7}$$

This model describes two plateaus, a zero-shear viscosity η_o and high-shear limiting viscosity η_∞. The flow behaviour index has the same meaning as that in the power-law expression and the parameter λ_c is a characteristic time of liquid. The high shear limiting viscosity is very small compared to the zero-shear viscosity and for most engineering

applications it can be neglected. The Carreau model is quite similar to another popular model, the Ellis model:

$$\frac{\eta}{\eta_o} = \left[1 + \left(\frac{\tau_{21}}{\tau_{1/2}}\right)^{\alpha-1}\right]^{-1} \tag{2.8}$$

Where α is related to the slope of the viscosity curve in the power-law region and $\tau_{1/2}$ is the shear stress at which the viscosity is equal to one half of the zero-shear viscosity η_o (Harnby et al., 1992)

2.6 Power Input

Power is energy per unit time which is added to the fluid by various mechanisms (Tatterson, 1994). The power is added to the fluid by an impeller. Mixing time, reaction time for fast chemical reactions and heat transfer coefficients are dependent on power. Power delivered to the process should be measured and calculated for any mixing operation. The selection of appropriate mixing system depends upon homogenization and power consumption (Marvos, 2001).

2.6.1 Newtonian Fluids

The impeller power is a function of impeller and tank geometry, viscosity and density of fluid, gravitational force and rotational speed of the impeller (Tatterson, 1991).

$$P = f(\rho, \mu, N, g, d, D) \tag{2.9}$$

The following general dimensionless equation is given by using Buckingham pi theorem (Uhl and Gray, 1966):

$$f\left(\frac{\rho N d^2}{\mu}, \frac{dN^2}{g}, \frac{P}{\rho N^3 d^5}, \frac{d}{D}, \frac{d}{z}, \frac{d}{c}, \frac{d}{p}, \frac{d}{w}, \frac{d}{h}, \frac{n_2}{n_1}\right) = 0 \tag{2.10}$$

where ρ is fluid density, μ is fluid viscosity, g is gravitational acceleration, P is power consumption, N is impeller speed, d is impeller diameter, D tank diameter, c clearance from vessel wall, w impeller blade width, p pitch of blades , n is number of blades and h is the length of blade.

Where $R_e = \frac{\rho N d^2}{\mu}$ is the Reynolds number

$Fr = \frac{dN^2}{g}$ is the Froude number

$Po = \frac{P}{\rho N^3 d^5}$ is the Power number

If we consider the geometrically similarity the above equation becomes:

$$f\left(\frac{\rho N d^2}{\mu}, \frac{dN^2}{g}, \frac{P}{\rho N^3 d^5}\right) = 0 \tag{2.11}$$

The above equation can be written in the correlation form:

$$Po = K_p (Re)^a (Fr)^b \tag{2.12}$$

The values of K_p, a and b are constants and independent of the size of the equipment (Harnby et al., 1997). The Froude number, which represents the inertial to gravitational forces ratio, is normally considered in the cases where vortex forms and it can be neglected if Reynolds number is less than around 300 (Skelland, 1967). For a higher Reynolds number, which is the ratio of inertial forces to viscous forces, the effects of a Froude number could be vanished by using a baffled tank or off-centre agitator. Reynolds number determines whether the flow is laminar of turbulent.

2.6.2 Non-Newtonian Fluids

The effective procedure for predicting the power consumption in non-Newtonian fluid using the fundamental viscometric data was proposed by Metzner and Otto (1957). They assumed that the average shear rate $\dot{\gamma}_a$ varies directly with impeller speed N:

$$\dot{\gamma}_a = k_s N \tag{2.13}$$

Here k_s is a proportionality constant, called the shear rate constant that depends upon the system geometry. In non-Newtonian fluid the apparent viscosity varies within the entire vessel due to variations in the shear rate. At an average shear rate, the apparent viscosity of non-Newtonian fluids is known as the average apparent viscosity μ_a. It is then assumed that Newtonian fluid having viscosity equal to μ_a will have same power consumption as the non-Newtonian fluid. Power for laminar mixing can be derived based on Stokes' drag and written as:

$$P \propto \frac{\mu N^2 d^3}{g_c} \tag{2.14}$$

Using the definition of Reynolds number, $R_e = \rho d^2 N/\mu$ and power number, $P_o = P/\rho d^5 N^3$ above equation for power expression can be written as:

$$P_o R_e = K_p \tag{2.15}$$

where P_o and R_e are Power number and Reynolds number respectively and K_p is a constant dependent on the mixer geometry. Typically, K_p is found in a range between 10 and 40000 for a variety of impellers. The plot of P_o versus R_e on log-log plot shows the power curve for mixing system. For laminar regime slope of the curve is –1. Power consumption can be very high in laminar mixing in comparison to turbulent mixing as

mixers are operated at low speeds and the torque on the shaft can be significantly high (Paul et al., 2004).

The value of k_s obtained by Metzner and Otto (1957) was 13 for the disk flat-blade turbine. For pseudoplastic fluids, k_s is approximately in the range of 10-13 for most impeller types, while slightly larger values 25-30 have been reported for close clearance impeller like anchors and helical ribbons. A literature review on the k_s value for anchor impellers by Beckner and Smith (1966), Bakker and Gates (1995), Calderbank and Moo-Young (1961), Shamlou and Edwards (1989), Sestak *et al.*(1986), Rieger and Novak(1973), Zinty and Houska (1986) provides different constant values and correlations for k_s. Murthy and Jayanti (2003a) were evaluated the correlation of Shamlou and Edwards (1989) and reported that k_s is a function of the geometric parameters of an impeller and not of the fluid rheology.

At high Reynolds numbers the flow is turbulent and mixing is faster due to the motion of turbulent eddies (Harnby et al., 1997). The power number is almost constant in turbulent region for baffled tanks as the power number depends mainly upon on the geometry of impeller:

$$P_o = K_p \tag{2.16}$$

For mixing tank without baffles, the power number is weakly depends upon the Reynolds number (Tatterson, 1991):

$$P_o = K_p (R_e)^a \tag{2.17}$$

One important parameter, which was the subject of the several research works, in anchor-agitated mixing processes, is power consumption and consequently Metzner and Otto (1957) concept. Power consumption of anchor agitators in the mixing of non-Newtonian fluids was investigated in several research work such as Foresti Jr. and Liu (1959), Calderbank and Moo-Young (1961), Beckner and Smith (1966), Nagata et al. (1972),

Rieger and Novak (1973), Edwards et al. (1976), Sestak et al. (1986), Shamlou and Edwards (1989), Foucault et al. (2004), Foucault et al. (2005) . Several researchers have also worked on power consumption determination using anchor impellers for Newtonian fluid (Foresti Jr. and Liu, 1959; Uhl and Voznick, 1960; Calderbank and Moo-young, 1961; Beckner and Smith, 1966; Takahashi et al., 1980; Shamlou and Edwards, 1989; Nomura et al., 1996; Foucault et al., 2004; Foucault et al., 2005).

Metzner and Otto (1957) were the first to develop a relation between the average shear rate and rotational speed of an impeller ($\dot{\gamma}_a = k_s N$). However later investigations revealed that k_s depends on the flow behaviour index n. Houska (1981) showed experimentally that the power consumption prediction based on unreliable values of k_s may lead to errors as large as 50-100%. Using the basic assumption of Metzner and Otto ($\dot{\gamma}_a = k_s N$), Sestak et al. (1986) derived an expression for k_s for pseudoplastic and thixotropic fluids experimentally for anchor impeller. They derived the following equation:

$$k_s = 35 n^{n/(n-1)} \tag{2.18}$$

Here n and k_s *are* flow behavior index and Metzner and Otto parameter respectively.

Foresti Jr. and Liu (1959) had developed a new method for estimating laminar-region power consumption from liquid properties, agitator speeds and gross dimensions, and vessel size. They studied the mixing of Newtonian and pseudoplastic fluids using flat blade turbine, anchor and two sizes of cone impellers.

Uhl and Voznick (1960) measured the power required for an anchor impeller using cylinder oil. Cylinder oils are high viscosity oils used for lubrication of piston ring/cylinder liner wall. They correlated the effect of clearance on power number for 24 inch and 10 inch diameter vessel by plotting the power number data versus *c/D* (clearance

over vessel diameter) ratio. They also investigated the effect of blade width on power consumption by plotting and power number versus Reynolds number data for 3 " and 2 " wide impeller blade. There was not much effect of blade width on power consumption due to absence of shear forces in the direction of blade width. Calderbank and Moo-young (1961) have presented a general correlation for the power input to stir Newtonian and non-Newtonian fluid with various types of agitators including anchor impeller. They validated the correlation for power with experimental data. Beckner and Smith (1966) studied the Newtonian and non-Newtonian fluid agitation using anchor impellers. They investigated the effect of clearance on power consumption. They used flat blade and 45° pitched blade anchor impellers and developed a generalized correlation for power input.

Hoogendoorn and Hartog (1967) measured power input for anchor, turbine, helical screw, helical ribbon, and paddle impellers for viscous flow region. Nagata et al. (1972) experimentally measured the power input for highly viscous non-Newtonian fluids agitated by anchor, turbine and paddle impellers. Edwards et al. (1976) carried out the experimental work in cylindrical vessel with anchor, helical ribbon and helical screw impellers to predict the power consumption for mixing of the thixotropic liquids like salad cream, tomato ketchup, yoghurt, paints and laponite solutions using Metzer-otto concept (1957). Power consumption for agitation of highly viscous non-Newtonian fluid was investigated experimentally by Rieger and Novak (1972) for anchor, pitched blade anchor, screw and helical impellers. They validated the results with Metzner-Otto (1957) concept.

Takahashi et al. (1980) proposed a new power correlation for anchor and helical ribbon impellers in highly viscous Newtonian liquids. They measured the power consumption for anchor and helical ribbon agitators under laminar flow regime for Newtonian fluid. On the basis of a physical model, they proposed a new power correlation that considered the geometrical parameters such as the impeller clearance, blade angle, blade length, and blade width and impeller diameter.

Shamlou and Edwards (1989) investigated the power consumption for anchor impeller mixer employing Newtonian and non-Newtonian fluid. They brought the data together

for viscous Newtonian and non-Newtonian liquids by using an average apparent viscosity concept and the following equation:

$$k_s = 33 - 172\left(\frac{c}{D}\right) \tag{2.19}$$

where k_s is a shear rate constant, c is a vessel wall clearance and D is a tank diameter. The range of c/D was $0.021 < c/D < 0.133$. They interpreted the power consumption in laminar region with the following model:

$$P_o R_e = 8.5\pi^3 \frac{(h/d)(w/d)n_b}{(c/D)^{0.5}} \tag{2.20}$$

Where h is impeller height, w is impeller blade width, d is impeller diameter, D is tank diameter *and* n_b is number of impeller blades.

Using experimental technique, Foucault et al. (2004) studied power consumption and the mixing time of a dual impeller composed of an anchor impeller as a wall scraping impeller and three types of impellers (Deflo turbine, Sevin turbine and hybrid turbine impellers) for Newtonian and non-Newtonian fluids. The hybrid-anchor combination impeller was found to be the most efficient for mixing in counter-rotating or co-rotating mode regardless of the fluid rheology.

Foucault et al. (2005) experimentally characterized the power consumption of coaxial mixer made up of a wall-scraping anchor and a radial discharge turbines rotating in co- and counter-rotating direction for Newtonian and non-Newtonian fluid. The power consumption of anchor was increased significantly in counter-rotating mode and decreased in co-rotating mode.

2.7 Mixing time

Mixing time is defined as the time required from the start of blending operation to the time when specific degree of uniformity in the concentration is achieved. It was shown by Uhl (1952) that anchor is suitable impeller as compared to turbine impeller for high viscosity Newtonian fluids and turbine impeller can achieve comparable mixing effectiveness for low viscosity fluids.

Hoogendoorn and Hartog (1967) measured the mixing time for several impellers such as anchor, inclined blade paddles, helical screw, helical ribbon and flat blade turbine. Using discoloration and thermal technique, they found that the turbine and anchor mixers were unsatisfactory for viscous mixing. In spite of this observation, anchor impellers have been widely used in food, paint, cosmetic, and pharmaceutical and food industries (Nagata et al., 1972; Kaminoyama et al., 1990).

Nagata et al. (1972) experimentally concluded that for highly viscous and non-Newtonian liquids, agitators that produced vertical circulations in vessel were most effective. They utilized multi-paddle and close clearance ribbon and screw impellers. The mixing rate of the anchor impeller was close to that of the ribbon impeller. However for high viscosity fluid, especially for plastic fluid, the mixing capacity of the anchor impeller was very low. Foucault et al. (2006) studied the mixing time of a dual impeller mixer composed of an anchor impeller and different types of three other impellers (Rushton turbine, Rayneri-sevin impeller or new hybrid dispersing impeller) for Newtonian and shear thinning fluids. They found that the Rushton turbine was more effective in terms of mixing time in both Newtonian and non-Newtonian fluids.

It was observed that few publications have been dedicated to determine the mixing time for anchor impeller using computational fluid dynamics (CFD).

2.8 Flow Patterns

Flow fields generated by an impeller in a mixing tank with a single phase liquid is useful in establishing whether there are any stagnant or dead regions in the vessel, and whether or not the particles are likely to be maintained in suspension. The efficiency of mixing tank and product quality are influence by flow patterns in the mixing tank. Flow patterns produced in a mixing tank are mainly dependent upon the impeller geometry. Stirrers used in mixing of non-Newtonian fluids are classified into three types:

1. Stirrers that rotates at high speeds and produces high local shear rates and relies on good momentum transport to carry the energy from an impeller into the far corners of the mixing tank. Turbine impeller is an example of this type (Ulbrecht and Patterson, 1985).
2. Stirrers which do not depend on adequate momentum transport due to viscous damping and therefore, are of large size to reach into the far corners of the mixing tank. Anchor and gate impellers falls in this category
3. Stirrers that rotates slowly without creating high gradients but have very good pumping capacity to reach every corner of the mixing tank. Helical screw and helical ribbon impellers.

The flow patterns for anchor impellers were studied by many researchers for Newtonian and non-Newtonian fluids using numerical analysis and experimental work (Peter and Smith, 1967; Murakami et al., 1972; Hiraoka et al., 1978; Kuriyama et al., 1982; Ohta et al., 1985; Kaminoyama et al., 1990; Rubert and Bohme, 1991; Bertrand et al., 1996; Marouche et al., 2002).

Peters and smith (1967) experimentally measured the velocity profiles generated by an anchor impeller for agitation of Newtonian fluid and viscoelastic fluids. They used cameras arranged with solenoid operated shutter releases. They discussed the conditions leading to a vortex formation behind the blade and the effect of these flow regimes on the performance of the anchor impeller. Murakami et al. (1972) experimentally investigated the mixing of a highly viscous fluid with anchor, paddle and helical ribbon impellers and

determined the flow patterns using cameras. For anchor impeller, the tangential flow was dominant and axial flow was very little. The radial flow was recognizable near the impeller.

2.9 Computational Fluid Dynamics Study

Computational fluid dynamics (CFD) is a numerical technique for the simulation of fluid flow, chemical reaction, mass transfer and many other phenomena. The general practice for the evaluation of stirred vessels has been done over the years through experimental investigation for a number of different impellers, vessel geometries and fluid rheology. Such an approach is usually costly and sometimes is not an easy task. On the other hand, the empirical correlations are often not suitable for all systems as they are commonly found for a specific system and therefore can only give general view of the mixing performance. Attempts are being made to use the science and fundamentals of mixing by using advanced computational fluid dynamics (CFD) method. With CFD, the various parameters contributing to the process can be examined in shorter time and with less expense, a task otherwise difficult by experimental techniques. However, this approach is limited by relative lack of sufficient detailed measurements for validation and corroboration. One advantage of CFD is that, once a validated solution is obtained, it can provide valuable information that would not be easy to obtain experimentally.

Hiraoka et al. (1978) established a numerical algorithm for two-dimensional laminar flow in stirred tank and studied the power input and velocity profile using anchor and paddle impellers for highly viscous fluid. Using numerical algorithms, two-dimensional flow in the horizontal plane with an anchor impeller was studied by Kuriyama et al. (1982) for Newtonian fluid. They used finite difference method to solve the governing equations. The computational velocity distribution and power consumption results were in good agreement with experimental results.

Bertrand et al. (1996) studied the flow behaviour of a yield stress fluid using three dimensional finite element methods and concluded that flow was mainly tangential and

there was formation of closed loops around the shaft. Ohta et al. (1985) presented a numerical method for the solution of two-dimensional flow problems in the vertical plane of an anchor agitated vessel for Newtonian fluid. Using calculated streamlines, they investigated the effect of impeller speed and vessel clearance on the axial flow pattern inside the tank.

With three-dimensional numerical analysis, extensive calculations related to velocity components, shear rate and apparent viscosity were performed by Kaminoyama et al. (1990). They studied the flow of pseudoplastic Ellis fluid in stirred vessels with three different impellers such as a six blade turbine, a paddle, and anchor impellers. Rubert and Bohme (1991) presented a finite element method to simulate the flow field for mixing of non-Newtonian fluid in a vessel equipped with an anchor impeller.

Abid et al. (1992) generated 3-D flow and showed that an increase in Reynolds number generally did not change the flow structures but may influence the appearance of the recirculation loops behind the blade. Kaminoyama et al. (1994) numerically analyzed the 3-D flow in anchor agitator tank and presented velocity (axial, radial, and tangential) profiles, and the distribution of shear rate, shear stress, and apparent viscosity.

Tanguy et al. (1994) analyzed simulation of flow field using three-dimensional finite element method for viscoplastic fluid with an anchor impeller and concluded that viscoplasticity affects the circulation patterns and power consumption in laminar regime for anchor impeller vessel. Bertrand et al. (1996) investigated numerically the mixing of yield stress fluids with an anchor impeller in the laminar regime using three-dimensional finite element method. The fluid rheology was modeled as a power law fluid. It was shown that Metzner-Otto (1957) concept was valid for yield stress fluids. They investigated experimental power correlations of Nagata (1975) regarding the mixing of yield stress fluid in laminar regime.

Marouche et al. (2002) conducted a numerical study on the behaviour of yield stress fluid and generated velocity field, power consumption, and flow pattern in a mixing tank equipped with an anchor impeller in the laminar regime using Carreau model of shear thinning fluid. Using finite element solver, Savreux et al. (2007) studied the 2-D mixing of viscoplastic fluids with a mixer having a static anchor impeller and a rotating tank. Using particle tracking, they showed that the increase in rotation velocity is not enough to improve the mixing quality.

Pedrosa and Nunhez (2000) worked on anchor impeller for non-Newtonian fluid, using computational fluid dynamics (CFD) package CFX-4.2, and calculated three components of velocity contours on two dimensional grids. Murthy and Jayanti (2003) investigated power consumption and the flow field created by an anchor impeller using the CFD code CFX for power-law fluid.

2.10 Research objective

The thorough review of the aforementioned published literature suggest that in the case of pseudoplastic fluids with yield stress, agitated with an anchor impeller, the 3-D CFD modeling works using finite volume method are very limited. Few research articles have been devoted regarding the study on power consumption and velocity profiles. Information concerning the mixing time (t_m), optimum blade width (w) and vessel clearance (c) is still inadequate.

In this study, CFD is employed to investigate the mixing behaviour of pseudoplastic fluid possessing yield stress using an anchor impeller. The major objectives of this study are:

- To generate a 3-D flow field for mixing of yield-pseudoplastic fluid in a flat bottom cylindrical tank equipped with two- and four-blade anchor impellers using computational fluid dynamics (CFD) modeling technique.
- To evaluate the effects of fluid rheology, agitator speed, number of impeller blades on power consumption, mixing time and flow patterns.

- To determine the optimum values of *c/D* (clearance to diameter) and *w/D* (width to diameter) ratios on the basis of minimum mixing time
- To evaluate the effect of clearance (*c*) and impeller blade width (*w*) on power consumption and mixing time.

3. EXPERIMENTAL WORK

This chapter covers physical and rheological properties of xanthan gum solution of different concentration and the detailed procedure of experimental work that was carried out.

3.1 Equipment Details

The mixing equipment designed, fabricated and utilized in this study was a flat-bottomed cylindrical tank having internal diameter 0.143 m (D) and height 0.178 m (H) and fitted with anchor impeller with two blades. The impeller was driven by a variable speed 1/8 hp motor (Lightnin, Model L5U10F). The detailed dimensions of the tank and impeller are given in the following Table 3.1.

Table 3.1 Detailed dimensions of experimental mixing tank

Parameters	**Dimensions (m)**
Vessel diameter (D)	0.143
Vessel Height (H)	0.178
Impeller diameter (d)	0.125
Impeller height (h)	0.125
Impeller blade width (w)	0.014
Impeller blade thickness (t)	0.009
Clearance from wall and bottom (c)	0.009
c/D	0.053
h/d	0.944
d/D	0.929
w/d	0.104

Further details about the geometrical characteristics of the stirred flat bottom tank with all internal dimensions are shown schematically in figure 3.1.

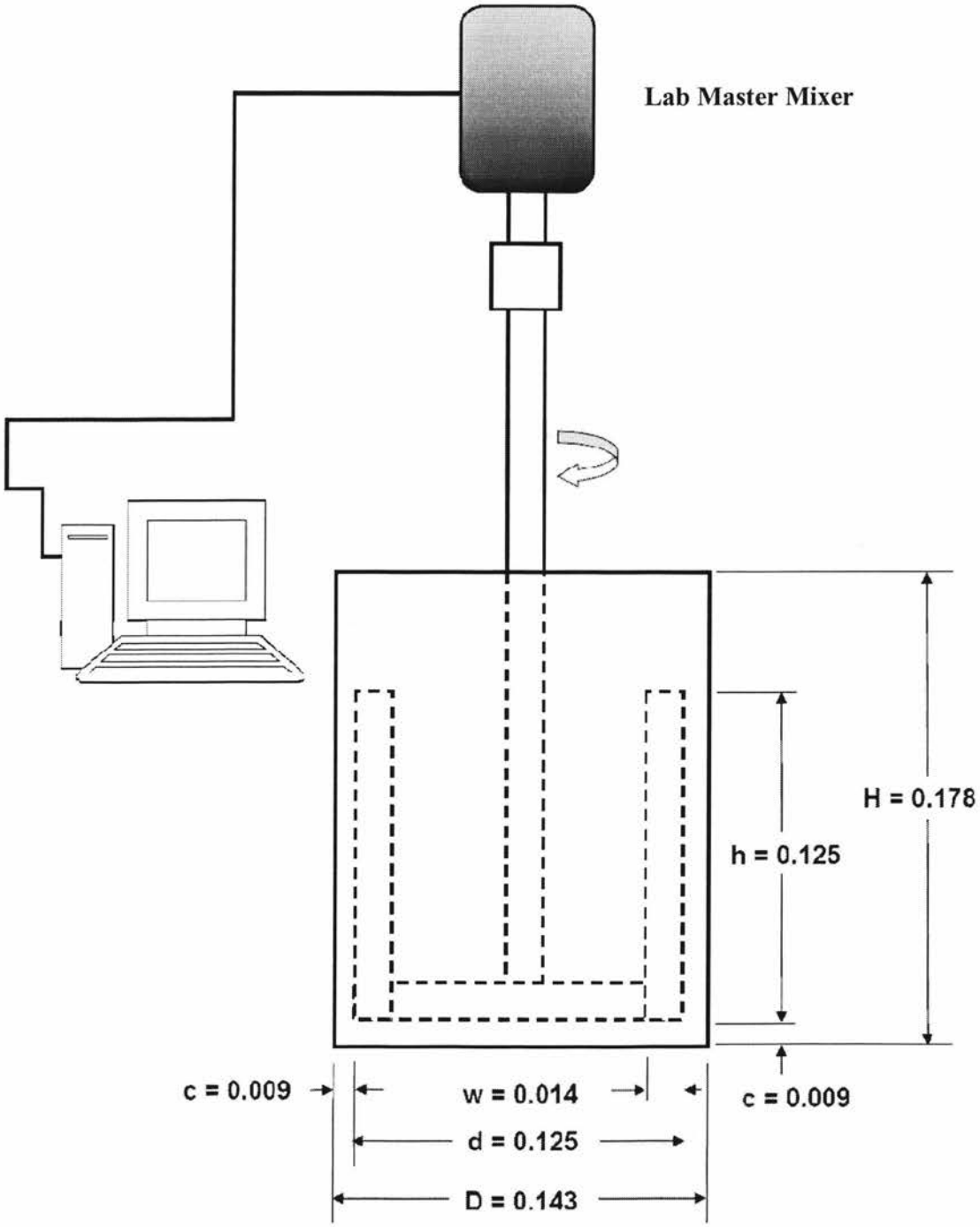

Figure 3.1 Schematic diagram of experimental mixing tank

3.2 Power Measurement Calibration

To ensure the accurate results, the mixer was calibrated with the following procedure as suggested by the manufacturer. Initially the mixer power was turned on. The shaft and impeller were removed from the equipment. The mixer was set to its minimum speed of 20 rpm and turned off. Then when the mixer was entered into the diagnostic mode, it initiated the power calibration program. The mixer was started and the revolution speed was increased to the maximum speed of 550 rpm, increasing 5 % each time. At each speed, it calibrated the measurement. The procedure took approximately 20 minutes to complete.

3.3 Power Measurement

The power input to the impeller (P) was determined from torque (M) and impeller rotational speed (N) measurements by using the following equation:

$$P = 2\pi NM \tag{3.1}$$

LabMaster mixer was connected to the anchor impeller shaft with a stainless steel chuck to accommodate radial, angular, and axial misalignment. Impeller torque and speed were measured using a rotary torque transducer with an encoder disk. The bearing and the shaft guiding system induces the friction torque. This friction torque was subtracted from all the measured torques.

3.4 Xanthan Gum Physical and Rheological Properties

3.4.1 Source

Xanthan gum is a microbial desiccation-resistant polymer prepared commercially by aerobic submerged fermentation from *Xanthomonas campestris* (Kennedy and Bradshaw, 1984). This biopolymer is used as a thickener, stabilizer and emulsifier (Garcia et al., 1998). It is widely used in many industries such as food, cosmetics, paper making,

enhanced oil recovery etc. The foremost function of xanthan gum in most foods is to boost the viscosity. When it is added to the liquid foods, it enhances the low shear viscosity while having very little effect on the viscosity of food at high shear rate (Speers and Tung, 1986) This phenomenon is known as shear thinning behaviour or pseudoplasticity which is a desirable property in many fluid foods as it results in superior suspending properties at low shear rates without rendering the food too viscous to mix or pour at higher shear rates.

3.4.2 Structural unit

Xanthan gum is a heteropolysaccharide made up of building blocks of D-glucose, D-mannose and D-glucuronic acid residues with the molar ratios of 2.8:3.0:2.0 (Rocks, 1971). The structure of xanthan gum is shown in figure 3.2. The basic repeating unit of xanthan gum consists of 16 monosaccharide residues, of which 13 are in the main linear chain and 3 are attached to a single-unit side chains.

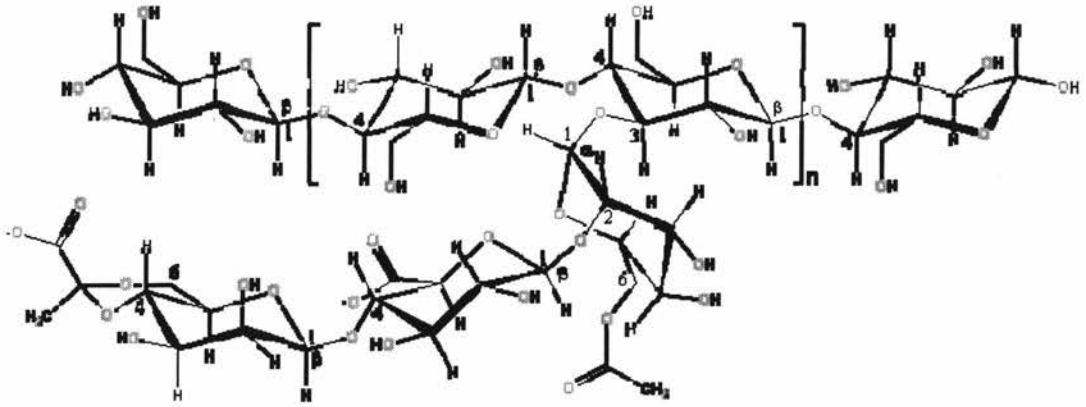

Figure 3.2 Xanthan gum molecular structure (Source: Chaplin, 2008)

Its most important property is its very high low-shear viscosity coupled with its strong shear-thinning character. The relatively low viscosity at high shear means that it is easy to mix, pour and swallow but its high viscosity at low shear gives good suspension and

coating properties and lends stability to colloidal suspensions. Several studies were done regarding viscosity or rheology of xanthan gum solutions (Whitcomb and Macosko, 1978; Galindo et al., 1989; Westra, 1989, Torees et al., 1993; Garcia-Ochoa and Casas, 1994; Podolsak et al., 1996; Renaud el al., 2005). Xanthan gum can be described as a yield-pseudoplastic fluid in most of the studies.

3.4.3 Effects of Temperature

Viscosity of xanthan gum solution decreases with rise in temperature. Variation in viscosity of xanthan gum solution with temperature was studied by Morris (1977) and found that the viscosity declines as the dissolution temperature is raised up to 40°C. Between 40°C and 60°C, the viscosity increases with increase in temperature. For temperatures higher than 60°C, the viscosity declines as the temperature is raised. Whitcomb (1997) measured viscosity as a function of temperature (5-95°C) for solutions of xanthan in distilled water. They found that there is a drop in viscosity with temperature beginning at 50°C. This behaviour is related to conformational changes of the xanthan molecule. The conformation shifts from an ordered (low dissolution temperature) to a disordered (high dissolution temperature) state (Ferguson and Kemblowski, 1991).

3.4.4 Effect of pH

García-Ochoa (2000) showed that the viscosity of xanthan solutions is unaffected by pH changes between 1 and 13 while it was shown that at pH 9 or higher, xanthan is gradually deacetylated (Tako and Nakamura, 1984) and at pH lower than 3, xanthan loses the pyruvic acid acetyl groups (Bradshaw et al., 1983). Either deacetylation or depyruvylation has hardly any effect on xanthan solution viscosity (García-Ochoa, 1994) and deacetylated or depyruvylated xanthan shows similar rheological properties as native xanthan (Bradshaw et al., 1983).

3.4.5 Effects of salts

The presence of salts in xanthan gum solution influences its viscosity. At low xanthan gum concentration, the viscosity decreases slightly when a small amount of salt is added

to the solution (Ferguson and Kemblowski, 1991). This effect has been associated with the reduction in molecular dimensions resulting from weakened intermolecular electrostatic forces (Smith and Pace, 1982). Viscosity increases at higher xanthan concentration when a large amount of salt is added (Rochefort and Middleman, 1987). This behaviour can be because of increased contacts between the polymer molecules (Milas et al., 1985). It was shown that the viscosity of a xanthan solution is not dependent on salt concentration when the salt content exceeds 0.1% w/v (Kang and Pettit, 1993).

For this study, the food grade xanthan gum (NovaXan, ADM, USA) in the powder form was used to prepare the xanthan gum solution.. The xanthan gum solutions were made with a concentration of 0.5%, 1.0%, and 1.5%. The rheological properties of the solutions were measured (Pakzad, 2007) at 22°C in a Bohlin CVOR-150 rheometer (Malvern instruments, USA) using a 40mm 1° cone and 60mm plate measuring system. The range of the shear rate applied in the controlled shear rate rheometer varied from 0.14-130 s^{-1}, which was supposed to be the range of that encountered in the mixing system. The temperature at which these measurements were made was the same as the bulk fluid temperature in the tank.

The rheology of xanthan gum solutions was modeled best (with high regression coefficients) by the Herschel-Bulkley model (Herschel and Bulkley, 1926), as shown in figure 3.3. Xanthan gum solution's apparent viscosity (η) is given by equation:

$$\eta = \frac{\tau_y}{\dot{\gamma}} + K\dot{\gamma}^{n-1} \qquad (3.2)$$

where $\dot{\gamma}$ is the shear rate, τ_y is the yield stress, and K and n are consistency index and flow behaviour index respectively.

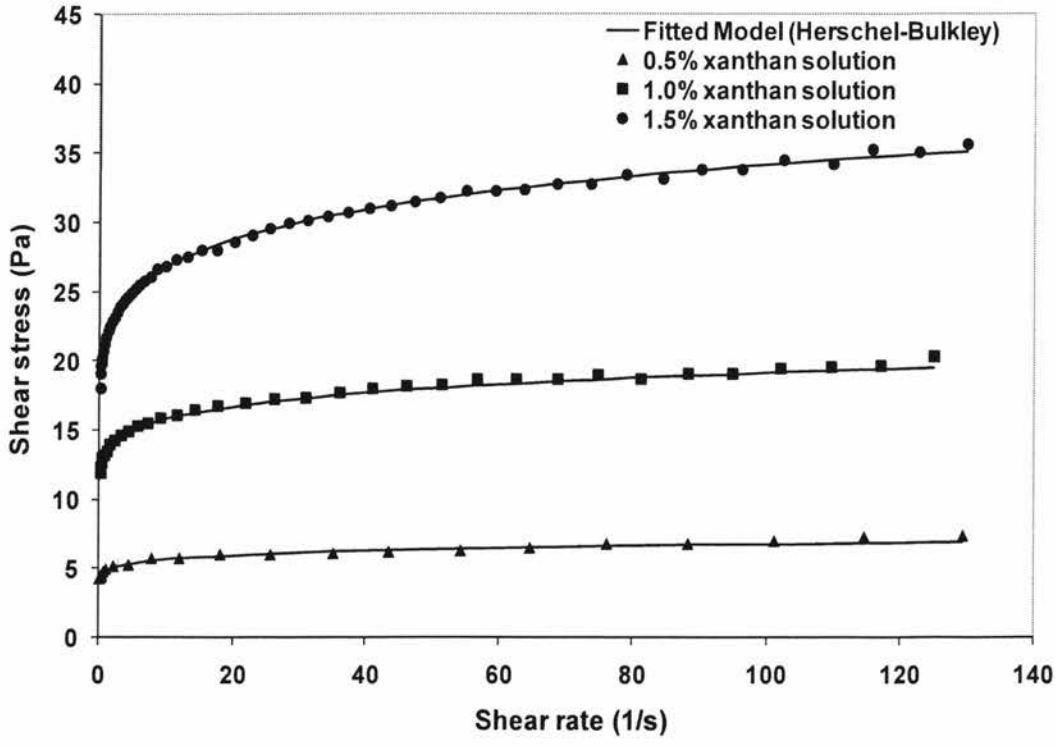

Figure 3.3 Shear stress (τ) versus shear rate ($\dot{\gamma}$) graph for xanthan gum solutions

The rheological characteristics of xanthan gum solutions are listed in Table 3.2.

Table 3.2 Rheological properties of xanthan gum solutions

Xanthan gum Concentration (%)	Consistency index, K (Pa s^n)	Power-law index, n -	Yield stress, τ_y (Pa)	Regression Coefficient, R^2
0.5	3	0.11	1.789	0.9905
1.0	8	0.12	5.254	0.9985
1.5	14	0.14	7.455	0.9992

3.5 Experimental Procedure

The fluid used for experiment as well as CFD simulation analysis was a xanthan gum solution in water with concentration of 0.5%, 1.0% and 1.5%. Weighted amount of xanthan gum was dissolved in the solution to prepare the solution of different concentration. Care was taken to prevent lumps and air bubble formation. For all experiments, the solution in the tank was kept overnight to reach the desired temperature and remove the possible air bubbles.

The experiment was carried out at various impeller speeds (20 to 100 rpm) to measure the impeller torque and power consumption for 0.5%, 1.0% and 1.5% xanthan gum solutions.

3.6 Experimental Conditions

Concentration of xanthan gum solutions: 0.5%, 1.0% and 1.5%
Impeller revolutions: 20-100 rpm
Temperature: Room temperature (22 °C)
Volume of the xanthan gum solution: 2.19 liter
Experimental mixing vessel geometry: as per the schematic diagram Figure 3.1

4. COMPUTATIONAL FLUID DYNAMICS (CFD)

Computational Fluid Dynamics (CFD) is a numerical technique that solves governing transport equations using different algorithms. In this study, the commercial packages Fluent 6.3 and MixSim 2.1 (Fluent Inc., USA) were used for CFD modeling. Fluent and MixSim uses the finite volume discretization method to solve the governing flow equations. This chapter is divided into two parts. In the first part governing equations, numerical methods and discretization schemes are discussed. The second part is dedicated to current CFD model development.

4.1 Performing a CFD Analysis

Computational fluid dynamics (CFD) packages involve three major elements (Shaw, 1992): Pre-processing, processing and post-processing.

4.1.1 Pre-processing

All tasks which take place before the numerical solution process are known as pre-processing. This involves following:

- Creating the system geometry (problem domain) that needs to be analyzed
- Specifying the fluid properties
- Selecting physical and chemical phenomena which is to be modeled
- Dividing flow domain into a number of smaller sub domains, called a mesh of cells
- Specifying appropriate boundary conditions.

4.1.2 Processing

During processing, mathematical equations of fluid flow are solved. The CFD solver performs the following functions: (1) Discretization of the domain, (2) Converting the

governing flow equations into algebraic equations, and (3) solving the algebraic equations by iterative methods.

4.1.3 Post-processing

Post processing is used to evaluate the data generated during CFD analysis. CFD postprocessors are equipped with data visualization techniques to display mesh and domain geometry, vector plots of velocity field, contours of velocity, 2D and 3D surface plots and many other output capabilities.

The following sections highlight the most important parts of computational fluid dynamics principles and the CFD analysis technique described above.

4.2 Governing Conservation Equations

After specifying system geometry and fluid properties, selecting the physical and chemical phenomena to be modeled becomes essential. This step is usually performed by choosing the appropriate transport equations that represent the model under study. Classical transport phenomena include continuity, motion, energy, and species transport equations. Modeling an isothermal, non-reacting mixing vessel requires adopting equations of motion and continuity.

In mixing process, the general governing transport equation represents mathematical statements of two conservation laws: (1) mass of a fluid is conserved; (2) the rate of change of momentum equals the sum of forces acting on the fluid. These statements represent continuity and momentum equations, respectively. These two equations can be written as follows (Patankar, 1980; Morison, 2001, Fluent, 2006):

4.2.1 Continuity Equation

The continuity equation is a statement of conservation of mass and given by:

$$\frac{\partial \rho}{\partial t} + \nabla.(\rho \vec{v}) = 0 \tag{4.1}$$

where ρ is a fluid density, $\vec{v}$ is a velocity vector. The first term in the above equation represents the dynamic change of density in the control volume and the second term shows the rate of mass flux passing through the control volume per unit volume.

For incompressible fluid, the density of fluid is not a function of space or time and remains constant (Morison, 2001). Therefore, above equation of conservation mass becomes

$$\nabla.\vec{v} = 0 \tag{4.2}$$

4.2.2 Momentum equation

The momentum equation is a statement of conservation of momentum, derived from Newton's second law of motion (Morison, 2001) given by $\vec{F} = m\,\vec{a}$. Newton's second law says that the net force on the fluid element equals its mass times the acceleration of the element. There are two sources for the force: (1) forces acting directly on the mass of the fluid element or volume (e.g., gravitational forces) known as body forces, and (2) forces acting on the surface of the fluid element or volume (e.g., pressure and friction) known as surface forces.

$$\frac{\partial}{\partial t}(\rho \vec{v}) = -\nabla \cdot (\rho \vec{v} \vec{v}) + \nabla \cdot \left(\overline{\overline{\tau}}\right) + \rho \vec{g} - \nabla p + \vec{F} \tag{4.3}$$

where p is statistic pressure, ρg is gravitational body force, F is external body force and $\overline{\overline{\tau}}$ is a stress tensor, created from the friction between the fluid and the surface of the fluid element and is given by following equation (Fluent, 2006):

$$\overline{\overline{\tau}} = \eta\left[(\nabla\vec{v}) + (\nabla\vec{v}^{T}) - \tfrac{2}{3}\nabla.\vec{v}I\right] \tag{4.4}$$

For incompressible fluids, the expression for the stress tensor is given by equation 4.4 with neglecting the last term we get:

$$\overline{\overline{\tau}} = \eta\left[(\nabla\vec{v}) + (\nabla\vec{v}^{T})\right] \tag{4.5}$$

where

$$\eta\left[(\nabla\vec{v}) + (\nabla\vec{v}^{T})\right] = \eta\overline{\overline{D}} \tag{4.6}$$

where η is apparent non-Newtonian fluid viscosity, I is identity matrix and $\overline{\overline{D}}$ is the rate of deformation or strain tensor. The non-Newtonian viscosity η is a function of the shear rate $\dot{\gamma}$, which is related to the second invariant of $\overline{\overline{D}}$ and is defined as the following (Bird et al., 2002):

$$\dot{\gamma} = \sqrt{\frac{1}{2}\left(\overline{\overline{D}} : \overline{\overline{D}}\right)} \tag{4.7}$$

4.3 General Form of a Transport Equation

All equations described above can be written in the form of a general transport equation for any scalar or vector quantity ϕ, (Patankar, 1980; Ferziger and Peric, 1995; Versteeg and Malalasekara, 1995) and used throughout this study to present the FV discretization practices.

$$\frac{\partial}{\partial t}(\rho\phi) + \nabla.(\rho\phi\,\vec{v}) - \nabla.(\Gamma_{\phi}\nabla\phi) = S_{\phi} \tag{4.8}$$

The first term in the above equation highlights the rate of change term for ϕ, the second term is a convective term and the third term is a diffusive term. The term in the right side is a source term (i.e. source of ϕ per unit volume). ϕ=1 in the continuity equation, and $\phi = \vec{v}$ in the momentum equation. Γ_ϕ is a diffusion coefficient. Γ_ϕ= 0 in the continuity equation, and Γ_ϕ= viscosity in the momentum equation

4.4 Introduction to Numerical Methods

The partial differential transport equation (Equation 4.8) explains the continuous movement of fluid in space and time. To solve these transport equations numerically, computational fluid domain is discretized; i.e. changed from continuous to discontinuous domain by series of connected control volume which is known as computational cells.

The following section describes the grid generation and numerical discretization methods. Only the finite volume method is discussed in more detail as it is used in this study.

4.4.1 Discretization of Flow Domain (Grid Generation)

Discretization of flow domain is also known as grid generation. After selecting physical and chemical phenomena to be modeled for a specified geometry (computational flow domain), the flow domain is divided into many sub-domains, or computational cells, or control volumes, which are also called a grid (or mesh) of cells.

The computational cells have different shapes. For two dimensional problems, triangular or quadrilateral cells are used; while for three dimensional domains tetrahedral, prisms, pyramids or hexahedral cells are used. Following figure 4.1 reveals the types of cells produced in Fluent 6.3 for three dimensional geometries (Fluent, 2006). The Fluent 6.3 and MixSim 2.1 mainly generate tetrahedral and hexahedral cells, with pyramid cells among the differently meshed zones. Tetrahedral and hexahedral cells generate good

quality meshes. However, they can result in a very large number of meshes for small-dimension elements such as baffle (Fluent, 2006).

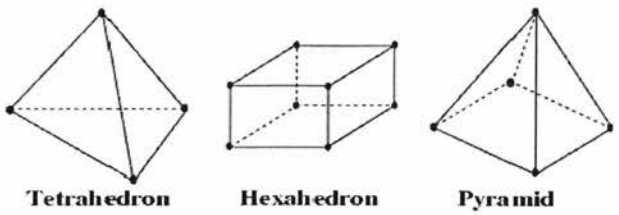

Figure 4.1 Types of computational cells

The density of the cells in a computational grid need to be fine enough to capture the flow details, but not too fine so that the overall numbers of cells in the domain are excessively high and require large computational time. The most important requirements placed on a gird generation are that there must be no holes between the grid cells, grid cells should not overlap, the grid should be smooth with no abrupt changes in the volume of grid cells, and the gird elements should be as regular as possible (Blazek, 2005). In Laminar flows, the grid near the boundaries should be refined to allow the solution to capture the boundary layer flow detail (Paul et al., 2004). The boundary layer grid should contain quadrilateral elements in two dimensional and hexahedral or prism elements in three dimensional domains.

Two different types of grids exist: (i) structured and (ii) unstructured grids. Evaluation of gradients and fluxes on structured grids is greatly simplified, because each grid can be accessed quickly and easily. The price paid for the enhanced flexibility in structured grids is a prolonged time (often weeks or months) required to generate grids for complex geometries. Unstructured grids, on the other hand, offer very flexible treatment of complex geometries. Quadrilaterals and triangles grids (in 2-D) and hexahedra, tetrahedral, prism and pyramid grids (in 3-D) can be placed independent of the complexity of the domain. These mixed grids result in a reduction in the number of grid cells, edges, faces and possibly nodes. Time required to build an unstructured, mixed grid for a complex configuration is significantly lower than that for a structured grid

(Blazek, 2005, Versteeg and Malalasekera, 2007). Fluent 6.3 and MixSim 2.1 use Gambit 2.2 to generate unstructured grids.

In the unstructured grids, the grids are finer near elements where the pressure, velocity, and temperature gradients are very high (e.g., impellers, baffles, tank walls) and coarser in areas where the gradients of velocity and temperature are small (Blazek, 2005). Since there are no small changes in flow behaviour to be captured, it is a waste to have a fine grid in such regions. The cost and accuracy of the solution directly depend upon the quality of the grids.

4.4.2 Discretization of Transport Equations

Several methods have been employed over the years to solve the momentum equations numerically, including the finite difference, finite element, spectral element, and finite volume methods. To apply CFD, the transport equations, which describe the continuous movement of a fluid in space and time, must be discretized or changed from a continuous to a discontinuous formulation. Discretization is the method of approximating the differential equations from a continuous domain to a discrete domain (Chung, 2002). All terms in the transport equations need to be discretized. Therefore, the discretization can be divided into spatial and temporal time.

4.4.2.1 Spatial Discretization

After generating a grid, the CFD solver implements the numerical technique to discretize convective, diffusion and source terms in transport equations. Three numerical techniques are known for spatial discretization: (i) finite difference, (ii) finite element, and (iii) finite volume.

The finite difference approach uses truncated Taylor series expansions for generating finite difference approximations of derivatives at each grid point for each term in the transport differential equation. The partial derivatives in the governing equations are replaced by the difference quotients leading to the system of algebraic equations for

dependent variables at each grid point. For simple geometry and structured grids the FDM is relatively simple and straightforward to easily achieve high order approximation (Blazek, 2005).

While the finite difference method is an approximation of the transport partial differential equation (PDE), the finite element method (FEM) is an approximation of the transport PDE solution. FEM divides the continuum field, or domain into cells or elements (triangular or a quadrilateral form in 2-D or tetrahedral or hexahedral form in 3-D) which can be rectilinear or curved. The grids are unstructured, which provide the most important advantage of the method when compared with FDM. A finite element method provides simple functions (linear or quadratic) valid on elements to describe the local variations of unknown flow variables. The approximation functions are defined at specified points called nodes. Nodes usually are located on the element boundaries to which the adjacent elements are connected. Now the nodal field variables become the new unknowns of algebraic equations. As known, the governing equation is satisfied by the exact solution of the variables, which is not possible by substituting the approximation functions for variables and therefore a residual is defined to measure the errors. Next, the residuals are minimized in some sense by multiplying them by a set of weighting functions and integrating. By minimizing the residual, a set of non-linear algebraic equations is obtained (Chung, 2002). The finite volume method is discussed later, with more details, in section 4.5.

4.4.2.2 Temporal Discretization

Two methods are used to perform temporal discretization by CFD solver:

(i) Explicit Method

(ii) Implicit method

Explicit time discretization scheme evaluates field variables at the current time level only. Although explicit time discretization schemes are numerically cheap, stability and convergence are hard to achieve using these schemes. Implicit time discretization scheme, on the other hand, evaluates field variables at different time levels. Larger time steps can be utilized with explicit time scheme without hampering the stability of the time

discretization. Another important advantage of implicit schemes is their superior robustness and convergence speed (Blazek, 2005). Finite volume temporal discretization is explained in the section 4.5.2.

4.5 Finite Volume Method

In this section the finite volume method is described in detail. Finite volume method is usually considered as a standard approach to perform the spatial discretization (Ranade, 2002). This method is widely used in CFD packages, such as Fluent 6.3 and MixSim 2.1. In finite volume technique the transport governing equations are integrated for each computational cell (or control volume) giving discrete equations that conserve each variable on a control volume basis. The volume integral can be converted to a surface integral by applying the divergence theorem. The remainder of this chapter will focus on finite volume discretization techniques.

4.5.1 Finite Volume Spatial Discretization

The steady state continuity equation and equation of motion can be expressed as follows in terms of an integral form for an arbitrary three dimensional control volume (CV):

$$\int_{CV} \nabla(\rho\vec{v}) dV = 0 \tag{4.9}$$

$$\int_{CV} \nabla(\rho\vec{v}) dV = \int_{CV} \nabla(\Gamma_\phi \nabla\phi) dV + \int_{CV} S_\phi dV \tag{4.10}$$

The divergence terms can be rewritten as integrals over the entire bounding surface of the control volume using Gauss' divergence theorem (Bird et al. 2002), resulting in the following equation:

$$\int_{A} (\rho\vec{v}) d\vec{A} = 0 \tag{4.11}$$

$$\int_A (\rho\phi\vec{v})d\vec{A} = \int_A (\Gamma_\phi \nabla\phi)d\vec{A} + \int_{CV} S_\phi dV \tag{4.12}$$

Here $\vec{A}$ is a surface area vector. If the above equations are applied to all control volumes or cells in the computational domain, and summed up for all the cells of computational domain the following equations will be obtained:

$$\sum_{\mathrm{f}}^{N_{\mathrm{faces}}} \rho_{\mathrm{f}}.\vec{v}_{\mathrm{f}}.\vec{A}_{\mathrm{f}} = 0 \tag{4.13}$$

$$\sum_{\mathrm{f}}^{N_{\mathrm{faces}}} \rho_{\mathrm{f}}\vec{v}_{\mathrm{f}}\phi_{\mathrm{f}}.\vec{A}_{\mathrm{f}} = \sum_{\mathrm{f}}^{N_{\mathrm{faces}}} \Gamma_\phi (\nabla\phi)_n \vec{A}_{\mathrm{f}} + S_\phi V \tag{4.14}$$

where subscript (f) refers to cell face, N_{faces} is the number of faces enclosing the cell , ϕ_f is value of ϕ convected through face (f), $\vec{A}_{\mathrm{f}}$ is area of face (f), $\rho_{\mathrm{f}}\vec{v}_{\mathrm{f}}.\vec{A}_{\mathrm{f}}$ is mass flux through the face, $(\nabla\phi)_n$ is magnitude of $\nabla\ \phi$ normal to face (f), and superscript arrows indicate the vector of transport property. The above equation 4.14 represents the flux balance in a control volume. The left side gives the net convective flux and the right side contains the net diffusive flux and the generation or destruction of the property ϕ within the control volume. Equation 4.14 as a general form is solved by Fluent. The diffusion term in the above equation 4.14 is central differenced and is always second-order accurate.

The pressure gradient term forms the main momentum source term in most cases. Pressure is also stored at cell centers. Therefore, an interpolation scheme is required to compute the face values of pressure from the cell values. For this purpose, Fluent provides several schemes such as first-order, linear, second-order, body-force-weighted and PRESTO schemes (Fluent, 2006), which will be explained in Section 4.6.1.

Face values ϕ_f are required for the convection terms in equation 4.14 and must be interpolated from the cell center values. This is accomplished using an upwind scheme. Upwinding means that the face value ϕ_f is derived from quantities in the cell upstream, or "upwind," relative to the direction of the normal velocity in equation 4.14. Fluent allows one to choose from several upwind schemes such as first-order upwind, second-order upwind, power law, and QUICK (Fluent, 2006) which will be discussed in Section 4.6.2.

Another important issue is the role played by the pressure appearing in the momentum equation as the source term, but there is no equation for pressure individually. Several methods have been proposed to estimate the pressure field which should be estimated. The most widely used methods for incompressible flows, implicit or semi implicit pressure correction methods are SIMPLE, SIMPLEC, and PISO (Fluent, 2006) which will be discussed in Section 4.7.

4.5.2 Finite Volume Temporal Discretization

For transient simulations, the governing equations must be discretized in both space and time. The spatial discretization for the time-dependent equations is identical to the steady-state case. Temporal discretization involves the integration of every term in the differential equations over a time step (Δt). The integration of the transient terms is straightforward, as shown below. A generic expression for the time evolution of a variable is given by the following:

$$\frac{\partial \phi}{\partial t} = F(\phi) \tag{4.15}$$

where the function $F(\phi)$ incorporates any spatial discretization. Fluent 6.3 and MixSim 2.1 discretize the time derivative with the backward first order differences and backward

second order differences. If the time derivative is discretized using backward differences, the first-order accurate temporal discretization is calculated as:

$$\frac{\phi^{m+1} - \phi^{m}}{\Delta t} = F(\phi) \tag{4.16}$$

The second-order discretization is given as:

$$\frac{3\phi^{m+1} - 4\phi^{m} + \phi^{m-1}}{2\Delta t} = F(\phi) \tag{4.17}$$

where ϕ is any scalar quantity (like concentration), Δt is time step, $m+1$ is the value of scalar quantity at next time step ($t + \Delta t$), m is the value of scalar quantity at current time step (t) and $m-1$ is the value of scalar quantity at previous time step ($t - \Delta t$). Once the time derivative has been discretized, a choice remains for evaluating $F(\phi)$; in particular, which time level values of ϕ should be used to evaluate F. Fluent 6.3 uses the two types of time integration schemes to evaluate $F(\phi)$: (i) implicit time integration (ii) explicit time integration.

Implicit time integration evaluates $F(\phi)$ at the future time level while the explicit time integration evaluates $F(\phi)$ at the current time level. The implicit scheme is absolutely stable with respect to time step size. The use of explicit time stepping is fairly limiting due to sensitivity of this integration scheme to time step, and is used mostly to capture the transient behaviour of moving waves (e.g., shocks).

By default, Fluent 6.3 uses implicit time integration for incompressible flow simulations, since for such applications solutions must be iterated to convergence within each time step (Fluent, 2006).

4.6 Discretization Schemes

Transport field variables (ϕ) are usually stored at the cell centers (nodes). Nodes are usually placed between control volumes such that the faces of control volume are positioned mid-way between adjacent nodes. However, face values of field variables are required to perform the calculations and must be interpolated from the cell values (Abbott and Basco, 1989). To obtain the face values of these variables as a function of values that are stored at the cell centers, a discretization scheme is required. Figure 4.2 shows the grid notations in one-dimensional geometry (Versteeg and Malalasekera, 2007). P shows the general nodal point and its neighbours in a one-dimensional geometry, W and E specify the nodes to the west and east, respectively. The west and east side faces of the control volume are specified by w and e respectively. The distances between the nodes W and P as well as between nodes P and E are specified by δx_{WP} and δx_{PE} respectively.

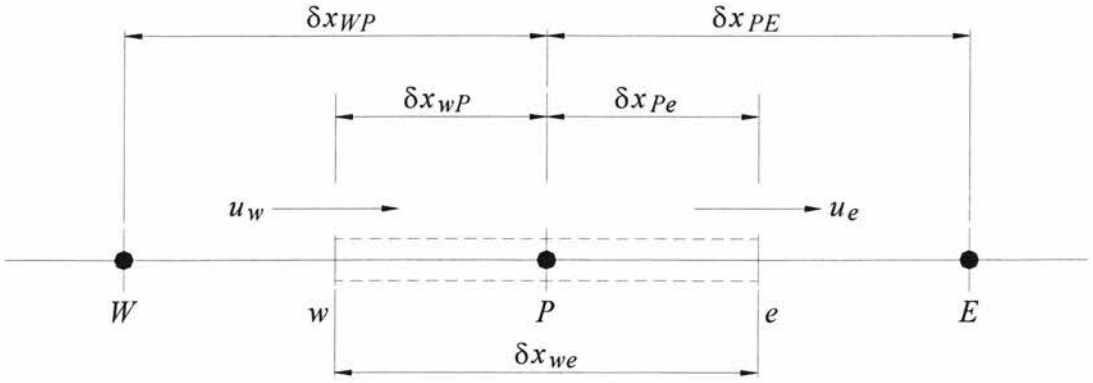

Figure 4.2 Grid notations (Source: Versteeg and Malalasekera, 2007)

4.6.1 Pressure Interpolation Scheme

The pressure gradient appears in the momentum equation in terms of $-\frac{dp}{dx}$, $-\frac{dp}{dy}$ and $-\frac{dp}{dz}$. Different schemes can be used to interpolate the pressure at the nodes of the cells

to the interface or cell faces. Fluent 6.3 and MixSim 2.1 uses the following pressure interpolation schemes:

- Linear scheme
- First order (standard) scheme
- Second-order scheme
- PRESTO (Pressure Staggering Option) scheme
- Body-force-weighted scheme

4.6.1.1 Linear scheme

The linear interpolation scheme assumes a piecewise linear profile for pressure between nodes of adjacent cells and computing face pressure as the average of the pressure values between two adjacent cells. At one-dimensional grid, the pressure gradient at face (e) can be expressed as follows (Fluent, 2006):

$$\left(\frac{\partial p}{\partial x}\right)_e = \frac{\frac{p_E + p_W}{2}}{\delta_{x_{PE}}} = \frac{(p_E + p_W)}{2\delta_{x_{PE}}} \tag{4.18}$$

4.6.1.2 First order or standard scheme

Having first order accuracy, the first order scheme deals with smooth uniform pressure fields. Under this scheme, the pressure at face (e) can be expressed as follows (Fluent, 2006):

$$\left(\frac{\partial p}{\partial x}\right)_e = \frac{(p_E - p_e)}{\delta_{x_{PE}}} \tag{4.19}$$

4.6.1.3 Second-order scheme

The second-order scheme reconstructs the face pressure in the manner used for second-order accurate convection terms. This scheme may provide some improvement over the

standard and linear schemes, but it may have some trouble if it is used at the start of a calculation and/or with a bad mesh (Fluent, 2006; Versteeg and Malalasekera, 1995).

$$\left(\frac{\partial p}{\partial x}\right)_e = \frac{(p_E - p_P)}{2\delta_{x_{PE}}} \tag{4.20}$$

4.6.1.4 PRESTO (Pressure Staggering Option)

The PRESTO (Pressure Staggering Option) scheme uses the discrete continuity balance for a staggered control volume about the face to compute the staggered (i.e., face) pressure. (Fluent, 2006) The PRESTO scheme is available only for quadrilateral and hexahedral meshes. For flows with high swirl numbers, high-Rayleigh-number natural convection, high-speed rotating flows, flows involving porous media, and flows in strongly curved domains, use the PRESTO scheme

4.6.1.5 Body-force-weighted scheme

The body-force-weighted scheme computes the face pressure by assuming that the normal gradient of the difference between pressure and body forces is constant. For problems involving large body forces, the body-force-weighted scheme is recommended (Fluent, 2006)

4.6.2 Convective Term Discretization Scheme

The effect of convective discretization scheme on the simulation of flow in stirred vessels was investigated in a few works such as Brucato et al. (1998), and Aubin et al. (2004). The following different schemes can be used to interpolate the momentum term defined at the nodes of the cells to the interface or cell faces:

- First-Order Upwind Scheme
- Second-Order Upwind Scheme
- Quadratic Upwind Scheme (QUICK)
- Power Law Scheme

4.6.2.1 First order upwind scheme

The first order scheme was first introduced by Courant et al., (1952) and then developed by Gentry et al. (1966) and Runchal and Wolfshtein (1969). In this scheme, quantities at cell faces ($\phi_f : \phi_e \ or \ \phi_w$) are determined by assuming that the cell-center values of any field variable represent a cell-average value and hold throughout the entire cell; the face quantities are identical to the cell quantities. Thus the face value is set equal to the cell-center value of the upstream cell. Thus, when a first-order unwind scheme is selected; the face value ϕ_f is set equal to the cell-center value of the upstream cell (Versteeg and Malalasekera, 1995):

$$\phi_e = \phi_P \quad \text{if } u_e > 0 \quad \text{or positive direction} \tag{4.21}$$

$$\phi_e = \phi_E \quad \text{if } u_e < 0 \quad \text{or negative direction} \tag{4.22}$$

4.6.2.2 Second order upwind scheme

The second order scheme developed by Barth & Jespersen (1989), involve more neighbour points and reduce the interpolation errors. Thus when a second-order upwind scheme is selected, the face value ϕ_f is computed by means of:

$$\phi_f = \phi + \nabla\phi.\Delta\vec{s} \tag{4.23}$$

where ϕ is the cell-centered value and $\nabla\phi$ represents the best estimate of the solution gradient in the cell computed from surrounding centroid data, and $\Delta\vec{s}$ is the displacement vector from the upstream cell centroid to the face centroid. This formulation requires the determination of the gradient $\nabla\phi$ in each cell. There are several methods for this purpose available in literature such as least-squares gradient reconstruction (Versteeg and Malalasekera, 2007). This gradient can be computed using the divergence theorem, which in a discrete form is written as:

$$\nabla\phi = \frac{1}{V}\sum_{f}^{N_{faces}} \tilde{\phi}_f \vec{A} \tag{4.24}$$

where the face values $\tilde{\phi}_f$ are computed by averaging ϕ from the two cells adjacent to that face and V is cell volume. The scheme shows significant improvement in comparison with the first order and provides suitable accuracy for many industrial cases of interest (Barth and Jespersen, 1989). Barth & Jespersen's second order upwind corresponds to a Taylor series expansion around the centers of cell face, where only the linear term in a Taylor series is retained.

4.6.2.3 Quadratic upwind scheme

For quadrilateral and hexahedral meshes, where unique upstream and downstream faces and cells can be identified, Fluent also provides the quadratic upwind scheme (QUICK) of Leonard (1979) and Leonard & Mokhtari (1990) for computing a higher-order value of the convected variable at a face. These schemes are based on a weighted average of second-order-upwind and central interpolations of the variable. The face value for any transport property can be obtained from a quadratic function passing through two bracketing nodes (on each side of the face) and a node on the upstream side as follows:

$$\phi_e = \frac{3}{8}\phi_E + \frac{6}{8}\phi_P - \frac{1}{8}\phi_W \tag{4.25}$$

The QUICK scheme will usually be more accurate on structured grids aligned with the flow direction (Fluent, 2006). This scheme can offer improvements over the second order scheme for swirling a flow.

4.6.2.4 Power law scheme

Power law scheme (Patankar, 1980) interpolates the face value of a variable using the exact solution to a one-dimensional convection-diffusion equation:

$$\frac{d}{dx}(\rho\vec{v}\phi)=\frac{d}{dx}\left(\Gamma\frac{d\phi}{dx}\right) \tag{4.26}$$

Here $\rho\vec{v}$ and Γ are constant across the interval δx. Equation 4.26 can be integrated to yield the solution describing how ϕ varies with x in terms of the Peclet number. The power-law expressions (Patankar, 1980) for cell-face value can be written as:

$$\frac{D_e-\frac{F_e}{2}}{D_e}=-P_e, \qquad \text{For } P_e<-10, \tag{4.27}$$

$$\frac{D_e-\frac{F_e}{2}}{D_e}=(1+0.1P_e)^5-P_e, \qquad \text{For } -10\le P_e<0 \tag{4.28}$$

$$\frac{D_e-\frac{F_e}{2}}{D_e}=(1-0.1P_e)^5, \qquad \text{For } 0\le P_e\le 10 \tag{4.29}$$

$$\frac{D_e-\frac{F_e}{2}}{D_e}=0, \qquad \text{For } P_e>10 \tag{4.30}$$

Here D_e is momentum conductance defined as μ/δ_x, Fe is strength of convection (for flow) given by $\rho.u_e$, P_e is $\rho.u_e.\delta_x/\mu$, μ is fluid viscosity, ρ is fluid density, and δ_x is element length as indicated in Figure 4.2.

4.7 Pressure-Velocity Coupling Schemes

Transport equations for velocity components (momentum equations) can be derived from the general transport equation 4.14 by replacing the variable ϕ by velocity. Then, the obtained velocity field must satisfy the continuity equation. The real difficulty in the calculation of the velocity field is the unknown pressure field (the pressure gradient term forms the main momentum source term). Therefore, the momentum equations can be solved only when the pressure field is estimated. Unless the correct pressure field is

employed, the resulting velocity field will not satisfy the continuity equation. The aim is to find a way to improve the estimated pressure, and subsequently the resulting velocity field will gradually get closer to satisfying the continuity equation.

The most frequently used velocity-coupling algorithms used with Fluent are: SIMPLE, SIMPLEC, and PISO for steady-state calculations.

4.7.1 SIMPLE Algorithm

The short form SIMPLE stands for Semi-Implicit Method for Pressure-Linked Equations. This algorithm, originally developed by Patankar and Spalding (1972), is in fact a guess-and-correct procedure for the calculating of pressure on a staggered grid arrangement. The core of the algorithm is as follows. A guessed pressure field is used in the solution of the momentum equations. The new velocities are computed, but these will not, in general, satisfy the continuity equation, so corrections to the velocities are determined. Based on the velocity corrections, a pressure correction is computed which, when added to the original guessed pressure, results in an updated pressure (Ranade, 2002). Following the solution of the remaining variables, the iteration is complete and the entire process repeated. SIMPLE is used generally for steady-state calculations (Fluent, 2006) and is a default scheme in MixSim.

4.7.2 SIMPLEC Algorithm

SIMPLEC (SIMPLE Consistent) was introduced by Van Doormal and Raithby (1984) This method follows the same steps as the SIMPLE algorithm with the difference that the SIMPLEC velocity correction equations neglect the terms that are less critical than those in the SIMPLE algorithm (Ranade, 2002). With SIMPLEC the pressure relaxation factor is generally 1.0, which enhances the conversion. However, in some problems the pressure-correction under-relaxation to 1.0 can lead to instability. For such cases SIMPLE is recommended (Fluent, 2006).

4.7.3 PISO Algorithm

The PISO (Pressure Implicit with Splitting of Operators) of Issa (1986) is a two-step corrector algorithm that uses two corrector steps. The first corrector step is the same as that of the SIMPLE algorithm. Then the corrected velocity and pressure fields are used to derive the second correction equation. For the second step, the first term in the right hand side is calculated using the first correction step (Versteeg and Malalasekara, 2007).

This method is a pressure-velocity calculation procedure developed originally for the non-iterative computation of unsteady compressible flows (Ranade, 2002). The PISO algorithm with neighbour correction is highly recommended for all transient flow calculations, especially for a large time step on highly skewed meshes (Fluent, 2006). For steady-state problems, PISO with a two-step correction procedure does not provide any advantage over the other methods such as SIMPLE or SIMPLEC with optimal under-relaxation factors (Fluent, 2006). This method solves the pressure correction equation twice, so the method requires additional storage for calculations.

4.8 Solution of Discretized Equations

By means of grid generation, specifying boundary conditions and the physical properties, the calculations can be started. The differential equations are approximated as a set of finite volume equations on the grid, and the resulting set of algebraic equations is then solved for the discrete values of the variables. Because of the nonlinearity of the equations that govern the fluid flow and related processes, an iterative solution procedure is required. The linearized form of the discretized equation can be written as follows:

$$a_p \phi_p = \sum_{nb} a_{nb} \phi_{nb} + S_\phi \tag{4.31}$$

Where ϕ is any transport property, subscript 'p' denotes the node at which governing equation is approximated, subscript 'nb' refers to the neighbour cells, a_p and a_{nb} are the linearized coefficients for ϕ_p and ϕ_{nb} respectively and S_ϕ is the source term.

Fluent employs two numerical methods: segregated or coupled solver to solve transport equations. With the segregated solution approach, a single variable is solved at a time all over the domain and the iteration of the solution is complete when the variable has been solved on the entire domain. The segregated approach, therefore, solves each discretized governing equation implicitly with respect to the equation's dependent variable, resulting in a system of linear equations with one equation for each cell in the domain (Abbott and Basco, 1989). For a coupled solution approach, all variables are solved simultaneously at the same time in a particular cell before the solver moves to the next cell.

As mentioned before, Fluent will solve the governing integral equations for the conservation of mass and momentum, and for energy and other scalars such as turbulence and chemical species. In the segregated or coupled approach, a control-volume-based technique is used. In both the segregated and coupled solution methods, the non-linear governing equations are linearized to produce a system of equations for the dependent variables in all computational cells. This process may take an implicit or explicit method with respect to the dependent variable.

Implicit: For a given variable, the unknown value in each cell is computed using a relation that has both existing and unknown values from neighbouring cells. Thus each unknown variable will appear in more than one equation in the system, and these equations must be solved simultaneously to give the unknown quantities.

Explicit: For a given variable, the unknown value in each cell is computed using a relation that includes only existing values. Therefore, each unknown will appear in only one equation in the system and the equations for the unknown value in each cell can be solved one at a time to provide the unknown quantities.

Fluent 6.3 and MixSim 2.1 solve transport equations using segregated and coupled solvers (Fluent Inc., 2006). The segregated approach solves the governing equations sequentially (i.e., segregated from one another). Coupled solver, on the other hand, solves the governing equation simultaneously (i.e., coupled together). Both solvers yield a system of equations represented by equation 4.31 for dependent variables in every computational cell. The segregated approach, therefore, solves each discretized governing equation implicitly with respect to the equation's dependent variable, resulting in a system of linear equations with one equation for each cell in the domain (Abbott and Basco, 1989). A point implicit Gauss-Seidel linear equation solver is used in conjunction with an algebraic multigrid (AMG) method (Versteeg and Malalasekera, 2007) to solve the equations for all dependent variables in each cell.

The coupled solution method allows using either implicit or explicit solvers. The coupled implicit approach solves for all variables in all cells at the same time. Each equation in the coupled set of governing equations under the implicit coupled solver is solved implicitly with respect to all dependent variables in the set. This results in a system of linear equations for each cell in the domain. A point implicit (Gauss-Seidel) linear equation solver is used in conjunction with an algebraic multigrid method to solve the resulting system of equations for all dependent variables in each cell. The coupled explicit approach, on the other hand, solves for all variables in one cell at a specific time. Each equation in the coupled set of governing equations under the explicit coupled solver is solved explicitly, resulting in a system of equations for each cell in the domain (Fluent, 2006).

4.8.1 Multigrid Scheme Concept

Multigrid methods (Shyy *et al.*, 1997) were originally developed by Brandt (1977). The basic idea is to accelerate the convergence speed of the iterative scheme (e.g. Gauss-Seidel iteration) by updating the corrections to the solution on coarser grids (Press *et al.*, 1992). The idea is that the low frequency components of the errors (global error) can be smoothed out more rapidly on the coarser grids. Thus, the success of this scheme depends on good damping of the errors.

The process starts from the original grid where the problem is defined, or the finest grid. A few iterations are carried out on the finest grid to reduce the high frequency errors. This step is called the pre-relaxation step because it is performed before moving to the next coarser grid level. Then the residual errors, controlling the accuracy of the solution on all coarse grids are injected into the coarser grids. The process of smoothing and injection continues down to the lowest grid, the coarsest one. Here the correction to the solution can be found rapidly and can be interpolated back up until the finest grid is reached again. Next, iterations are carried on the fine grids to remove high-frequency errors formed on the coarse grids by the multigrid cycles. These iterations are referred to as post-relaxation sweeps because they are performed after returning from the coarser grid level.

4.8.2 The Gauss-Seidel Method

Gauss-Seidel is the simplest among all iterative methods (Patankar, 1980) in which the values of the variables are calculated by visiting each grid point in a certain order. Only one set of dependent variable (ϕ) is held in computer storage. In the beginning, these represent an initial guess or a value from the previous iterations. As each grid point is visited, the corresponding value of dependent variable in the computer storage is altered as follows:

If discretization equation is written by equation 4.31 then ϕ_{nb} at the visited grid point is calculated from

$$\phi_p = \frac{\sum_{nb} a_{nb}\phi_{nb} * + S_\phi}{a_n} \tag{4.32}$$

Here ϕ_{nb} * stands for the neighbour-point value present in the computer storage. For neighbours that have already visited during the current iterations, ϕ_{nb} * is the freshly calculated value; for yet-to-be-visited neighbours, ϕ_{nb} * is the latest available value for the neighbour-point variable. When all grid points have been visited in this manner, one

iteration of the Gauss-Siedel method is complete. The segregated implicit scheme was used to solve linearized discretized equations in this work.

4.8.3 Convergence Norms

Iterative numerical solutions, such as CFD, are approximations to the exact solution of the governing equations, depending on the appropriateness of numerical schemes used, initial guesses, and iterations.

The solution of each governing equation at each iterative step is based on orientation from the initial guesses that are refined through repeated iterations. Therefore, the right hand side of equation 4.31 is a non-zero value, representing the error or residuals in the solution. The total residual, often known as an unscaled residual, is the sum over all cells in the computational domain of the residuals in each cell and expressed as follows (Fluent, 2006; Ranade, 2002):

$$R^{\phi} = \sum_{allCells} \left| \sum_{nb} a_{nb}\phi_{nb} - a_p\phi_p + S_{\phi} \right| \tag{4.33}$$

Since the total residual defined above depends upon the magnitude of the variable being solved, it is customary to either normalize or scale the total residual to gauge its change during the solution process. R^{ϕ} is known as the "unscaled " residual. The convergence evaluation using an unscaled residual is a difficult task since no scaling is employed (Fluent, 2006). Fluent scales the residual using a scaling factor representative of the flow rate of ϕ over the entire domain. The "scaled" residual is defined as:

$$R^{\phi} = \frac{\sum_{allCells} \left| \sum_{nb} a_{nb}\phi_{nb} - a_p\phi_p + S_{\phi} \right|}{\sum_{allCells} \left| a_p\phi_p \right|} \tag{4.34}$$

For the momentum equations the denominator term $a_p\phi_p$ is replaced by $a_p v_p$, where v_p is the magnitude of the velocity at cell P. For the continuity equation, the unscaled residual for the segregated solver is defined as (Fluent, 2006):

$$R^c = \sum_{all\ cells} |rate\ of\ mass\ reaction\ in\ cell\ P| \tag{4.35}$$

and the segregated solver's scaled residual for the continuity equation is defined as:

$$\frac{R^c_{iteration\,N}}{R^c_{iteration\,5}} \tag{4.36}$$

The denominator ($R^c_{iteration\,5}$) is the largest absolute value of the continuity residual in the first five iterations (Fluent, 2006).

4.8.4 Under-relaxation

Convergence and stability are two mathematical concepts that are used to determine the success or failure of a CFD solution. Convergence is the property of a numerical method to produce a solution that approaches the exact solution as the control volume size is reduced to zero. Convergence criteria are preset conditions for the normalized or scaled residuals that determine when an iterative solution is converged and the solution is no longer changing. Stability is associated with the damping errors as the numerical method proceeds. When unstable or divergent behaviour is obtained, under-relaxation factors can be used to control the computed variables.

The solution of a single differential equation, solved iteratively, makes use of information from the preceding iteration so that the new value (ϕ_{n+1}) is expressed as follows:

$$\phi_{n+1} = \phi_n + \Delta\phi \tag{4.37}$$

Rather than using the full computed change in the variable ($\Delta\phi$) and in order to make the convergence process stable, it is often necessary to use a fraction of the computed range (Paul et al., 2004) so that:

$$\phi_{n+1} = \phi_n + \alpha.\Delta\phi \tag{4.38}$$

where α is known as under relaxation factor and usually takes a value from zero to one. Small under-relaxation factors facilitate convergence, but they require longer computational time (Fletcher, 1991). The value of an under-relaxation factor can be changed during computation process.

4.9 CFD Modeling of Agitated Tanks

To model the geometry of the impeller in an agitated tank, 3-D simulation methodologies were developed to explicitly present impeller rotation in a vessel. Different solution methods are available to capture the rotating impeller motion. Fluent 6.3 uses the following two methods to model impeller rotation in agitated tanks: Multiple Reference Frame (MRF) Model and Sliding Mesh (SM) Model.

4.9.1 Multiple Reference Frame (MRF) Model

A multiple reference frame model (MRF) is a steady state approach allowing for the modeling of baffled tanks with complex rotating or stationary internals (Luo et al., 1994). A rotating frame is used for the region containing the rotating components while a stationary frame is used for regions that are stationary. In the rotating frame containing the impeller, the impeller is at rest. In the stationary frame containing the tank wall, the tank is at rest.

A momentum equation inside the rotating frame is solved in the frame of the enclosed impeller while those outside the rotating frame are solved in the stationary frame. A steady transfer of information is made at the MRF interface as the solution progresses.

While the solution of the flow field in the rotating frame in the region surrounding the impeller imparts the impeller rotation to the region outside this frame, the impeller itself does not move during simulations. The impeller position is static, implying that the orientation of impeller blades relative to the baffles does not change. With this model, the rotating frame section extends radially from the centerline of shaft out to a position that is about midway between the blade's tip and the wall. The axially rotating frame section extends above and below the impeller. In the circumferential direction, it extends throughout the entire angle of the vessel (Fluent, 2006).

4.9.2 Sliding Mesh (SM) Model

The sliding mesh (Luo et al., 1993) model provides a time-dependent description of the periodic interaction between impellers and baffles. In this model, the grid surrounding the rotating components physically moves during the simulations, while the stationary grid remains static. The velocity of the impeller and shaft relative to the moving mesh region is zero as is the velocity of the tank, baffles, and other internals in the stationary mesh region.

The motion of the impeller is realistically modeled because the grid surrounding it moves as well, giving rise to a time accurate simulation of the impeller-baffle interaction. The motion of the grid is not continuous, but it is in small discrete steps. After each such motion, the set of transport equations is solved in an iterative process until convergence is reached. The grid moves again, and convergence is once again obtained from another iterative calculation. During each of these quasi-steady calculations, information is passed through an interface from the rotating to the stationary regions back again.

The sliding mesh model is the most rigorous and informative solution method for stirred tank simulations. Upon comparing numerical predictions obtained from applying different impeller modeling methodologies, several investigators observed that steady state approaches, like MRF, can provide reasonable predictions to flow field features and power consumption. About one-seventh of the CPU-time can be saved using steady state

MRF techniques (Brucato et al., 1998). Instead of performing a single calculation to obtain a converged result, as is the case with steady state flows, sliding mesh simulations advance forward in time using small time steps. This requires some level of convergence at each of the time steps. The goal of the sliding mesh model is a solution for the final, periodic steady-state condition.

MRF was successfully used for modeling stirred vessels to simulate the impeller rotation by several researchers (Harvey et al., 1997; Kelly & Gigas, 2003; Khopkar et al., 2004; Sommerfeld and Decker, 2004; Kukukova et al., 2005; Lane et al., 2005; Deglon and Meyer, 2006; Khopkar et al., 2006; Kerdouss et al., 2006; Yue-Lan et al., 2007).

4.10 CFD Model Description

Fluent is a CFD package that solves the momentum and continuity equations using a finite volume method. In this study the computational fluid dynamics (CFD) package Fluent 6.3 (Fluent Inc., USA) was used to discretize the conservation of mass and momentum equations in laminar regime and to generate steady-state 3-D flow fields inside the mixing tank.

4.10.1 Geometry

A specialized pre-processor for mixing applications, MixSim version 2.1.10 (Fluent Inc., USA) was used for defining the mixing tank geometry. The detailed geometrical dimensions of mixing tank defined in the preprocessor were same as the one that was used in the experimental study (Table 3.1)

4.10.2 Impeller modeling

The impeller rotation can be modeled using multiple reference frames (MRF) and sliding mesh (SD) methods. These both techniques were designed to capture the motion of a rotating impeller in a stationary tank without need of any empirical data. The steady-state simulation is performed by utilizing a multiple reference frame (MRF) model. The

transient interaction between the impeller(s) and blades is predicted by the sliding mesh (SM) model (Fluent, 2006). The review on the subject can be found in Deen et al. (2002) and Brucato et al. (1998). The MRF technique was used in this study. A rotating frame was used for region containing the shaft and impeller while the stationary frame was used for regions that are stationary containing tank wall. The angular velocity of rotating frame is same as that of the shaft and impeller. The conservation equations for impeller grid region were solved in rotating frame whereas for stationary region, the equations were solved in the stationary frame of the mixing tank. A steady transfer of information was made at the MRF interface as the solution progressed.

4.10.3 Defining Fluid Physical Properties

Xanthan gum was defined as a new material in MixSim 2.1 material library. The xanthan gum rheology has been described by the Herschel-Bulkley model (Galindo et al., 1989; Macosko et al., 1994). The detailed fluid rheology of xanthan gum solutions (0.5%, 1.0%, and 1.5%) is described in Chapter 3.

The difficulties with modeling with the Hershel-Bulkley model are that it becomes discontinuous at less shear rates because the non-Newtonian viscosity becomes unbounded at small shear rates (Ford, 2004). This discontinuous behaviour causes major difficulties in numerical analysis. To overcome this problem it can be assumed that for low shear rates ($\dot{\gamma} \leq \tau_y / \mu_0$), the xanthan gum solution will act like a very viscous fluid with viscosity μ_0. As the shear rate is increased and the yield stress (τ_y) is passed, the xanthan gum fluid behaviour is described by a power-law model (Fluent, 2006). So apparent viscosities of xanthan gum solutions are described as follows to overcome this discontinuity:

$$\eta = \mu_0 \qquad \text{for } \tau \le \tau_y \tag{4.39}$$

$$\eta = \frac{\left[\tau_y + K\left[\dot{\gamma}^n - \left(\frac{\tau_y}{\mu_0}\right)^n\right]\right]}{\dot{\gamma}} \qquad \text{for } \tau > \tau_y \tag{4.40}$$

where μ_0 is yielding viscosity. μ_0 can be estimated from experimental rheological curves. It can be assumed to be the slope of the line of shear stress versus shear rate curve before yielding as shown in the figure 4.3.

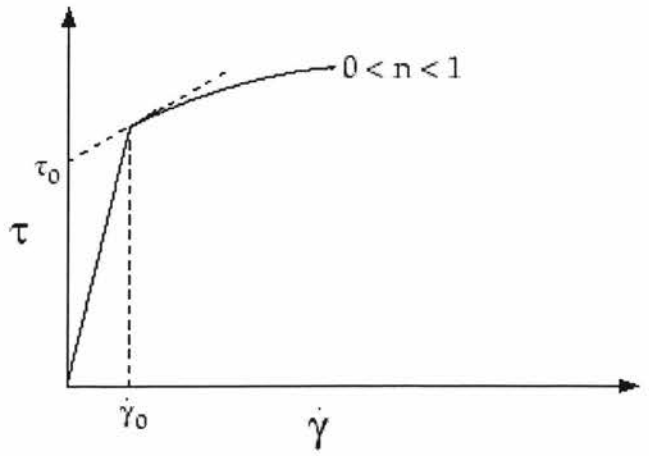

Figure 4.3 Shear stress (τ) versus shear rate ($\dot{\gamma}$) plot for the Herschel-Bulkley model

Therefore, the xanthan gum fluid rheologies were modeled as a Herschel-Bulkley fluid based on the parameters listed in table 4.1.

Table 4.1 Fluid rheological parameters

Xanthan gum Concentration	Consistency index, K(Pa.s^n)	Power-law index, n	Yield stress, τ_y (Pa)	μ_0 (Pa.s)	Density kg/ m^3
0.5%	3	0.11	1.789	13.30	997.36
1.0%	8	0.12	5.254	22.61	991.80
1.5%	14	0.14	7.455	32.36	989.76

4.10.4 Boundary Conditions

The most common boundary conditions that occur when solving the laminar flows are:

4.10.4.1 Inlet

At inlet boundaries, velocity (or pressure), and composition of the incoming fluid stream are known. All other scalar, except pressure, can be set equal to input values. When velocity is known, the boundary condition for pressure is not required since the pressure-velocity coupling schemes depend on the pressure gradient and not on the absolute pressure. CFD codes generally fix the absolute pressure at one inlet node (atmospheric pressure for open tanks), and set the pressure correction to zero at that node (Ferziger and Peric, 1995; Versteeg and Malalasekara, 2007).

4.10.4.2 Outlet

Surface normal gradients for all the variables are zero except pressure (Ferziger and Peric, 1995; Versteeg and Malalasekara, 2007). This boundary condition means that the conditions downstream of the outlet boundary should not influence the flow within the solution domain. For pressure boundary condition, static pressure (atmospheric pressure for open tanks) is defined.

4.10.4.3 Symmetry plane

A symmetry surface is one across which the flux of all quantities is zero. The tank surface is considered as a symmetry surface. At symmetry surface the normal velocity and concentration are set equal to zero to ensure that there is no connective or diffusive flux across the tank surface (Ferziger and Peric, 1995; Versteeg & Malalasekera, 2007; Ranade, 2002).

4.10.4.4 Impermeable no-slip walls

At the impermeable wall boundaries, usually a no slip boundary condition is used. For velocity, this boundary condition implies that the traverse fluid velocity is equal to that of the surface and setting the normal velocity equal to zero. For species concentration, a zero flux boundary condition is applied at the wall of the vessel, implying that the wall is impermeable and that the species cannot penetrate the wall (Versteeg & Malalasekera, 2007; Ferziger and Peric, 1995; Ranade, 2002). The convection flux through the wall is zero.

4.10.5 Grid generation

In grid generation the flow domain was discretized into small control volumes or cells. The conservation equations for the entire domain were solved in each cell. Gambit was used as a geometry and grid generator in MixSim package for generating tetrahedral meshes [Figure 4.4(a), 4.4(b)].

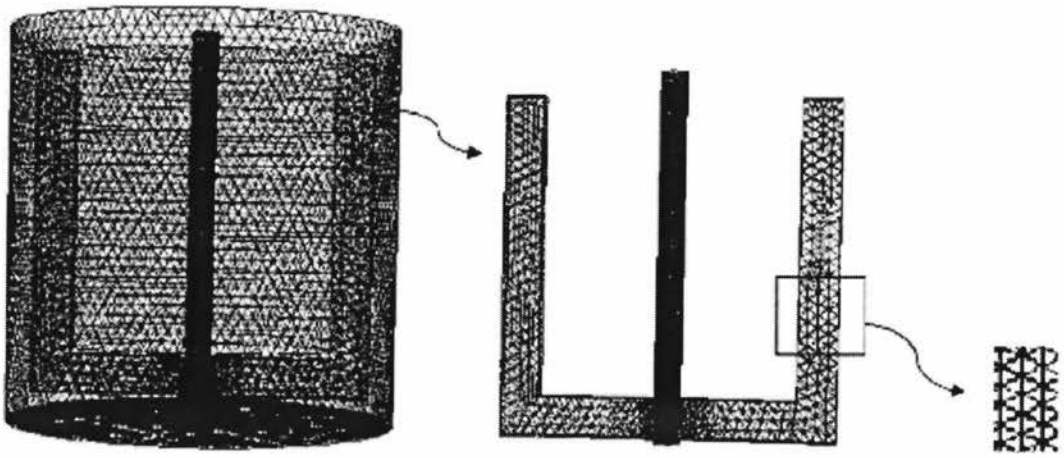

Figure 4.4 (a) Numerical grids for a tank with a two-blade anchor impeller

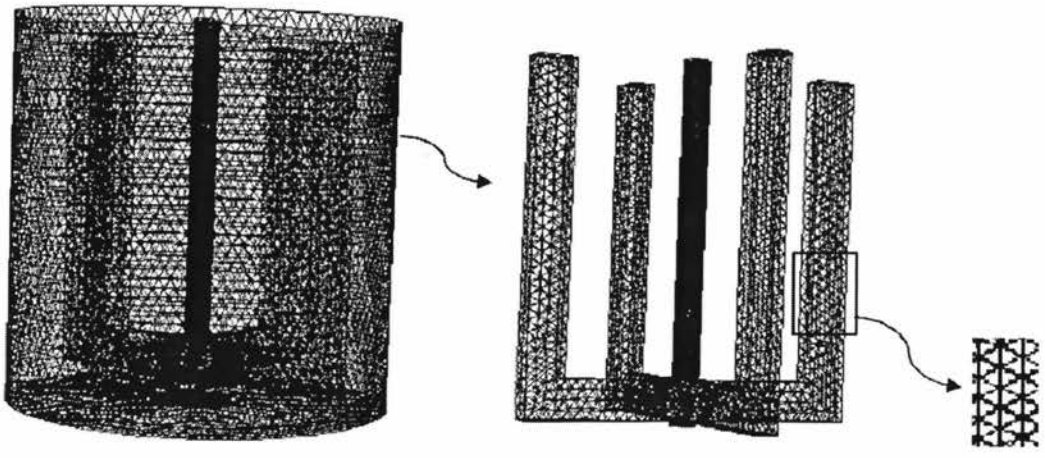

Figure 4.4 (b) Numerical grids for a tank with a four-blade anchor impeller

The grid quality is an important aspect for CFD. Good quality grids require proper resolution, smoothness and low skewness. The finer meshes were required near the vessel wall and for the impeller region where the velocity gradient were high. If the grids were too fine the computational time would be very high and if it were too coarse the results would not be accurate. Therefore it would be very essential to optimize the number of grids required.

The quality of the grid has been checked using a grid histogram for the equiangle skewness, Q (Figure 4.5). The grid quality was assessed using skewness of the cells. It is an indication of how close cells are to a perfect equilateral element. Zero value of skewness describes perfect equilateral and that of one describes poorly shaped element. 96% of the cells generated had a skewness smaller than 0.6, indicating an excellent mesh formation (Fluent, 2006).

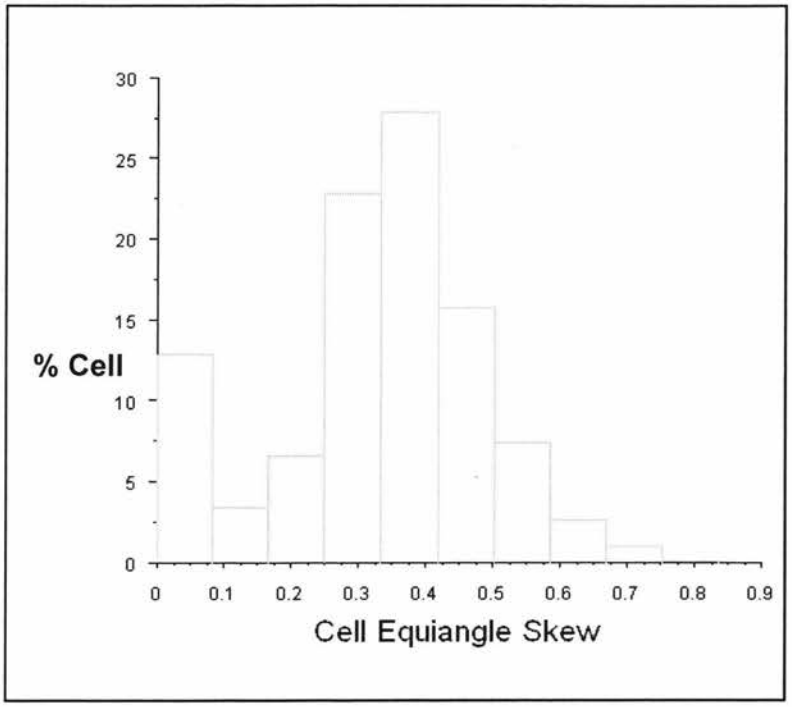

Figure 4.5 Grid Histogram

4.10.6 Grid Independence

The grid independency study was performed to insure that the numbers of grids used were sufficient to capture most of the important features of the flow. For grid independency, four different grids were generated (40765, 81191, 159824, and 318546) in the laminar region for Reynolds number, Re = 8.42. It was observed that there was not a significant difference in the calculated power number for all four grids (Table 4.2).

Table 4.2 Power number for 1.5% xanthan gum solution (50 rpm) using different mesh number

Cells	Power (W)	Power Number (Po)
40,765	0.287212	16.32801
81,191	0.287684	16.35486
159,824	0.292741	16.64239
318,546	0.293637	16.69333

A further requirement was that the additional grids did not change the calculated velocity profiles in regions of high-velocity gradients. Figure 4.6(a), 4.6(b) and 4.6(c) show the radial, tangential and axial velocity profiles as functions of horizontal and vertical positions, where large transport gradients in the flow exist.

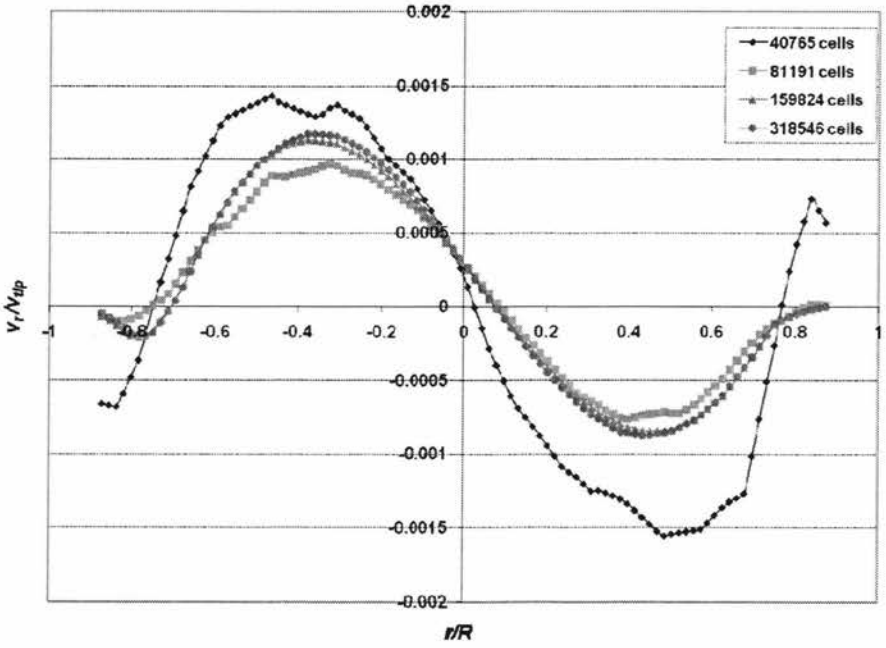

Figure 4.6 (a) Effect of grid numbers on radial velocity (x = 0.03, y = - 0.06245 to 0.06245, z = 0.016145 m)

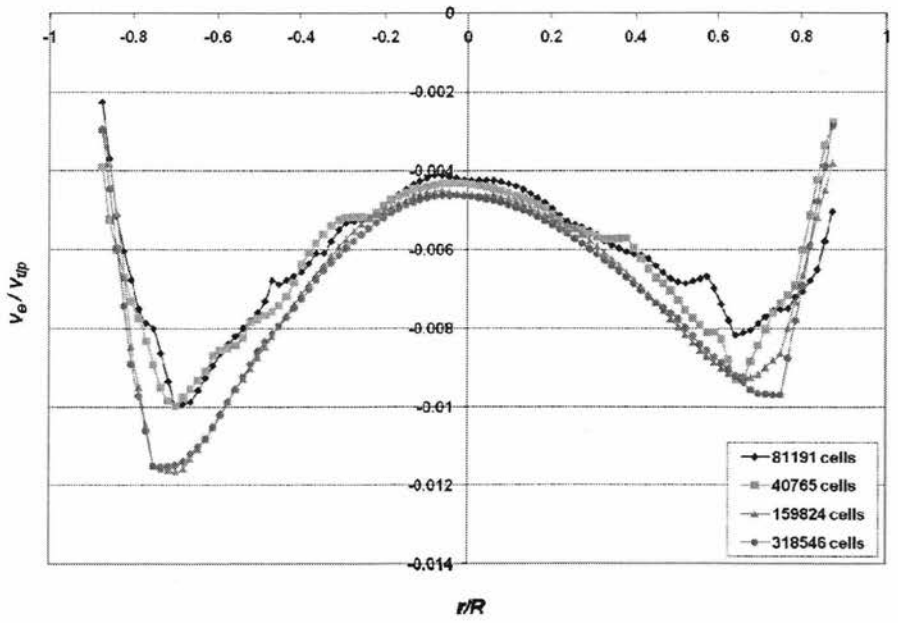

Figure 4.6 (b) Effect of grid numbers on tangential velocity (x = 0.015, y = - 0.07145 to 0.07145, z = 0.016145 m)

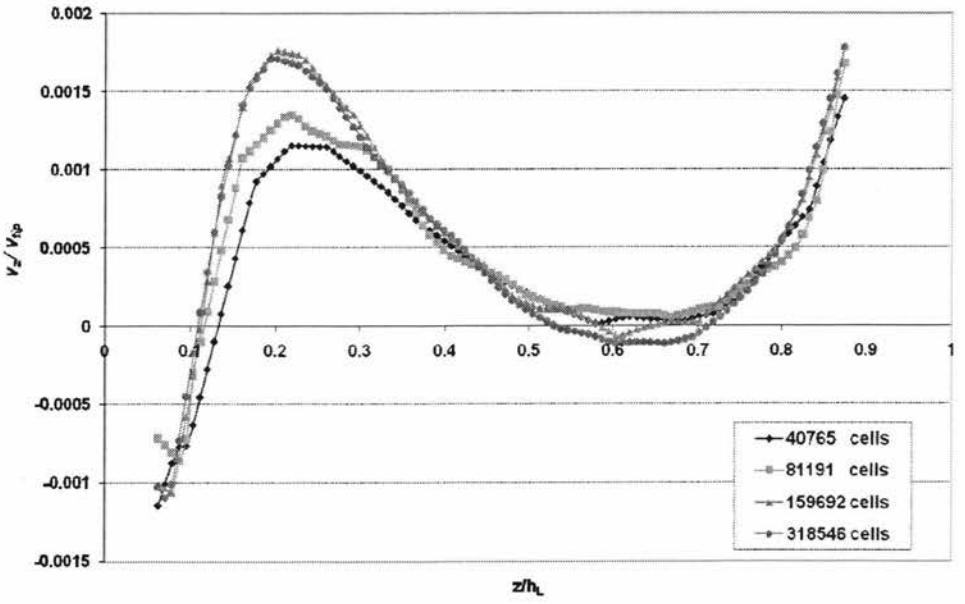

Figure 4.6 (c) Effect of grid numbers on axial velocity (x = 0.015, y = 0.055305 to 0.06245, z = 0.009 to 0.1249 m)

It is observed from figure 4.6 that the two largest grids (159824 and 318546) give very similar profiles of all three velocities while the velocity profiles for 40765 and 81191 grids are clearly different from the fine meshes.

The discrepancy between velocity profiles can be qualified in terms of the root-mean-square (*RMS*) deviation (Arratia *et al.*, 2006):

$$RMS = \frac{\left[\frac{1}{n}\sum_{1}^{n}(u_1 - u_2)^2\right]^{1/2}}{\left[\frac{1}{n}\sum_{1}^{n}(u_2)^2\right]^{1/2}} \tag{4.41}$$

where n is the number of nodes in the velocity field. Table 4.3 shows the *RMS* values among four different grids.

Table 4.3 RMS value for 1.5% agitated at 50 rpm using different mesh number

Cells	40,765 and 81,191	81,191 and 159,824	159,824 and 318546
Radial velocity on horizontal position [Figure 4(a)]	65.6%	15.5%	4.3%
Tangential velocity on horizontal position [Figure 4(b)]	10.3%	14.75%	3.9%
Axial velocity on axial position [Figure 4(c)]	22.1%	22.7%	7.9%

The difference between the tangential and radial (impeller is tangential- radial flow impeller) velocity profiles for the 159824 and 318546 grid simulations is less than 5%, therefore 159,824 control volume cells were considered suitable for this problem and were used for all CFD simulations.

A modification was made on the previous model and numbers of the blade for anchor impeller were changed from two-blades to four-blades. Gambit 2.2.30 (Fluent Inc., USA) was again utilized to discretize the flow domain with an unstructured tetrahedral mesh consisting of 165,994 cells shown in figure 4.4(b).

4.10.7 Performing Numerical Calculations

Once the model is defined and grids are generated the solutions can be started. The numerical scheme selected in Fluent was the segregated solver. Using this approach, the governing equations are solved sequentially.

In the segregated algorithm, the individual governing equations for the solution variables are solved one after another (Fluent, 2006). Each governing equation, while being solved, is segregated from other equations. Therefore, the segregated algorithm is memory-efficient, but relatively slow. All iterations consist of the following steps (Fluent, 2006):

- Update fluid properties
- Solve the momentum equations, one after another, using the recently updated values of pressure and face mass fluxes
- Solve the pressure correction equation using the recently obtained velocity field and the mass-flux
- Correct face mass fluxes, pressure, and the velocity field using the pressure correction obtained from above step
- Check for the convergence

All these steps are continued until the convergence criteria are reached. The governing equations are discretized using the finite-volume method. The convective terms of the governing equations are discretized using the second-order upwind differencing scheme. A first order upwind scheme was initially used for the momentum equations for 50 iterations and when the convergence ($<10^{-2}$) was reached; the solution was used as the initial conditions for the calculation of a second order upwind scheme. It is important to note that this scheme is more accurate than first order and power law scheme (Aubin et al., 2004) and more stable than QUICK scheme. The pressure interpolation scheme selected was also second order. The pressure-velocity coupling method used was SIMPLE.

Convergence was monitored (Figure 4.7) dynamically by checking the residuals for each conservation variable: mass, x-velocity, y-velocity, and z-velocity. Simulations were considered converged when the scaled residuals dropped below 10^{-5}.The under-relaxation factors for momentum and pressure were set at 0.3 and 0.7 (default) respectively.

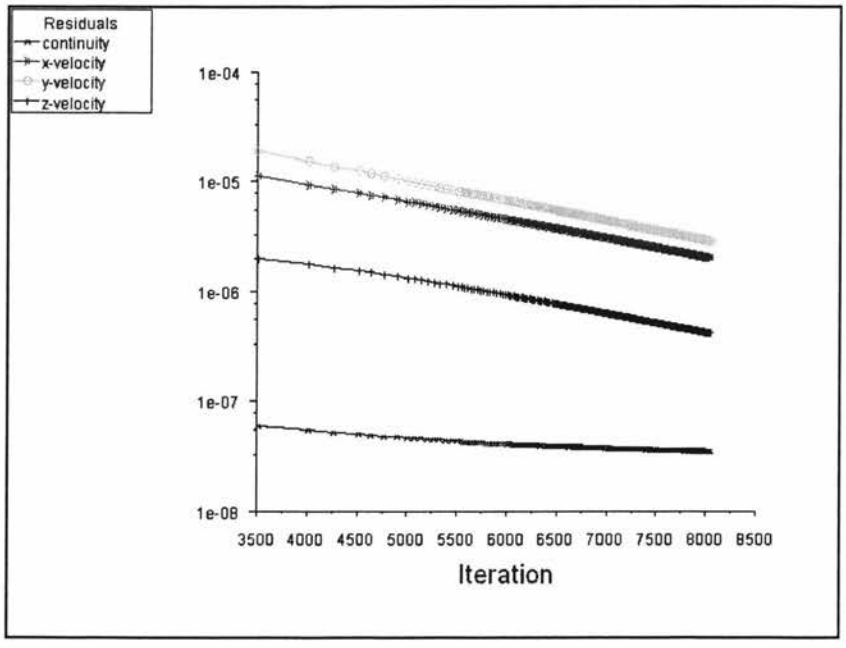

Figure 4.7 Typical convergence history of the scaled residuals

A no-slip boundary condition is imposed on all walls. The free liquid surface is modeled with no vortex, flux and stress conditions. The simulations were considered converged when the scaled residuals for each transport equations were reached below 10^{-5}. Problem requires around 7000-9000 iterations for convergence. The computations were performed on a 3.60 GHz Intel Pentium IV CPU having 2.00 GB of RAM. The CPU time varied between 6 and 8 hours.

4.10.8 Species transport to Investigate Dynamics of Mixing Process

In order to simulate the mixing time, once the flow fields had been calculated, the calculations were switched to transient and the simulations for the tracer homogenization were performed. The tracer, having the same physical properties as the bulk fluid, was added 6cm under the liquid surface. The virtual probes were placed at four points (Figure 4.8).

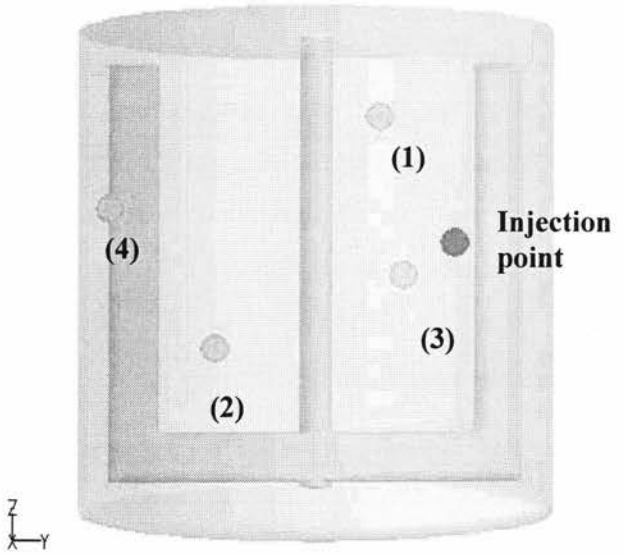

Figure 4.8 Location of the injection point and monitoring locations known as probes; all locations are specified by their x, y, z coordinates in meter. Injection point: 0.02, 0.04, 0.08; Probes location: (1): -0.02, 0.02, 0.12; (2): 0.03,-0.03, 0.05; (3): -0.06, 0.03, 0.07; and (4): 0.03, -0.06, 0.09

The mass fraction of tracer in the vessel was recorded during the time-dependent simulation. The mixing time (t_{95}) was defined as the time needed for the normalized tracer concentrations at all four monitoring points to reach 95% of the steady state value. To model the flow of the tracer, the following species transport equation was solved:

$$\frac{\partial}{\partial t}(\rho w) + \nabla.(\rho \bar{v} w_t) = \nabla.\rho D_m \nabla \phi \tag{4.42}$$

where w_t is the local mass fraction of the tracer, $\bar{v}$ is the mean velocity vector, ρ is the fluid density and D_m is the molecular diffusivity of the tracer in the mixture which is assumed to be 10^{-9} as a typical value of liquids (Montante et al., 2005)

The influence of the time step on the tracer concentration profiles was checked by performing the simulations with time steps of 0.1 and 1s. Although the differences can be observed in the traced concentration at the beginning of its dispersion inside the vessel, the predicted mixing times (t_{95}) were almost the same for 0.1 and 1s. (Refer Table 4.4 and Figure 4.9 (a), 4.9(b)). On the other hand, the computational time required to reach the homogenous level using the time step of 0.1s was more than 12 h while the computational time required to achieve homogeneity using the time step of 1s was 3-5 h. Therefore, the time step used for all simulations was set to 1s. The value of species residual for a converged solution was set equal to 10^{-5}. The CPU time was varied between 3-5 h.

Table 4.4 Mixing time comparison for 1.5% xanthan solution agitated at 50 rpm

Time step (s)	t_{95} **(min)**
0.1	9
1	8.53

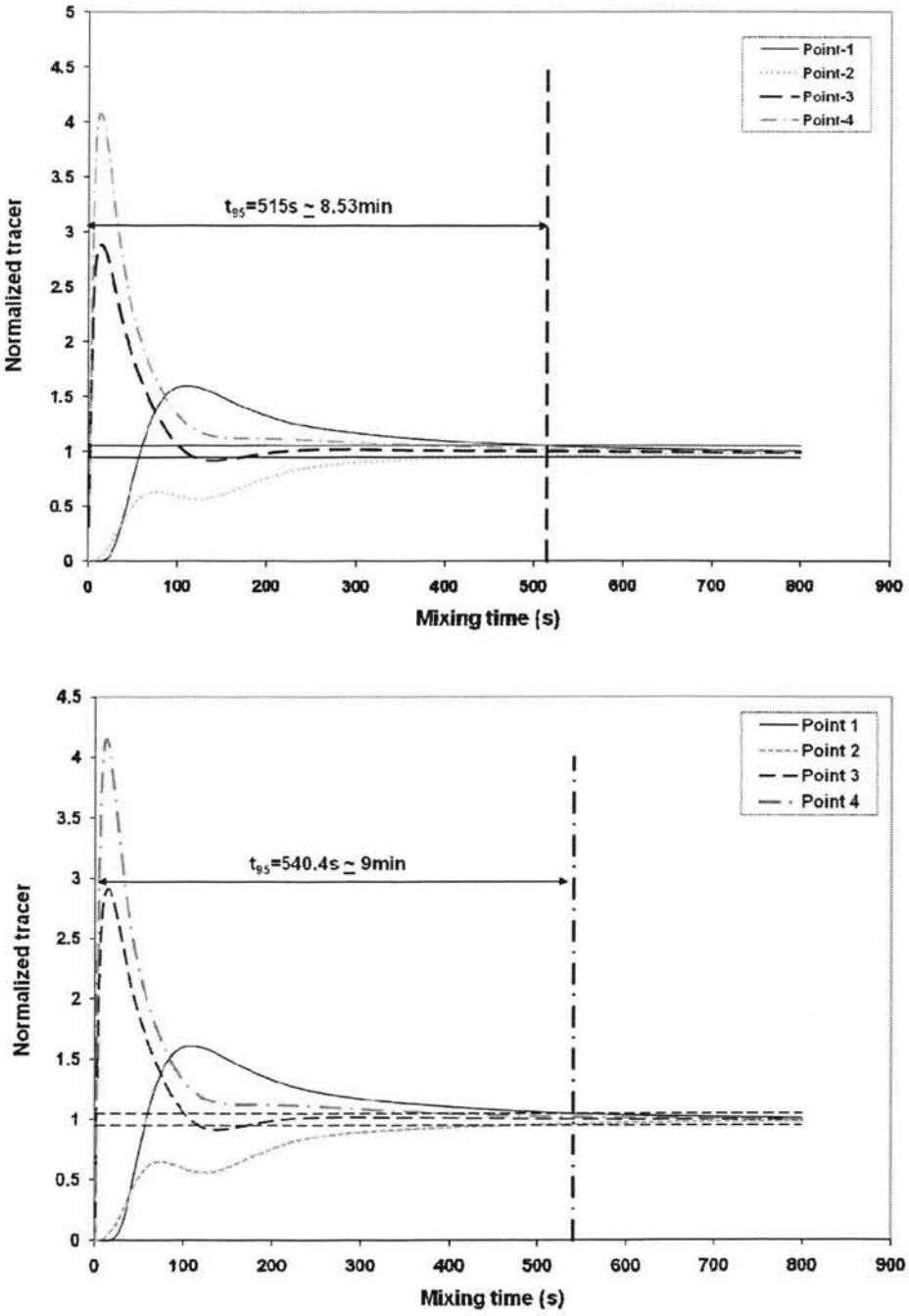

Figure 4.9 Comparison of normalized tracer concentration versus mixing time (1.5% xanthan gum solution, 50 rpm): (a). Time step: 0.1 s (b) Time step size: 1.0 s, For monitoring point 1: -0.02, 0.02, 0.12; monitoring point 2: 0.03,-0.03, 0.05; monitoring point 3: -0.06, 0.03, 0.07; and monitoring point 4: 0.03, -0.06, 0.09

5. RESULTS AND DISCUSSIONS

5.1 Power Consumption

In this study the performance of an anchor impeller was evaluated on the basis of power consumption and mixing time. The power consumption is defined as the energy transferred from impeller to solution per unit time. In stirred tank, the power consumption depends on the fluid rheology, flow regime, impeller and tank geometry. Power input and power number to the impeller were estimated using the following equations:

$$P = 2\pi NM \tag{5.1}$$

$$P_o = \frac{P}{\rho d^5 N^3} \tag{5.2}$$

where P_o is the power number and ρ is the density of the fluid.

The Reynolds number for non-Newtonian fluids using Metzner-Otto (1957) concept of apparent viscosity can be estimated as per the following:

$$R_e = \frac{\rho N d^2}{\eta} \tag{5.3}$$

Apparent viscosity η is defined as:

$$\eta = \tau / \dot{\gamma}_a \tag{5.4}$$

According to Metzner-Otto relationship the average shear rate is given by:

$$\dot{\gamma}_a = k_s N \tag{5.5}$$

where $\dot{\gamma}_a$ is an average shear rate and k_s is a Metzner-Otto constant.

Using equations 5.3, 5.4 and 5.5 we get the following equation for Reynolds number:

$$R_e = \frac{\rho N d^2}{\eta} = \frac{\rho N d^2}{\tau/\dot{\gamma}_a} = \frac{\rho N d^2}{\tau/k_s.N} = \frac{\rho N d^2.k_s}{\tau} \tag{5.6}$$

Shear stress defined by Herschel Bulkley model (Equation 3.2) was inserted in the Equation 5.6 to obtain the expression for Reynolds number:

$$R_e = \frac{\rho N d^2.k_s}{\left[\tau_y + K(k_s.N)^n\right]} \tag{5.7}$$

A literature review on k_s shows different constant values and correlations (Beckner and Smith, 1966; Calderbank and Moo- Young, 1961; Sestak *et al.*, 1986; Rieger and Novak, 1973; and Shamlou and Edwards, 1989). Since the exact value of k_s is not known for anchor impeller, the correlation of Shamlou and Edwards (1989), evaluated by Murthy and Jayanti (2003) was applied to find the k_s. They reported that k_s is a function of the geometric parameters of impeller and not of the fluid rheology.

$$k_s = 33 - 172\left(\frac{c}{D}\right) \tag{5.8}$$

where c is the impeller clearance from wall and D is the tank diameter. The parameter k_s is a weak function of impeller type. The value of k_s used here is 22.17.

To validate the model, the CFD power consumptions results were compared with the experimental power input data for 0.5%, 1.0% and 1.5% xanthan gum solutions (Figure 5.1(a), 5.1 (b), 5.1 (c)).

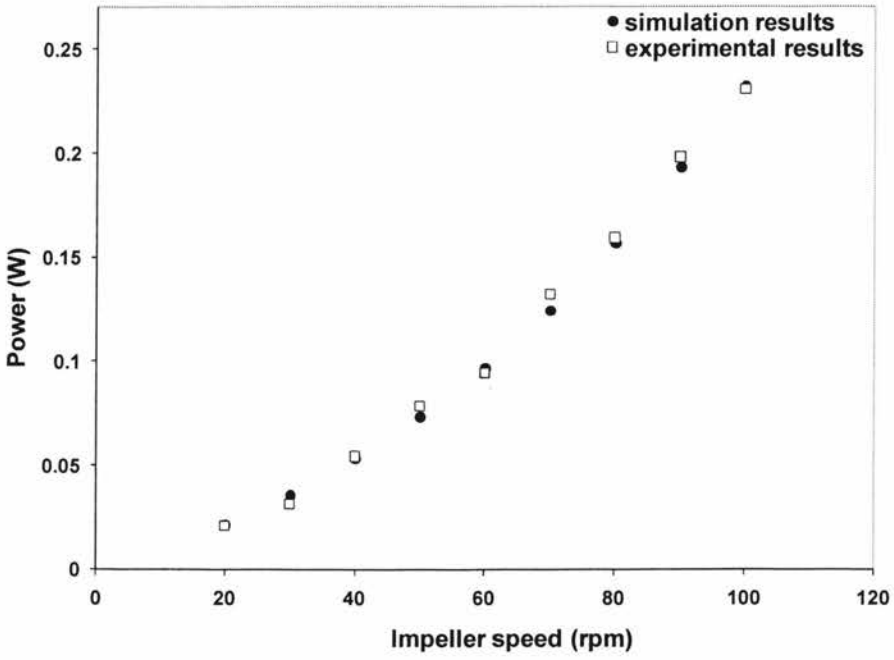

Figure 5.1 (a) Power consumption versus impeller revolution speed for two-blade anchor impeller (0.5% xanthan gum solution)

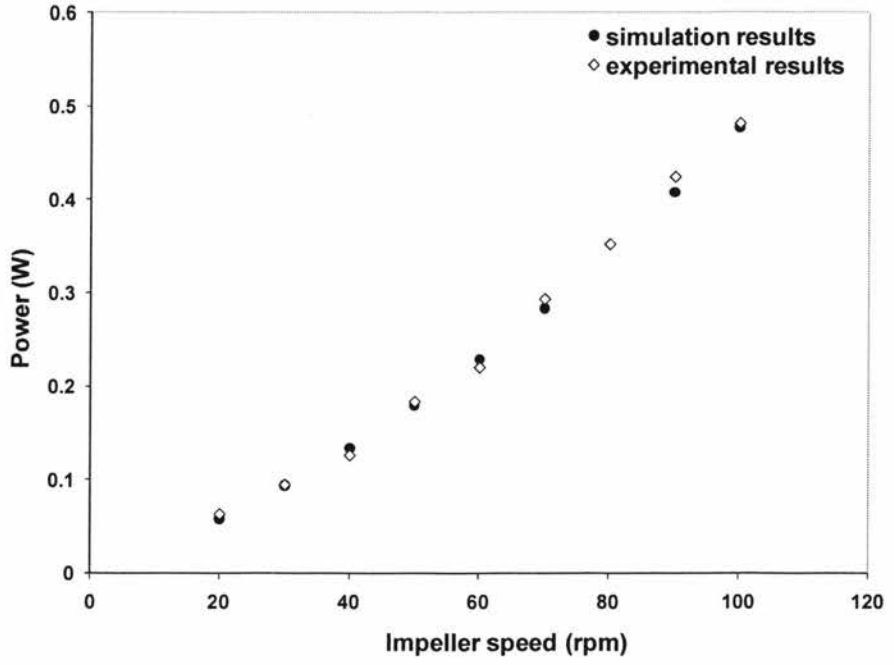

Figure 5.1 (b) Power consumption versus impeller revolution speed for two-blade anchor impeller (1.0% xanthan gum solution)

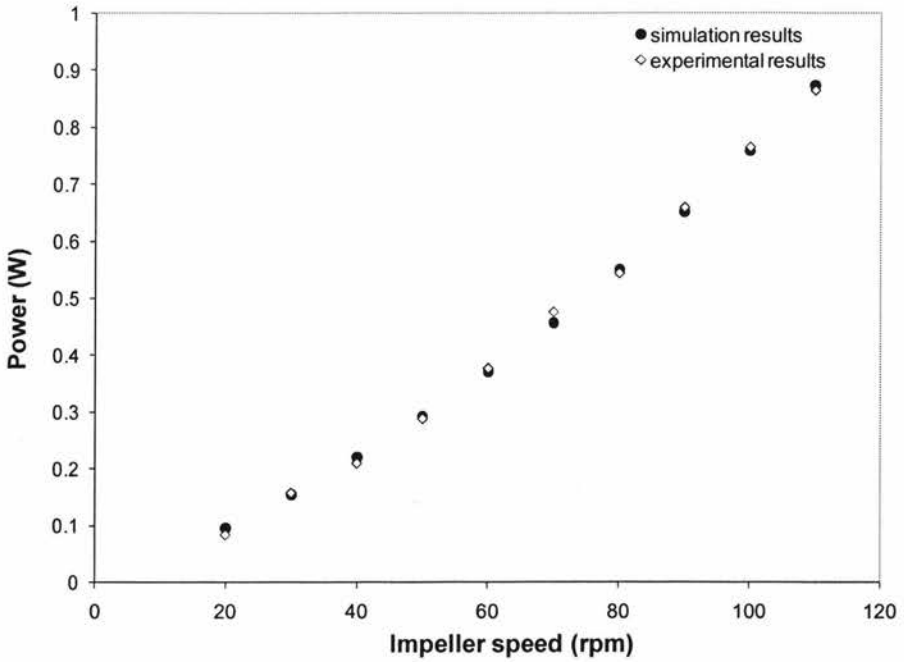

Figure 5.1 (c) Power consumption versus impeller revolution speed for two-blade anchor impeller (1.5% xanthan gum solution)

It can be observed from figures 5.1(a), 5.1 (b), 5.1 (c) that power consumption increases with an increase in the impeller speed for both CFD and experimental work. The CFD results were found in good agreement with the experimental results.

Figure 5.2(a), 5.2 (b), 5.2 (c) shows the power consumption versus impeller speed graphs for two- and four-blade impeller. It shows that when impeller speed increases the power consumption also increases. For a four-blade impeller the power consumption is higher as compared to the two-blade impeller. The reason for this is more torque is needed for the four-blade impeller rotation.

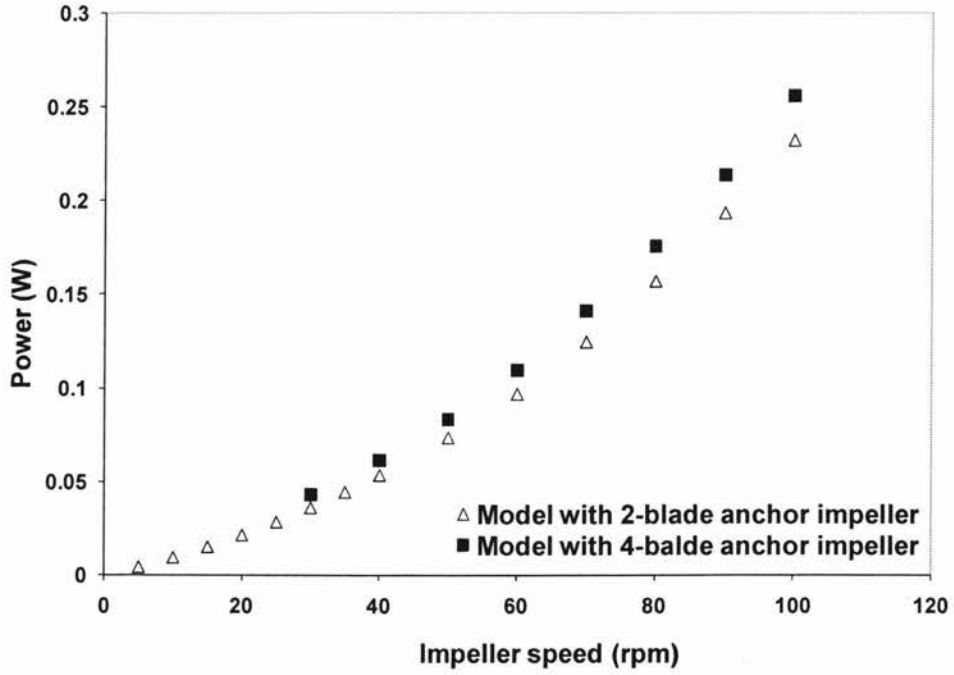

Figure 5.2 (a) Simulated power consumption versus impeller speed (0.5% xanthan gum solution)

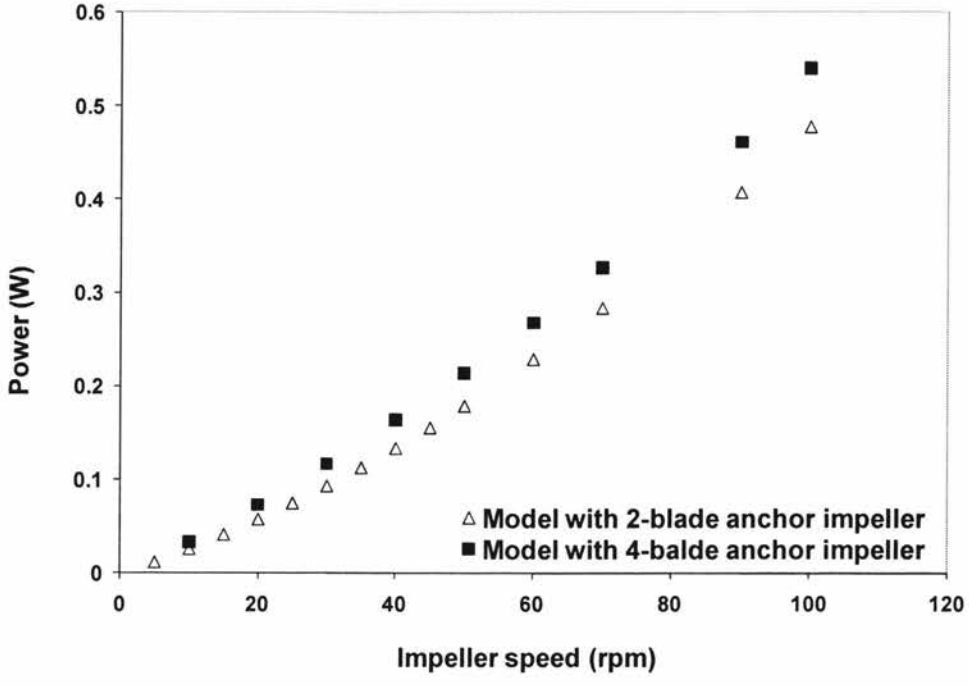

Figure 5.2 (b) Simulated power consumption versus impeller speed (1.0% xanthan gum solution)

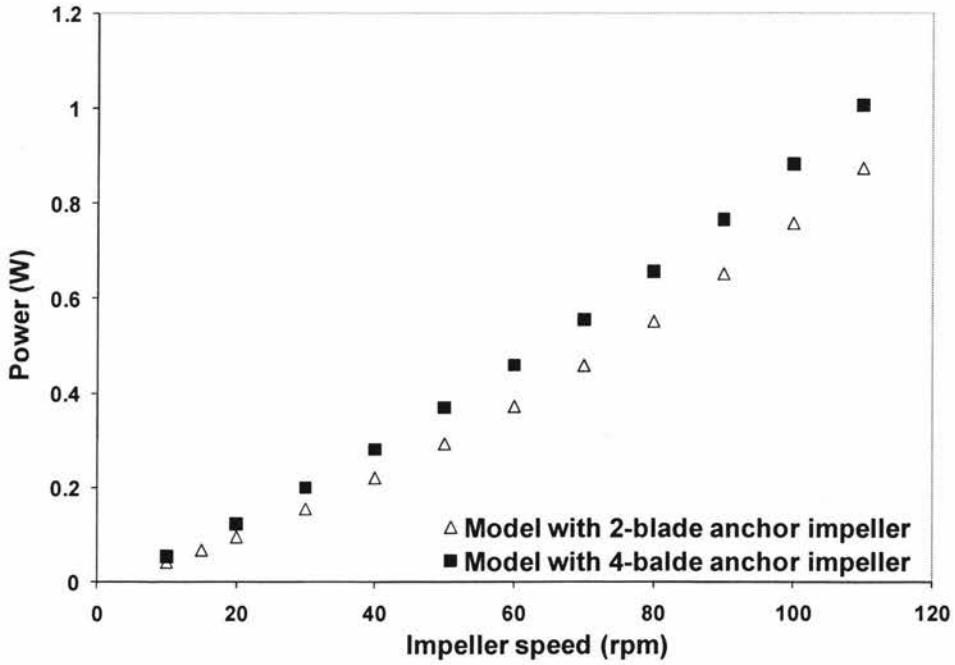

Figure 5.2 (c) Simulated power consumption versus impeller speed (1.5% xanthan gum solution)

Figure 5.3(a), 5.3 (b) shows the simulated power consumption for two- and four-blades anchor impeller respectively. It shows the effect of rheology on power consumption. It is observed that when the concentration of the fluid increases the power consumption also increases. Power consumption for 1.5% concentration is higher than 0.5% and 1.0% xanthan gum fluid for the same impeller speed. This is due to rise in the yield-stress of xanthan gum solution when the concentration increases. Therefore, more impeller torque is required to keep the entire fluid in motion. Table 4.1 (Chapter 4) reveals the effect of yield-stress on xanthan gum solution for various concentrations. When the viscosity of the fluid increases the power consumption also increases. The 1.5% xanthan gum solution is more viscous as compared to 1.0% and 0.5% solution.

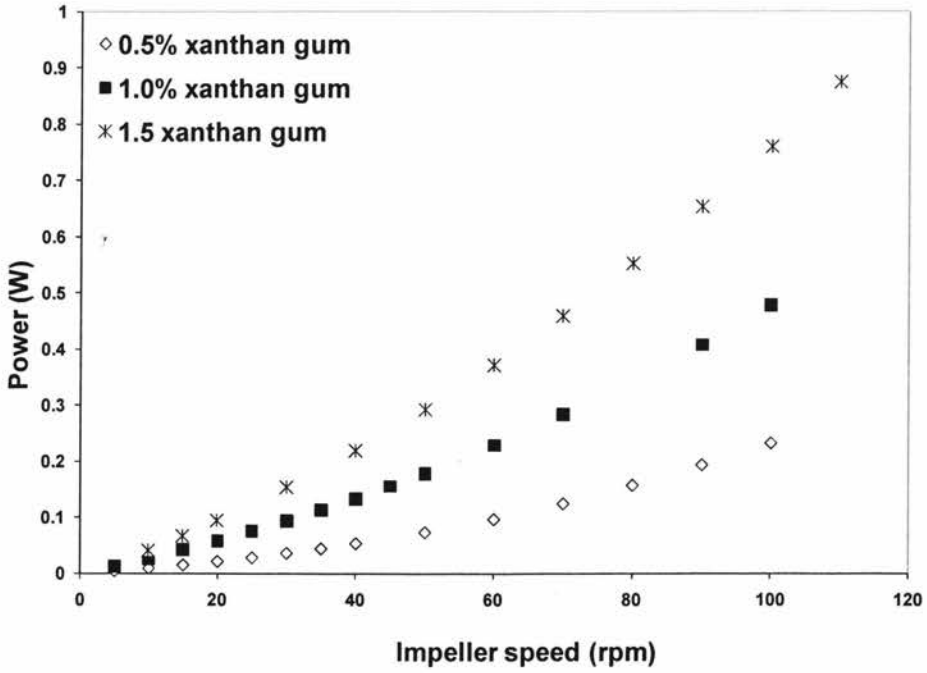

Figure 5.3 (a) Simulated power consumption versus impeller speed for two-blade anchor impeller

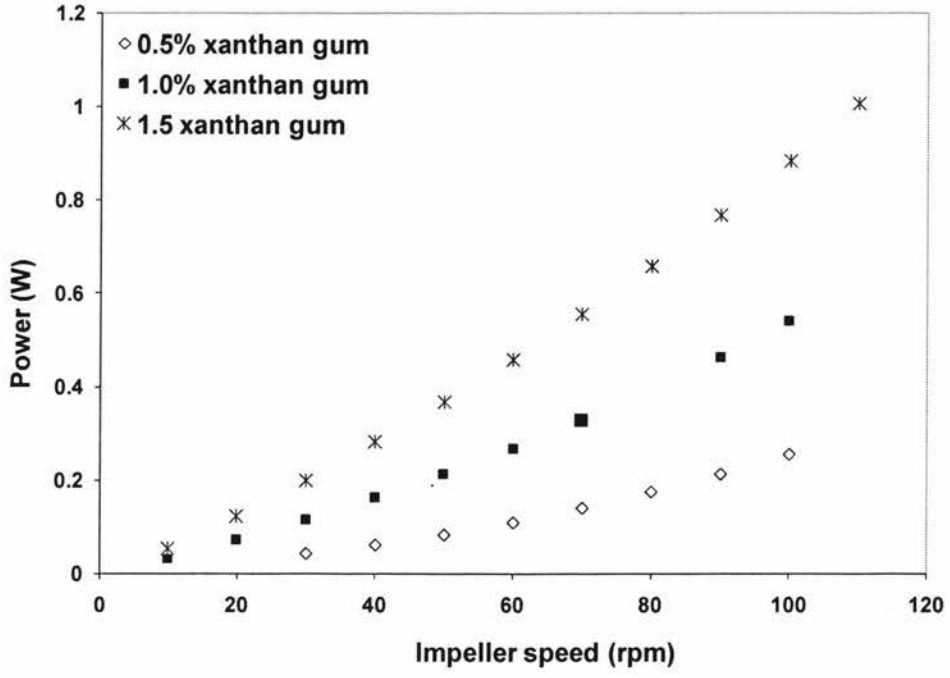

Figure 5.3 (b) Simulated power consumption versus impeller speed for four-blade anchor impeller

Figure 5.4(a), 5.4 (b), 5.4 (c) shows the power number (P_o) versus Reynolds number (Re) plot for mixing of xanthan gum solution. The trend in the power number curves for all concentrations were similar to typical power curves found in the literature. The power number data falls along the line of slope -1 at low Reynolds number ($Re < 10$), which is in good agreement with that reported in the literature (Lee et al., 1957; Nienow et al., 2005; Pakzad et al., 2008) indicating that the flow is laminar. In the laminar region $P_o \propto \mathrm{Re}^{-1}$ and the power input depends mainly on the viscosity (Paul et al., 2004). At $Re > 10$, the data start moving away from the line of slope -1 slowly. This is due to fact that in the transitional region the power number changes slightly with the Reynolds numbers and in the turbulence region the power number is independent of the Reynolds number and remains almost constant with increase in the Reynolds number (Harnby et al., 1997; Chhabra and Richardson, 1999). From figure 5.4(c) it is observed that CFD results are in good agreement with the experimental results.

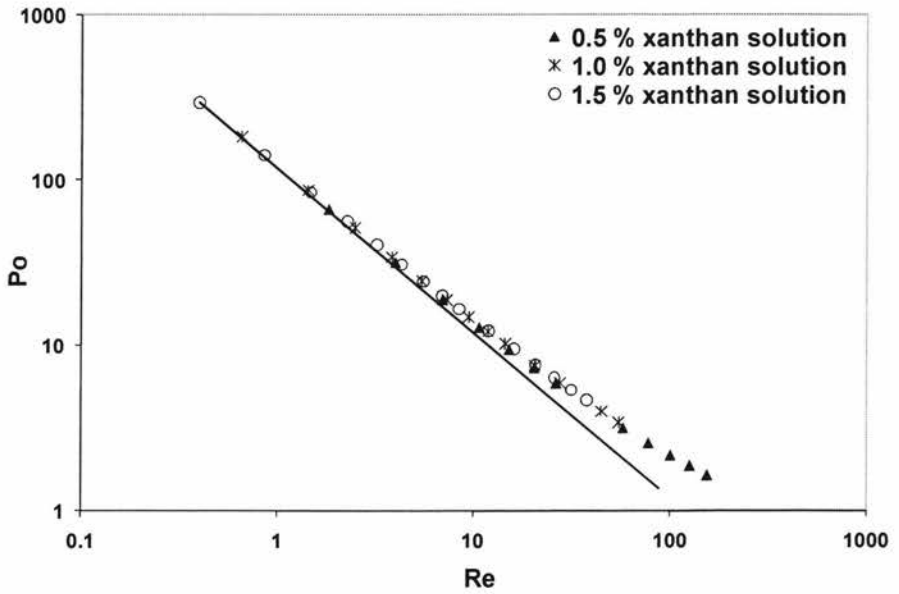

Figure 5.4 (a) CFD Power number versus Reynolds number for two blade anchor impeller

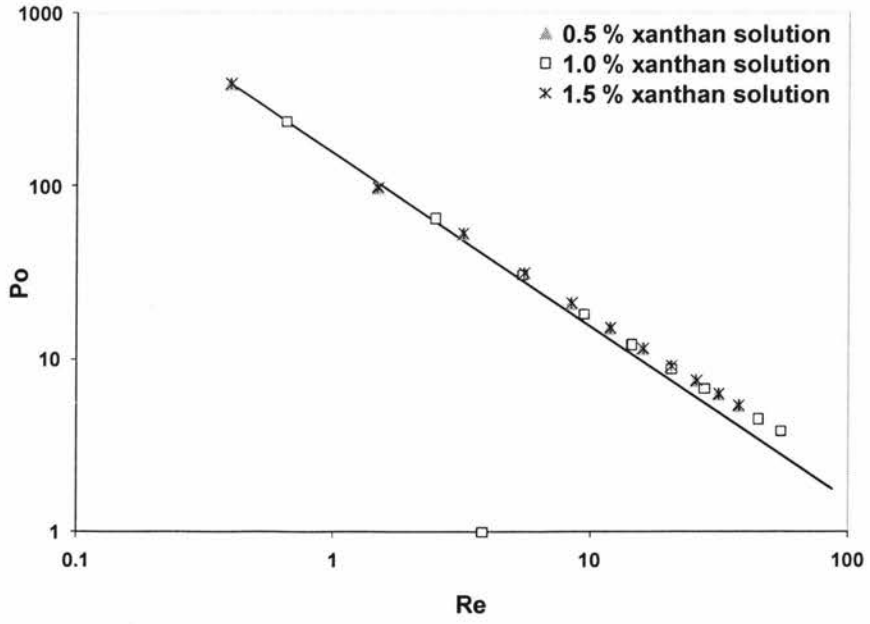

Figure 5.4 (b) CFD Power number versus Reynolds number for four blade anchor impeller

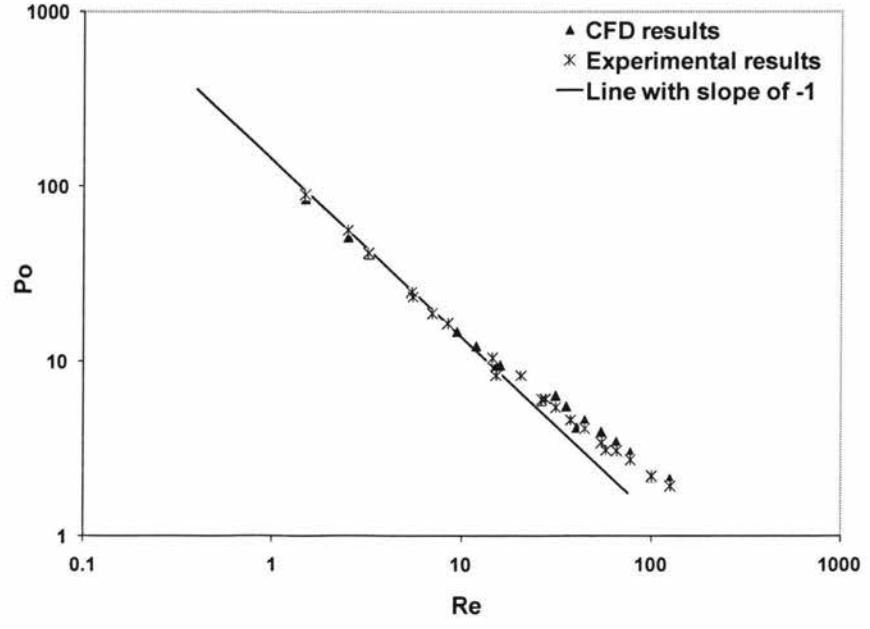

Figure 5.4 (c) Power number versus Reynolds number for 1.5% xanthan gum agitated with two blade anchor impeller

5.2 Mixing time

The key factor that determines the effectiveness of the mixing operation is mixing time or blending time, which is often used to evaluate quantitatively the mixing performance of stirred tanks. Mixing time is defined as the time required toachieve the desired uniformity of the tracer concentration in entire vessel. This specific degree of uniformity is usually the expected equilibrium concentration of the tracer. If there is no tracer initially present in the tank, then a mixing time (t_m) can be defined as the time from tracer injection to time when we get,

$$m = \frac{|C - C_\infty|}{C_\infty} \tag{5.9}$$

Here m is the maximum acceptable deviation from homogeneous condition, C is the tracer concentration and C_∞ is the mean tracer concentration at time equal to infinity (Harnby et al., 1997). The mixing time, t_{95} is defined as the time taken for the tracer concentration to reach 95% of steady state value i.e the time from tracer injection to the time when the value of m is 0.05. In figure 4.9 the lower boundary is average (steady state) minus 5% of average value and the upper boundary represents the average plus 5% of average value. The numerical simulations were performed to understand the effect of impeller rotational speed, number of blades, clearance, width and rheological properties of the solution on the mixing time. Three separate xanthan gum solutions (0.5%, 1.0% and 1.5%) with different rheological properties were used for this study. The mixing times were obtained from the simulated normalized tracer concentration profiles. All the simulations gave a reasonable trend of the mixing time as a function of impeller speed as shown in figure 5.5(a), 5.5(b), 5.5(b). It is obvious from figure 5.5 that when the impeller speed increases, the mixing time decreases. It was also observed that the mixing time for four-blade is less than that with the two-blade anchor impeller as expected.

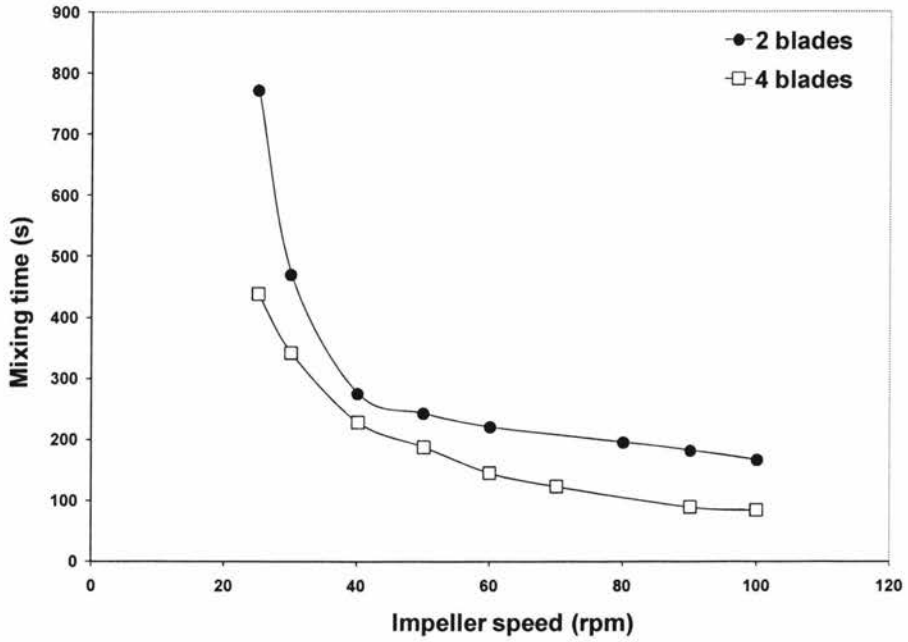

Figure 5.5 (a) Mixing time as a function of the impeller speed for 0.5% xanthan solution agitated by anchor impeller

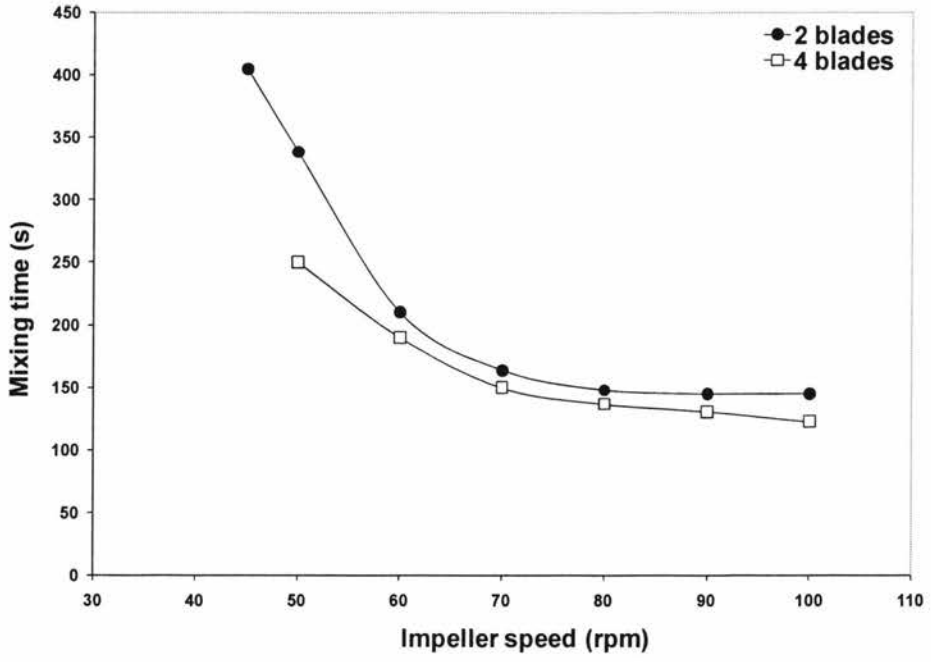

Figure 5.5 (b) Mixing time as a function of the impeller speed for 1.0% xanthan solution agitated by anchor impeller.

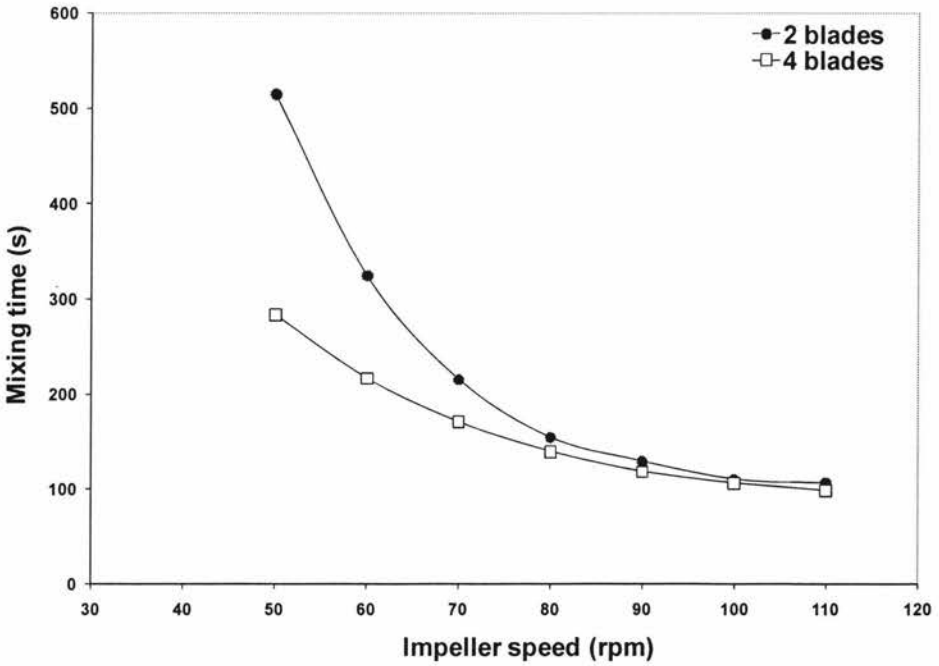

Figure 5.5 (c) Mixing time as a function of the impeller speed for 1.5% xanthan solution agitated by anchor impeller.

To understand the results better, two measures from the literature were used to evaluate the efficiency of close clearance agitators. First is the mixing time number and second is the specific power of mixer. The mixing time number, K_m, also known as dimensionless mixing time, is defined as:

$$K_m = Nt_m \tag{5.10}$$

Here N is the impeller rotational speed and t_m is the mixing time. The mixing time is constant for a specific geometry of close clearance impeller in laminar flow regime (Hoogendoorn and Den Hartog, 1967; Coyle et al., 1970; Coulson et al., 1990; Tatterson, 1991). The plot of Nt_m as a function of Reynolds number is shown in Figure 5.6(a), 5.6(b), 5.6(c).

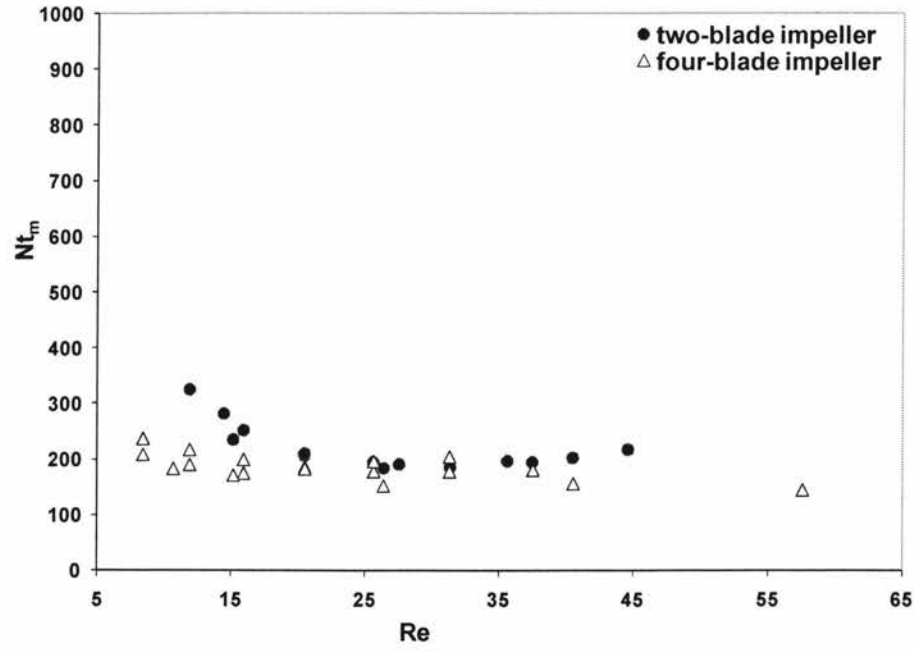

Figure 5.6 (a) Mixing time number (Nt_m) versus Reynolds number plot for 1.5% xanthan gum agitated with two-blade anchor

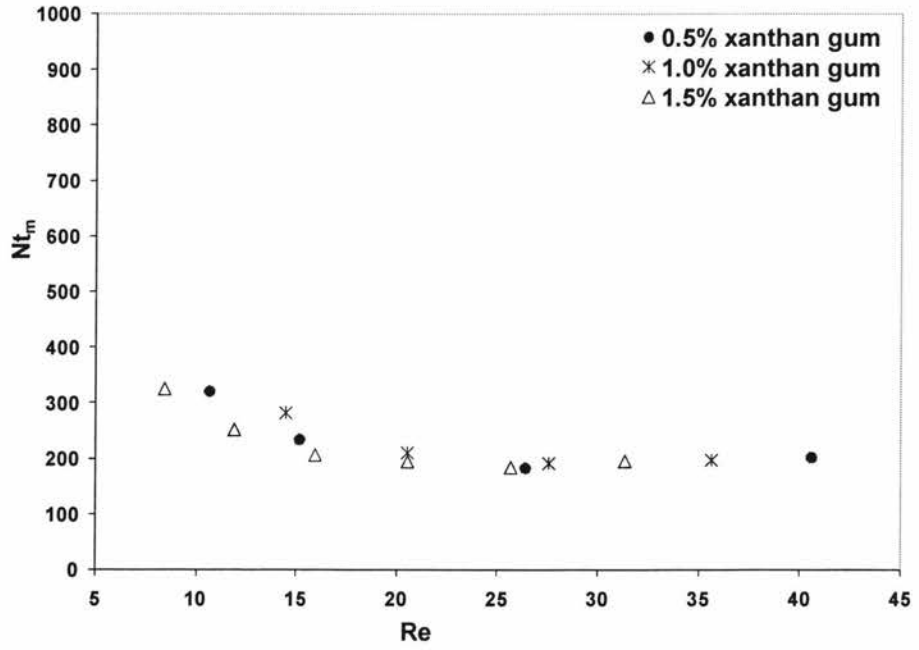

Figure 5.6 (b) Mixing time number (Nt_m) versus Reynolds number plot for two-blade anchor

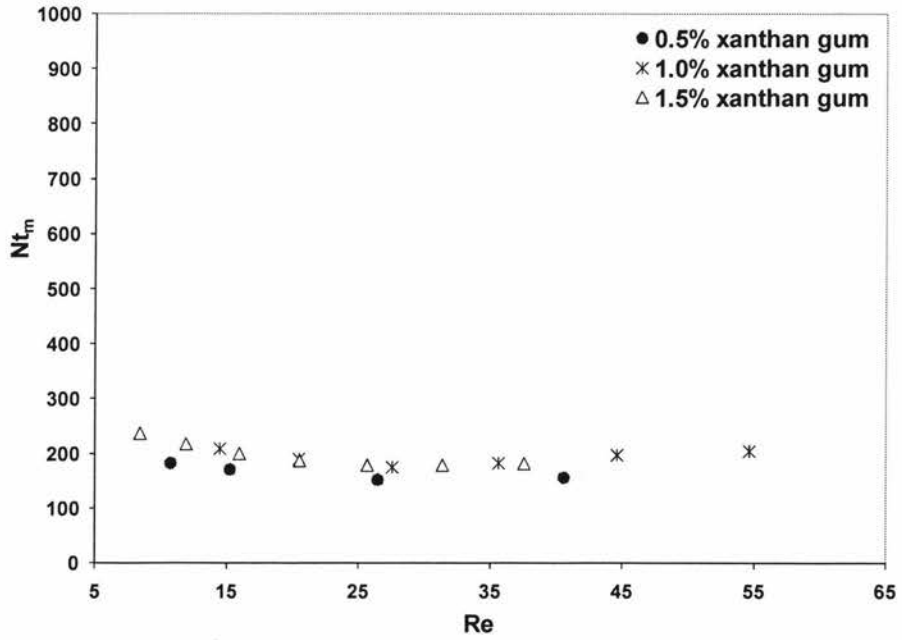

Figure 5.6 (c) Mixing time number (Nt_m) versus Reynolds number plot for four-blade anchor

The average K_m values obtained for the two-blade and four-blade impellers are 214 and 185 respectively. From the definition of K_m, it is clear that four-blade anchor requires less impeller rotations as compared to two-blades. Thus the mixing time for four-blade impeller is less as compared to two-blade anchor impeller. It was noticed by Havas et al. (1978) and Ford et al. (1972) that the value of K_m is closely related to the method used to determine the mixing time. Other additional criteria are the location of probes and injection area, liquid height, physical properties of tracer, and bottom clearance (Takahashi, 1994).

In order to evaluate the mixing efficiency, the relationship between the mixing time and power consumption per unit volume (specific power consumption) for the mixing vessel is useful. Figure 5.7(a), (b), (c) shows the plot of mixing time versus specific power consumption. As expected the mixing time decreases with increase in the power consumption (Nomura et al., 1996; Pour et al., 2007).

A similar trend is found in the literature and also observed by Ihejirika and Ein-Mozaffari (2007) for close clearance impeller.

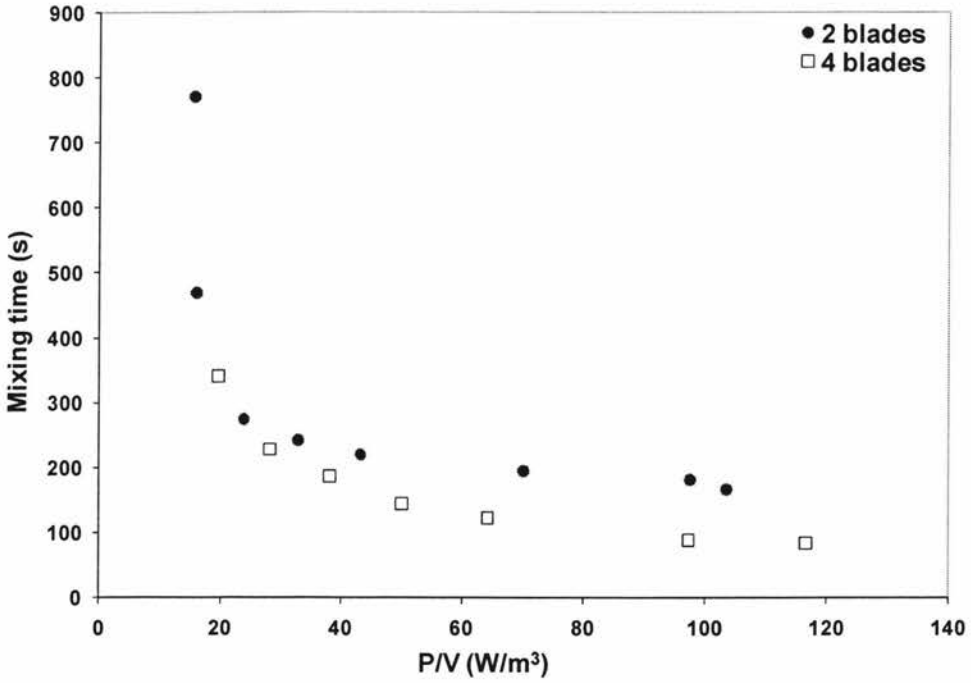

Figure 5.7 (a) Mixing time versus impeller specific power consumption (0.5% xanthan gum)

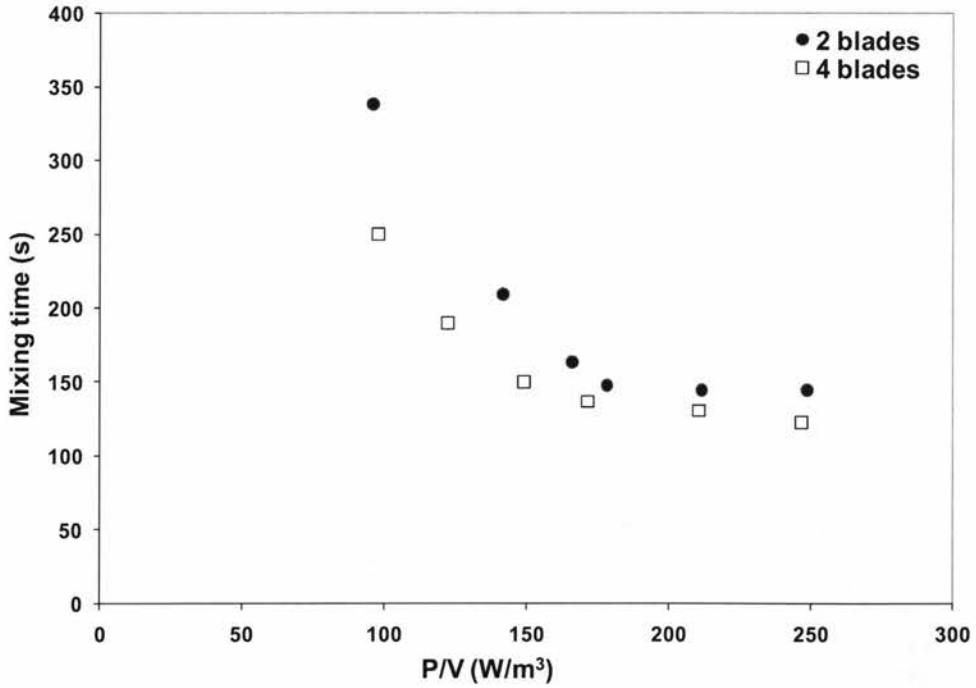

Figure 5.7 (b) Mixing time and specific power consumption relation (1.0% xanthan gum)

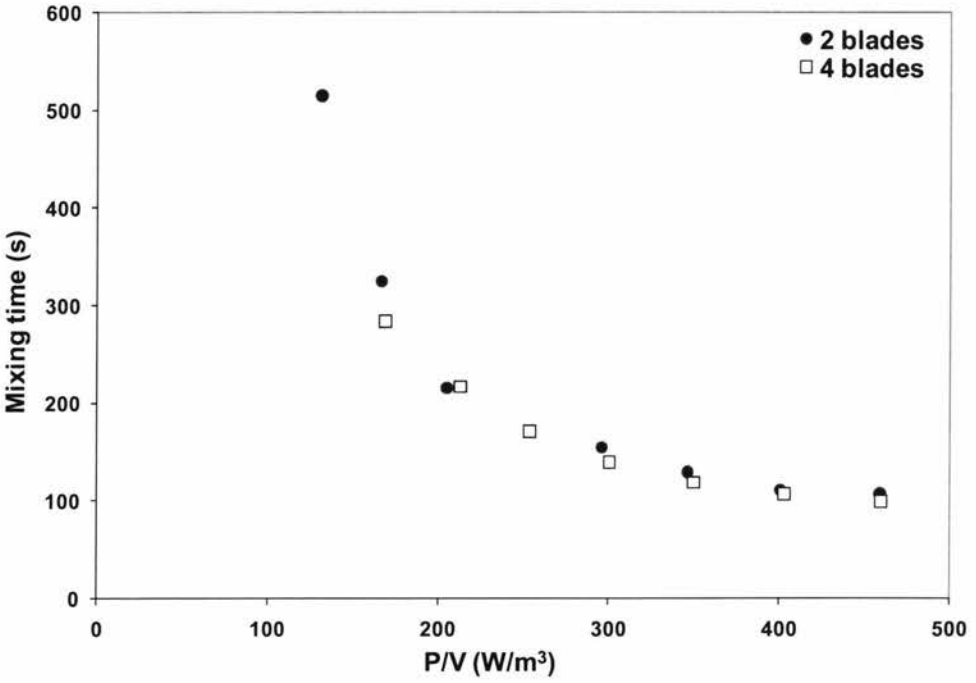

Figure 5.7 (c) Mixing time and specific power consumption relation (1.5% xanthan gum)

5.3 Flow Patterns

The mixing performance is a function of the flow pattern generated by the impeller. Parameters such as impeller geometry, rotational speed and liquid viscosity affect the flow pattern generated by the impeller in the mixing tank (Paul *et. al.*, 2004). The flow pattern is a very important factor in movement of fluid into entire vessel (Murakami et al., 1972). Figure 5.8 shows the CFD velocity contour for mixing of xanthan gum solution.

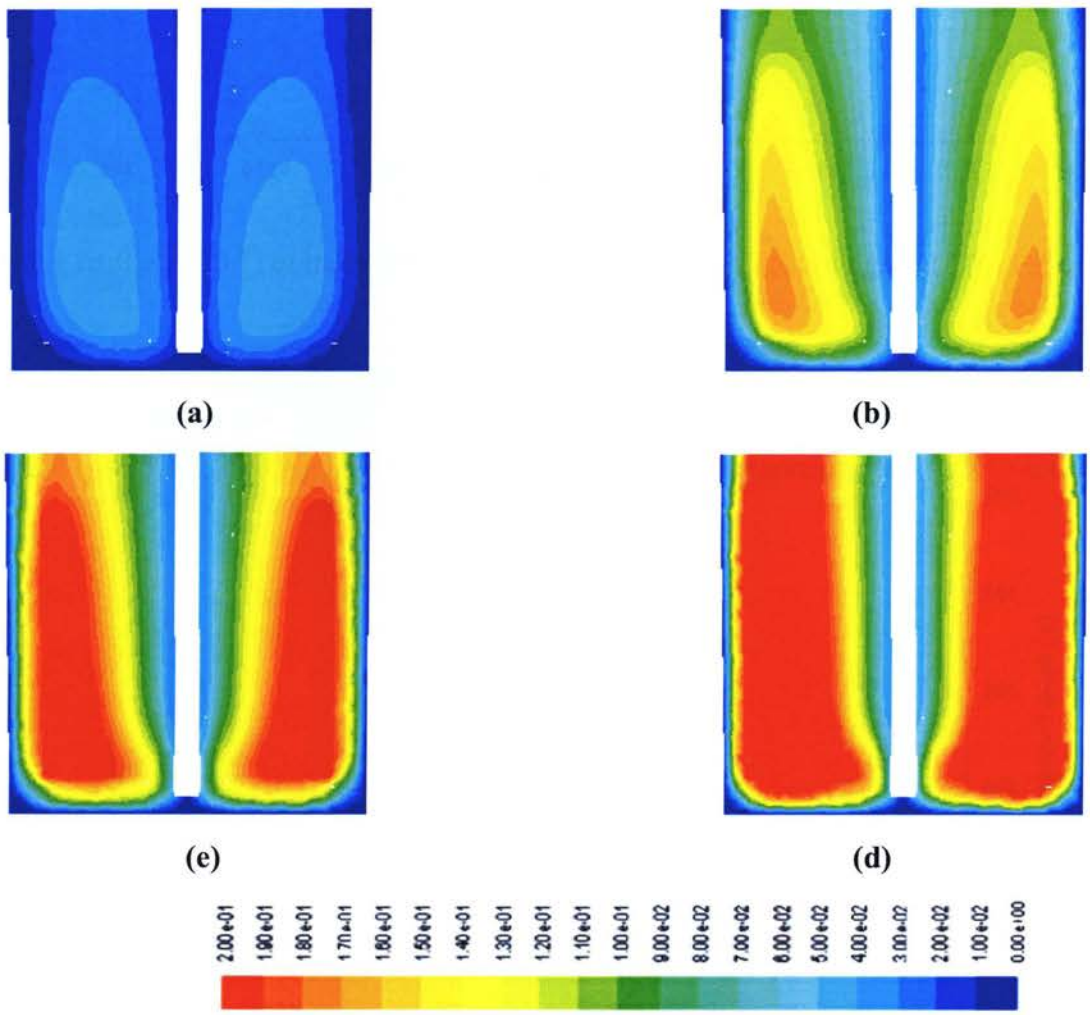

Figure 5.8 Velocity magnitude contours (m/s) for 1% xanthan gum solution agitated with 2-balde anchor impeller: (a) 25 rpm (Re = 3) (b) 60 rpm (Re = 20) (c) 80 rpm (Re = 35) (d) 100 rpm (Re = 54)

From figure 5.8 it can be observed that two circulation loops exists in the tank between impeller and shaft. With increase in impeller speed the size of these circulation loops increases and better mixing is observed with increase in impeller speed. The circulation loops are also observed by other researchers for mixing in close clearance impellers (Nomura et al., 1996; Iranshahi et al., 2007).

Figure 5.9 shows the CFD velocity magnitude contours for 0.5%, 1.0% and 1.5% xanthan gum solution.

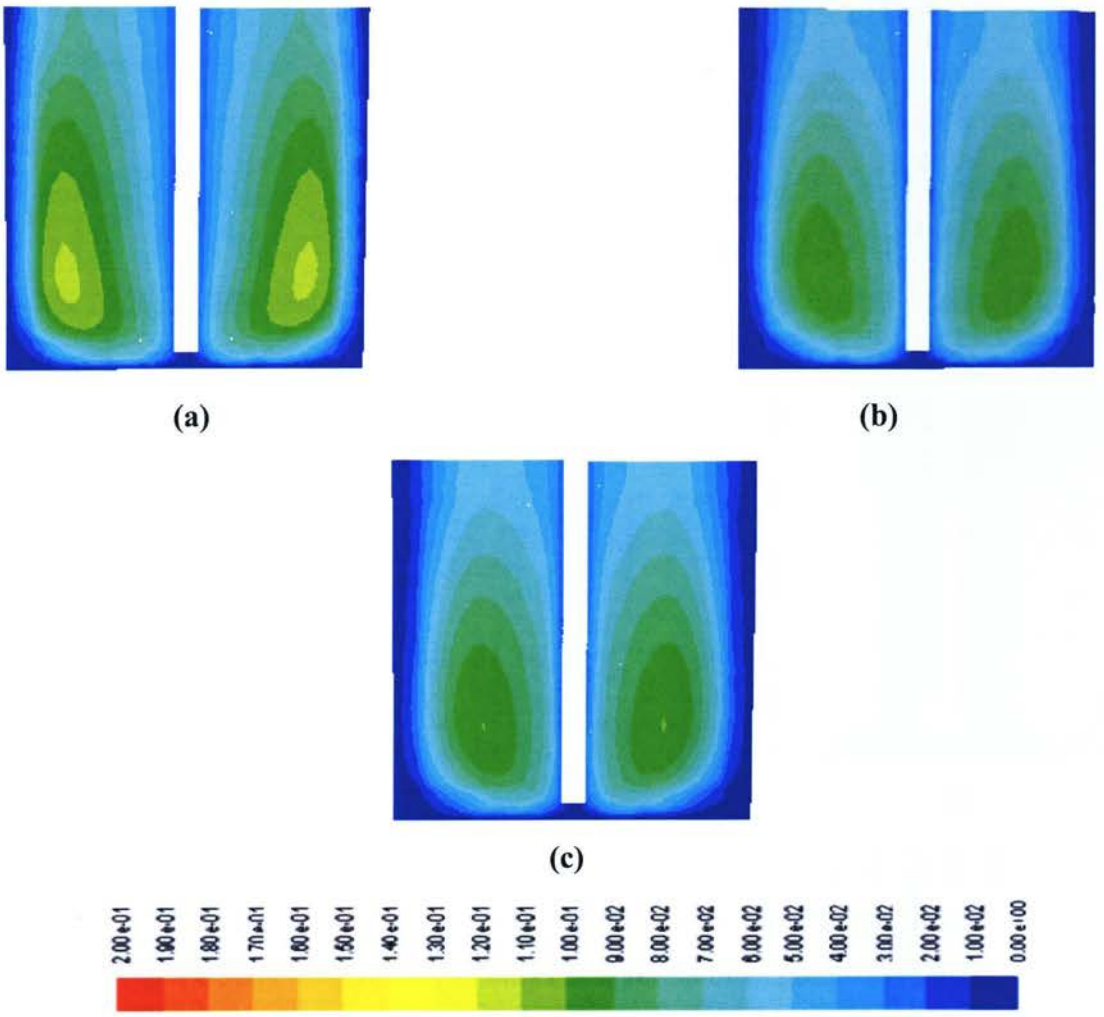

Figure 5.9 Velocity magnitude contours (m/s) for xanthan gum solution agitated with 2-balde anchor impeller at 40 rpm: (a) 0.5% xanthan gum (b) 1.0% xanthan gum (c) 1.5% xanthan gum

It was observed from the figure 5.9 that the velocity magnitude decreases when the concentration of fluid increases at a constant impeller speed. The reason for this observation is that when the concentration increases there is an increase in the yield-stress and viscosity of the xanthan gum solution.

Figure 5.10 reveals the comparison of CFD velocity contours for two- and four-blade anchor impeller with different concentration of xanthan gum solution. From the figures, it was observed that the circulation zones are bigger in size for four-blade impeller as compared to two-blade impeller. The velocity is higher in four-blade impeller which leads to the higher power consumption but reduction in the mixing time in comparison to two-blade anchor impeller.

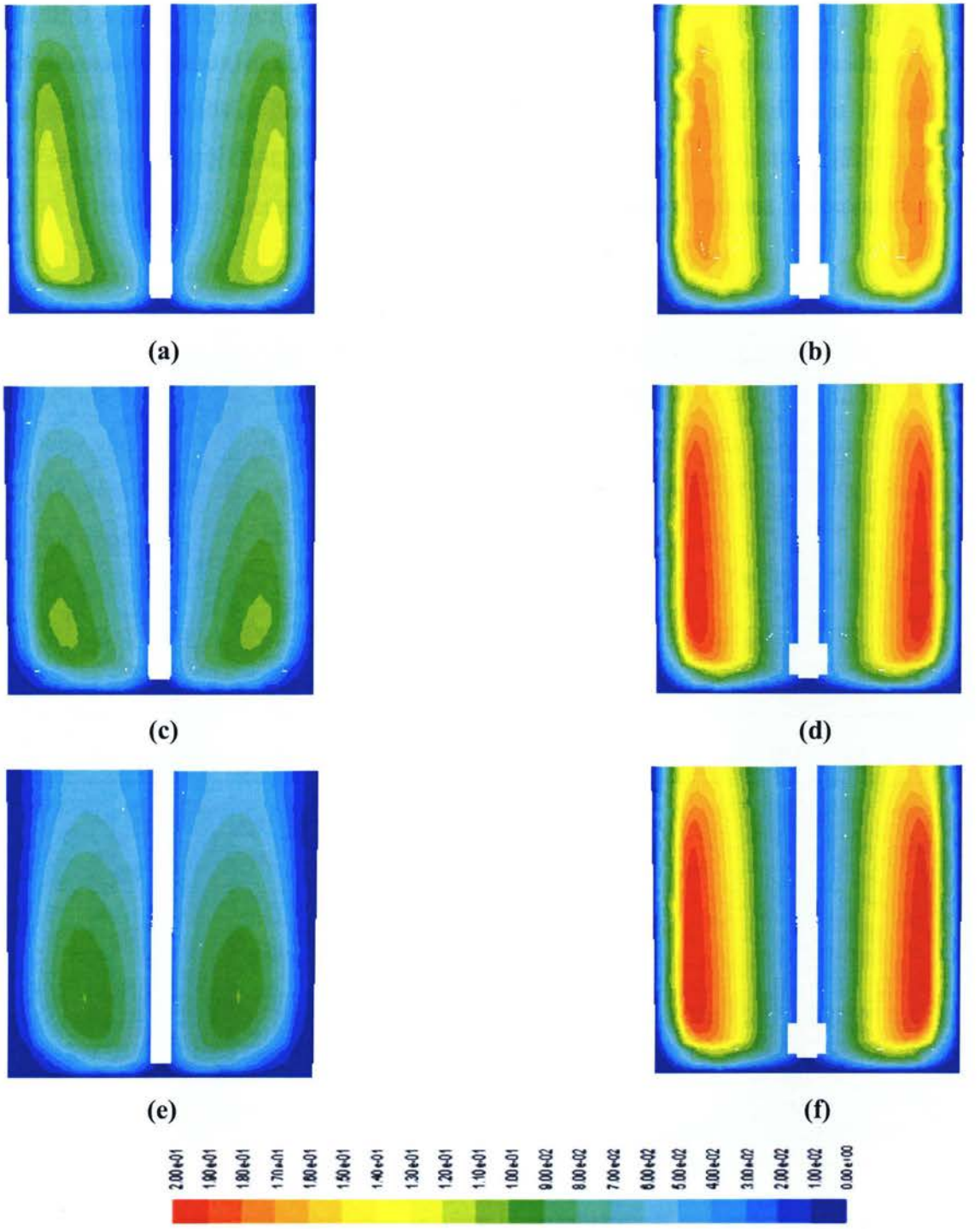

Figure 5.10 Velocity magnitude contours (m/s) for xanthan gum solution agitated with anchor impeller: (a) 0.5% xanthan gum agitated at 40 rpm with 2- blade impeller (b) 0.5% xanthan gum agitated at 40 rpm with 4- blade impeller (c) 1.0% xanthan gum agitated at 40 rpm with 2- blade impeller (d) 1.0% xanthan gum agitated at 40 rpm with 4- blade impeller (e) 1.5% xanthan gum agitated at 40 rpm with 2- blade impeller (f) 1.5% xanthan gum agitated at 40 rpm with four-blade impeller

Figure 5.11 reveals the CFD velocity vectors for mixing of xanthan gum at different impeller speed. From figure it can be seen that the magnitude of vector increases with increase in impeller speed. The flow pattern is mainly tangential and radial. Peter and Smith (1967), Murakami et al. (1972), Kuriyama et al. (1982) and Bertrand et al. (1996) have observed the same pattern in their works.

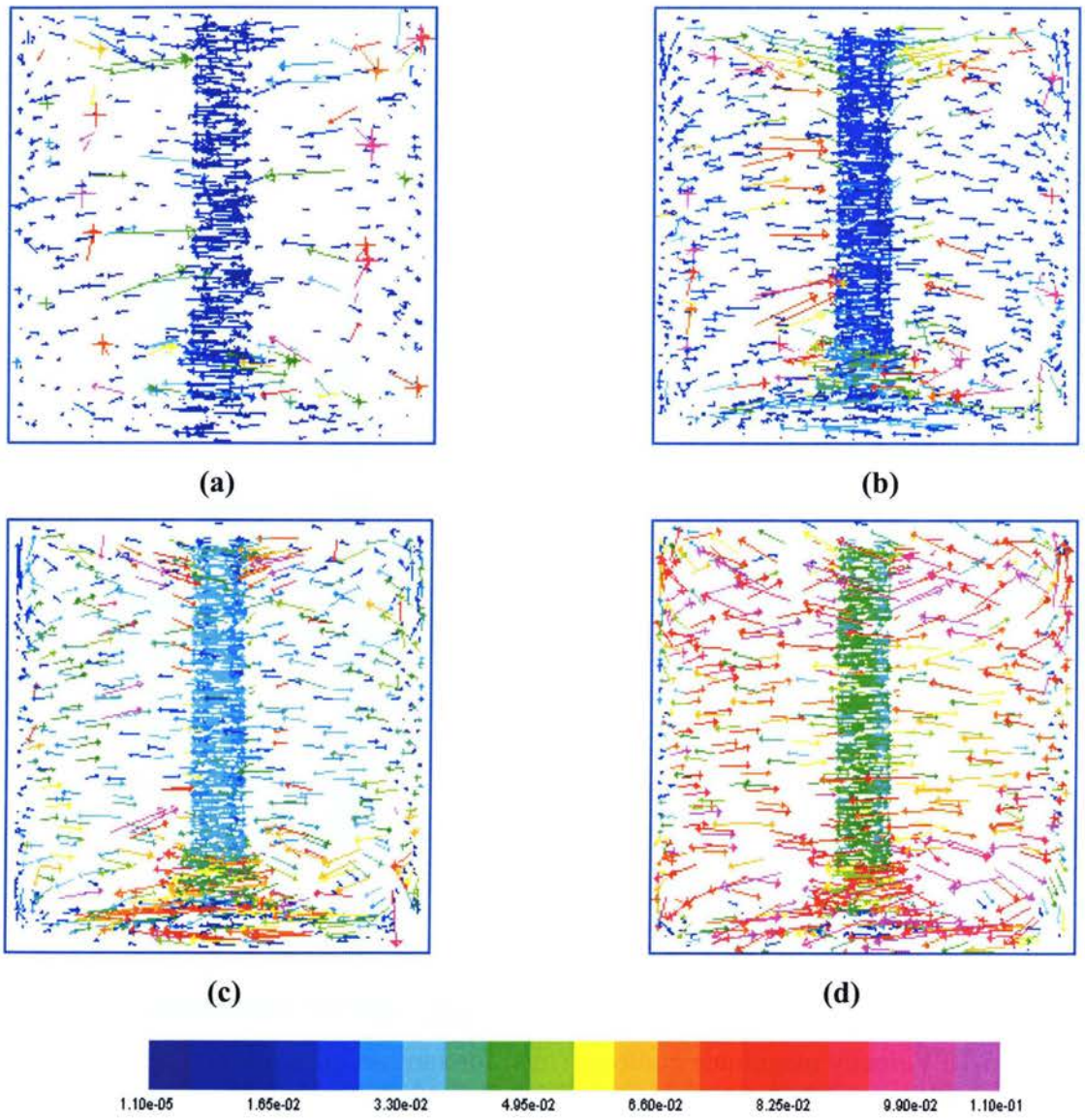

Figure 5.11 Velocity vector for 0.5% xanthan gum solution agitated with two-blade anchor impeller: (a) 30 rpm (b) 50 rpm (c) 70 rpm (d) 90 rpm

The tangential flow is dominant and becomes smaller with distance away from the impeller which was also observed by Murakami et al. (1972). The axial flow is less than tangential flow. Radial flow is recognizable near impeller. The magnitude of velocity vector is very less at the centre around the shaft and it increases with increase in impeller speed. The velocity vectors are more prominent at bottom due to the horizontal arm of anchor.

Figure 5.12 shows the CFD velocity vectors for mixing of xanthan gum with two- and four-blade anchor impeller. From the figures we can see that the magnitude of the velocity vectors is higher during mixing of xanthan gum using four-blade impeller. This leads to less mixing time to get desired degree of homogeneity for mixing with four-blade anchor impeller.

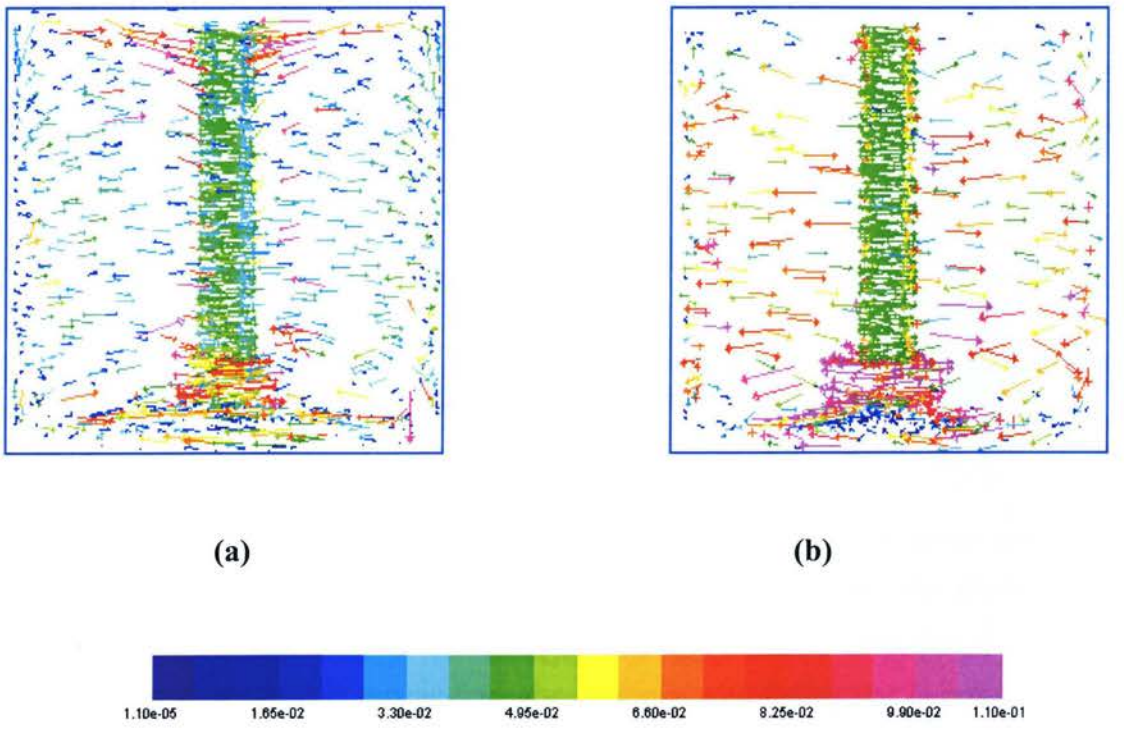

Figure 5.12 Velocity vector for 1.0% xanthan gum solution agitated at 90 rpm: (a) two-blade anchor impeller (b) four-blade anchor impeller

5.4 Effect of Clearance on Power Consumption and Mixing Time

The power consumption and mixing time were calculated for several values of *c/D*. Figure 5.13 shows the power number versus *c/D* plot for 1.5% xanthan gum solution agitated at 60 rpm (*Re* = 11.9). The plot illustrates that when *c/D* increases the power number decreases, which is in good agreement with theory and literature (Paul et al., 2004). This is due to fact that when the clearance is increases, the torque required to drive the impeller is decreases. Also, it was shown experimentally by Beckner and Smith (1966) and Uhl and Voznick (1960) that the power number decreases with an increase in *c/D* ratio for anchor impellers at fixed Reynolds number. For different *c/D* values, the mixing time were determined.

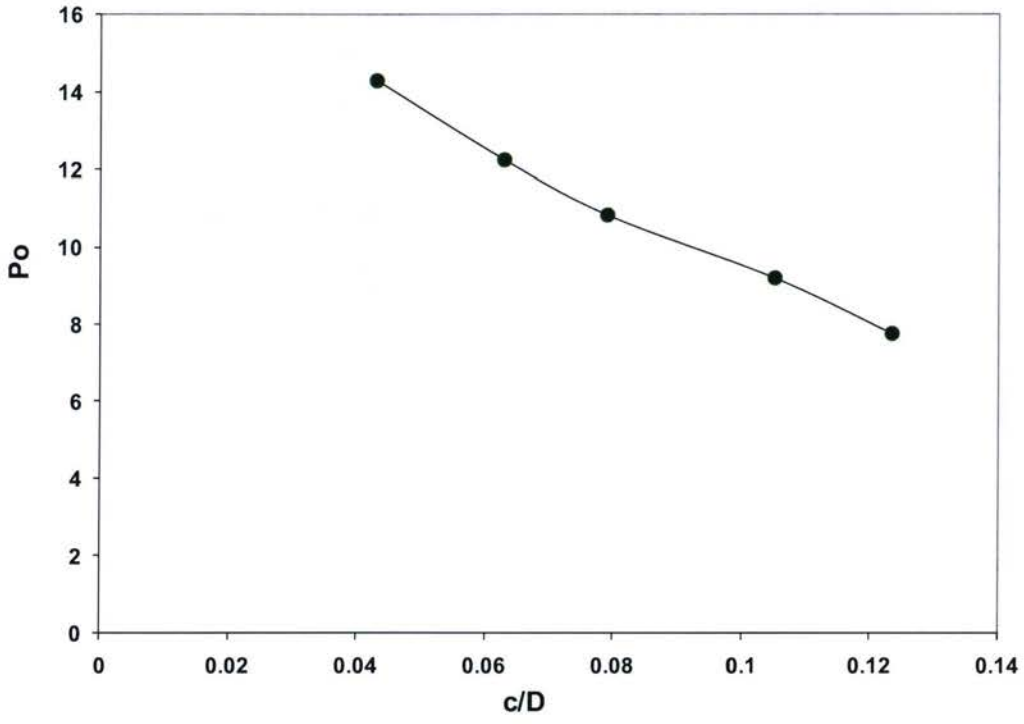

Figure 5.13 Power number as a function of *c/D* ratio for 1.5% xanthan gum agitated at 60 rpm in two-blade anchor impeller

Figure 5.14 shows the plot of non-dimensional mixing time versus *c/D*. The U-shaped curve was obtained. It was observed that when the *c/D* ratio increases the mixing time decreases up to *c/D* value of 0.079. With further increase in the *c/D* the mixing time also increases. For the *c/D* value of 0.079 the optimum dimensionless mixing time was obtained.

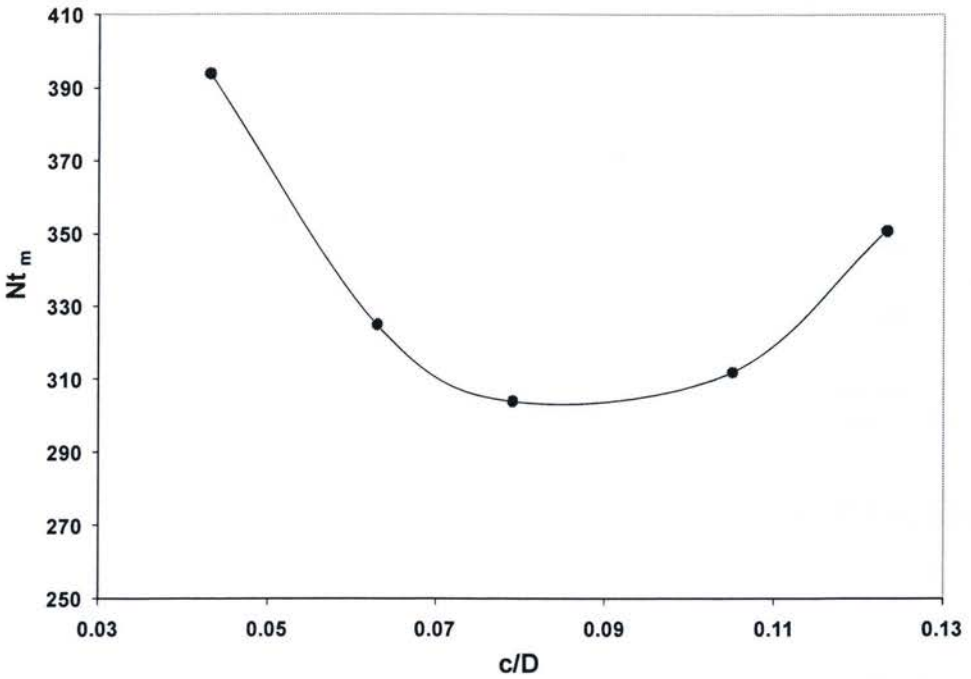

Figure 5.14 Dimensionless mixing time as a function of *c/D* ratio for 1.5% xanthan gum agitated at 60 rpm in two-blade anchor impeller

Figure 5.15 shows the plot of dimensionless mixing time versus power number at different *c/D* values. The U-shaped curve was obtained. Initially, the dimensionless mixing time decreases with an increase in the power number. Onwards from *c/D* value of 0.079, the dimensionless mixing time also increases with further rise in power number. Thus for a *c/D* value of 0.079 the optimum power number, P_o and mixing time number, Nt_m were achieved.

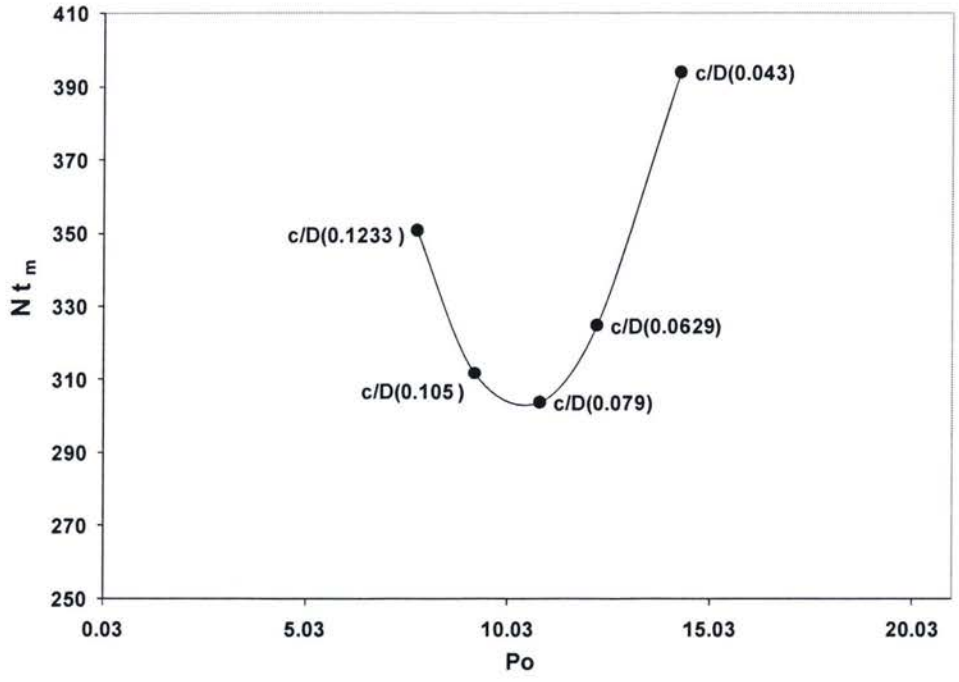

Figure 5.15 Dimensionless mixing time as a function of Power number for 1.5% xanthan gum agitated at 60 rpm in two-blade anchor impeller

5.5 Effect of Impeller Blade Width on Power Input and Mixing Time

At different values of *w/D* the power consumption and mixing time were obtained. Figure 5.16 shows the power number versus *w/D* plot for 1.5% xanthan gum agitated with two-blade anchor impeller at 60 rpm (*Re* = 11.9). The plot illustrates that when *w/D* increases the power number doesn't increases significantly, which is in good agreement with theory. This is reasonable because of the absence of shear forces in the direction in which the blade was moving.

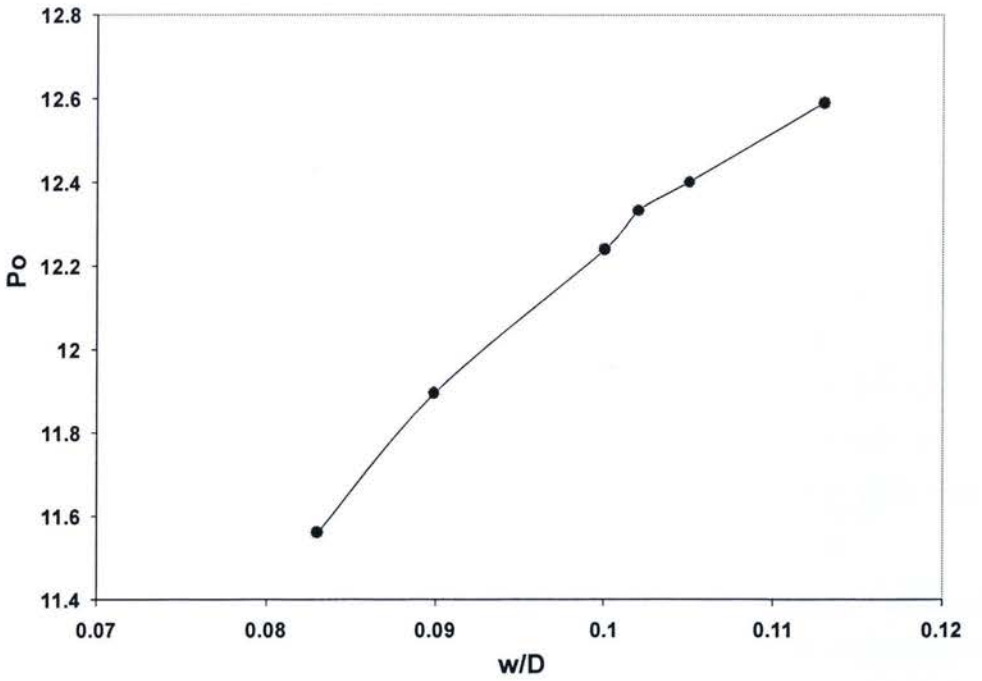

Figure 5.16 Power number as a function of w/D ratio for 1.5% xanthan gum agitated at 60 rpm in two-blade anchor impeller

Figure 5.17 shows the plot of dimensionless mixing time versus *w/D*. The U-shaped curve was obtained. Initially, when *w/D* increases the mixing time decreases up to a *w/D* value of 0.102. After the *w/D* value of 0.102, with further increase in *w/D* the mixing time also increases. Figure 5.18 shows the relationship between dimensionless mixing time, Nt_m and power number, *Po*. When the *w/D* increases, the power number increases and the mixing time decreases up to *w/D* = 0.102. With further increase in *w/D*, the dimensionless mixing time also increases. Therefore, for a *w/D* value of 0.102 the optimum power number, *Po* and mixing time number, Nt_m were achieved. The optimum *w/D* and *c/D* ratio determined in this study were quiet well in agreement with other works and literature (Peter and Smith, 1969; Takahashi et al., 1980; Murthy and Jayanti, 2003, Bertrand et al. 1996; Rieger and Novak, 1973; Hoogendorn and Den Hartog, 1967).

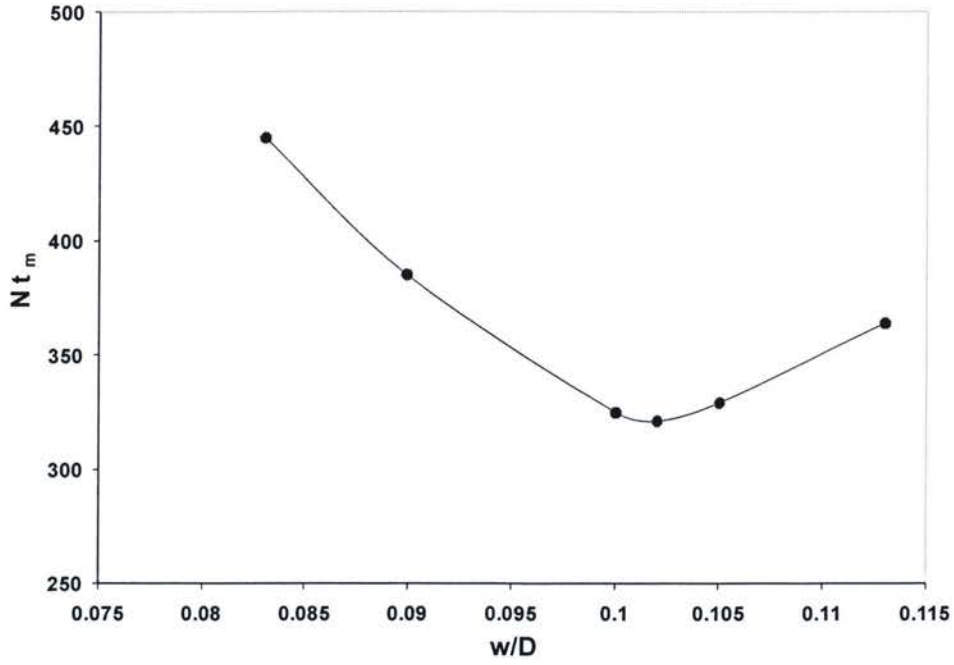

Figure 5.17 Dimensionless mixing time as a function of w/D ratio for 1.5% xanthan gum agitated at 60 rpm in two-blade anchor impeller

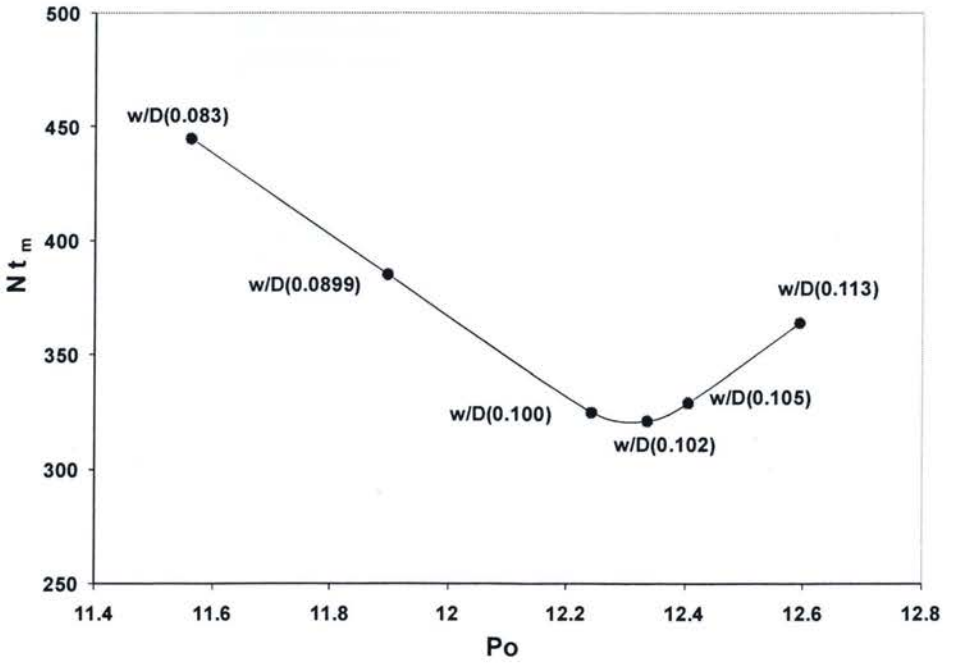

Figure 5.18 Dimensionless mixing time as a function of w/D ratio for 1.5% xanthan gum agitated at 60 rpm in two-blade anchor impeller

6. CONCLUSION AND FUTURE RECOMMENDATIONS

6.1 Conclusion

In this study, computational fluid dynamics (CFD) technique was used to generate the 3-D flow domain for mixing of yield-pseudoplastic fluids with two- and four-blade anchor impellers. The multiple reference frames (MRF) method was applied to capture the motion of the impeller in a stationary mixing tank. Effects of fluid rheology, impeller speed and geometry on flow patterns and power consumptions were studied. The flow patterns observed were mainly tangential. Power consumption was found to increase with an increase in the fluid concentration as well as impeller speed. With an increase in the clearance, power input was decreased but the effect of impeller width on power consumption was not significant. Power curves determined using CFD were found in good agreement with experimental data and those reported in the literature.

To determine the mixing time, once the flow fields were calculated the tracer was added to the fluid and unsteady state simulations for tracer homogenization were performed. It was found that mixing time for a four-blade impeller was less than that for a two-blade impeller with fixed impeller speed. To evaluate the performance of the impeller, dimensionless mixing time (Nt_m) were plotted against the Reynolds number (Re) and were found to remain almost constant with an increase in the Reynolds number. The dimensionless mixing time for two- and four-blade anchor impellers were 214 and 185 respectively. To determine the mixing efficiency the mixing time was plotted against the specific power consumption. Mixing time reduced with an increase in the specific power consumption and remained almost constant with further increase in specific power. Optimum values of c/D and w/D ratios on the basis of mixing time were determined and were in good agreement with those observed in the literature. Optimum c/D and w/D values were 0.079 and 0.102 respectively. However, it was not possible to have an exact comparison of mixing time number and efficiency with the previous research work as the fluid, geometry and method used in this study were different from them.

6.2 Recommendations for Future Work

Based on the present study and the published research the following is suggested for further research.

- Velocity profiles should be verified experimentally using Ultrasonic Doppler Velocimetry (UDV).
- Mixing time should be determined by Electrical Resistance Tomography (ERT) technique.
- The Herschel-Bulkley model was used as an approximation for rheological behaviour of xanthan gum solutions in this study. Another model may be used to impose the CFD results.

NOMENCLATURE

a_p = linearized coefficients equation 4.1

a_{nb} = linearized coefficients equation 4.2

$\vec{A}$ = surface area vector, m^2

c = clearance from wall and bottom, m

C = Tracer concentration, %

C_∞ = Tracer concentration at time equal to infinity, %

d = Impeller diameter, m

$\overline{\overline{D}}$ = rate of strain tensor, s^{-1}

D = tank diameter, m

D_e = diffusion conductance on the face, e

D_m = molecular diffusivity of the tracer, m^2/sec.

E = the east node

F = strength of the convection, N

F_e = strength of the convection on the face e, N

$\vec{F}$ = external (body) force, N

F_z = axial force imparted by the impeller, N

$F(\Phi)$ = A function that incorporates any spatial discretization

g = gravitational acceleration, ms^{-2}

h = Impeller height, m

I = unit tensor

k_s = Metzner-Otto constant, dimensionless

K = fluid consistency index, Pa-s^n

K_p = proportionality constant of the power number, dimensionless

K_m = mixing time number, dimensionless

m = consistency index

M = impeller torque, N-m

n = flow behaviour index, dimensionless

$\vec{n}$ = normal vector

n	=	number of nodes
n_b	=	number of impeller blades
N	=	impeller speed, s^{-1}
$N.t_m$	=	dimensionless mixing time
N_f	=	axial force number, dimensionless
N_{faces}	=	number of faces enclosing the cell
p	=	pressure, Pa
P	=	general nodal point
P	=	power input, W
P_e	=	Peclet number, dimensionless
P_o	=	Impeller Power number, dimensionless
Q	=	equiangle skewness
$\Delta\vec{s}$	=	displacement vector from the upstream cell centroid to the face centroid, m
$R^c_{\text{iteration } N}$	=	unscaled continuity residual
$R^c_{\text{iteration } 5}$	=	continuity residual in the first five iteration
R^{Φ}	=	scaled residual
$R^{\Phi}{}_s$	=	unscaled residual
R_e	=	Reynolds number, dimensionless
S_{Φ}	=	generalized source term, variable unit
t_m	=	mixing time, s
$\vec{v}$	=	velocity vector, m/s
$\bar{v}$	=	mean velocity, m/s
V	=	fluid volume in tank, m^3
V_{tip}	=	impeller tip velocity, m/s
V	=	cell volume, m^3 (equation 4.14)
V_θ	=	tangential velocity, m/s
V_r	=	radial velocity, m/sec.
V_z	=	axial velocity, m/sec.
w	=	impeller blade width, m
w_t	=	local mass fraction of the tracer, dimensionless
W	=	west node

z	=	axial co-ordinate, m
z/H	=	dimensionless axial co-ordinate
r/R	=	dimensionless radial co-ordinate

Greek Letters

α	=	under-relaxation factor
η	=	non-Newtonian viscosity, Pa.s
η_∞	=	viscosity at infinite shear rate, N.s/m^2
η_0	=	viscosity at zero shear rate, N.s/m^2
ρ	=	Fluid density (kg/m^3)
τ	=	shear stress, Pa
$\bar{\bar{\tau}}$	=	viscous stress tensor, Pa
$\tau_{1/2}$	=	Shear stress at which viscosity drops to half of its zero shear value, Pa
τ_y	=	yield stress, Pa
$\dot{\gamma}$	=	Shear rate, s^{-1}
$\dot{\gamma}_a$	=	Average shear rate in mixing tank, s^{-1}
δx	=	characteristic length (cell width), m
δx_{WP}	=	distance between nodes W and P, m
δx_{PE}	=	distance between nodes P and E, m
$\Delta\vec{r}$	=	displacement vector from the upstream cell centroid to the face centroid, m
Γ	=	free source inhomogeneous domain, dimensionless
Φ	=	generalized conserved quantity, variable unit
$\widetilde{\phi}_f$	=	averaged Φ at face, variable unit
Γ_φ	=	generalized diffusion coefficient, variable unit
μ_a	=	apparent viscosity, Pa.s
μ_o	=	yielding viscosity, Pa.s
λ_c	=	characteristic time (parameter), s

Subscripts

av	=	average
cv	=	control volume
e	=	referred to east
f	=	face
n	=	normal to surface
p	=	general nodal point
r	=	radial component
nb	=	neighbour cell
tip	=	impeller tip
w	=	referred to west
y	=	yield stress
95	=	95% mixing time
z	=	axial component
θ	=	tangential component

Abbreviations

AMG	=	algebraic multigrid
CFD	=	computational fluid dynamics
CPU	=	central processing unit
ERT	=	electrical resistance tomography
FDM	=	finite difference method
FEM	=	finite element method
FVM	=	finite volume method
MRF	=	multiple reference frame
PDE	=	partial differential equation
PRESTO	=	PREssure STaggering Option
PISO	=	pressure implicit with splitting of operators

RAM = random access memory

RMS = root-mean-square

SIMPLE = semi-Implicit Method for Pressure-Linked Equation

SIMPLEC = SIMPLE consistent

SM = Sliding Mesh

Mathematical Operations

$\frac{\partial}{\partial t}$ = partial derivative with respect to time

$\frac{\partial}{\partial x}$ = partial derivative with respect to space

$\int_{CV}$ = integration on control volume

$\int_{A}$ = integration on control volume area

∇ = del or nabla operator

BIBLIOGRAPHY

Abid, M., Xuereb, C. and Bertrand, J. "Hydrodynamics in vessels stirred with anchor and gate agitators: Necessity of 3-D modeling", *Chem. Eng. Res. Des.*, 377-384 (1992)

Abbot, M. B. and Basco, D.R. "Computational Fluid Dynamics - An introduction for engineers", *Longman scientific & technical, England* (1989)

Ahmad, J., Ramaswamy, H. S. and Ngadi, M. O. "Rheological Characteristics of Arabic Gum in Combination with Guar and Xanthan Gum Using Response Surface Methodology: Effect of Temperature and Concentration", *Int. J. Food Prop.*, 8(2), 179-192 (2005)

Amanullah, A., Hjorth, S. A. and Nienow, A. W. "Cavern sizes generated in highly shear thinning viscous fluids by Scaba 3SHP1 impeller." *Food Bioprod. Process.,* 75, 232-238 (1997)

Arratia P. E., Kukura J., Lacombe J., and Muzzio F. J. "Mixing of Shear-Thinning Fluids with Yield Stress in Stirred Tanks." *AIChE J.*, 52 (7), 2310-2322 (2006)

Aubin J., Fletcher D. F. and Xuereb C. "Modeling turbulent flow in stirred tanks with CFD, the Influence of the modeling approach, turbulence model, and numerical Scheme" *Exp. Thermal and Fluid Sci.*, 28, 431-445 (2004)

Bakker A. and Gates L. E. "Properly Choose Mechanical Agitators for Viscous Liquids", *Chem. Eng. Prog.*, 91, 25-34 (1995)

Barth, T.J. and Jesperson, D.C., "The design and application of upwind schemes on unstructured meshes", *27th Aerospace sciences meeting, Reno, Nevada,* AIAA-89-0366, 1-12 (1989)

Beckner, J.L. and Smith, J.M. "Anchor-agitated systems: Power input with Newtonian and pseudo-plastic fluids", *Trans. Instn. Chem. Eng.*, 44, T224-T236 (1966)

Bertrand, F., Tanguy P.A. and Brito-De La Fuente, E. "A New perspective for the mixing of yield stress fluids with anchor impellers", *J chem. Eng. Jpn.*, 29(1), 51-58 (1996)

Bird, R. B., Stewart, W E., and Lightfoot, E. N. "Transport phenomena, 2nd edition", *John Wiley & Sons Inc, New York* (2002)

Blazek, J. "Computational fluid dynamics, principles and applications", *Elsevier Science Pub. Co.* (2005)

Bourne, J.R., Buerli, M. and Regenass, W. "Heat transfer and power measurements in stirred tanks using heat flow calorimetry", *J chem. Eng. Jpn.,* 36, 354-354 (1980)

Brandt, A. "Multi level adaptive solutions to boundary value problems" *Math. of Comput.,* 31, 333-390 (1977)

Brucato A., Ciofalo M., Crisfi F. and Micale G. "Numerical prediction of flow fields in Baffled Stirred Vessels: a comparison of alternative modeling approaches." *Chem. Eng. Sci.*, 53, 3653-3684 (1998)

Buwa, V., Dewan, A., Nasser, A. F. and Durst F. "Fluid dynamics and mixing of single-phase flow in a stirred Vessel with a grid disc impeller: experimental and numerical investigations." *Chem. Eng. Sci.*, 61, 2815-2822 (2006)

Calderbank, P.H. and Moo-Young, M.B. "The power characteristics of agitators for the mixing of Newtonian and non-Newtonian fluids", *Trans. Instn. Chem. Engrs.*, 39, 337-347 (1961)

Chaplin, M., "Xanthan gum", *http://www.lsbu.ac.uk/water/hyxan.html* (2008)

Chung, T.J. "Computational fluid dynamics", *Cambridge University Press* (2002)

Courant, R., Isaacson, E. and Rees, M. "On the solution of non-linear hyperbolic differential equations by finite differences." *Comm. Pure Appl. Math.*, 5, 243-255 (1952)

Coulson, J.M., Richardson, J.F., Brackhurst, J.R and Harker, J.H. "Chemical engineering, Volume 1, 4th Edition", *Pergamon Press,Oxfor,* (1990)

Coyle, C.K., Hirschland H.E., Michel, B.J and Oldshue, J.Y. "Mixing in viscous fluids", *AIChE J.,* 16(6), 903 (1970)

Deen, N.G., Solberg, T., Hjertager, B.H. "Flow generated by an aerated ruston impeller: two-phase PIV experiments and numerical simulations", *Can. J. Chem. Eng.*, 80, 1-15 (2002)

Deglon, D.A. and Meyer, C.J. "CFD modeling of stirred tanks: numerical considerations", *Minerals Eng.*, 19(10), 1059-1068 (2006)

Edwards, M.F., Godfrey, J.C. and Kashani, M.M. "Power requirement for the mixing of thixotropic liquids", *J J. non-Newtonian fluid mech.*, 1, 309-322 (1976)

Eklund, D.E., and Teirflolk, J.E. "Dispersion of talc for use as a coating pigment", *TAPPI Journal*, 64, 63 (1981)

Ferziger, J.H. and Peric, M. "Computational methods for fluid dynamics", *Springer-Verlag Berlin Heidelberg, New York* (1995)

Ferguson, J. and Kemblowski, Z. "Applied Fluid Rheology" *Elsevier Applied Science, New York* (1991)

"Fluent 6.3 User's Guide Documentation." *Fluent Inc.*, (2006)

Foresti, R., Jr. and Liu, T., "How to measure power requirements for agitation of non-Newtonian liquids in the Laminar Region", *Ind. and eng. Chem.*, 51(9), 860-864 (1959)

Ford C. "CFD simulation of mixing dynamics in agitated pulp stock chests." *MASc Thesis, University of British Columbia* (2004)

Ford, D.E, Mashelkar, R.A. and Ulbrecht, J. "Mixing times in Newtonian and non-Newtonian fluids", *Process Tech. Int.*, 17(10), 803-807 (1972)

Fradette, L., Thome, G., Tanguy, P.A. and Takenaka, K. "Power and mixing time study involving a Maxblend impeller with viscous Newtonian and non-Newtonian fluids", *Trans IChemE, Part A, Chem. Eng. Res. Des.*, 85(A11), 1514-1523 (2007)

Foucault, S., Ascanio, G. and Tanguy, P.A. "Coaxial mixer hydrodynamics with Newtonian and non-Newtonian fluids", *Chem. Eng. Technol.*, 27(3), 324-329 (2004)

Foucault, S., Ascanio, G. and Tanguy, P.A. "Power characteristics in coaxial mixing: Newtonian and non-Newtonian fluids ", *Ind. Eng. Chem. Res.*, 44, 5036-5043 (2005)

Galindo E., Torrestiana B., and García-Rejón A. "Rheological characterization of xanthan fermentation broths and their reconstituted solutions." *Bioproc. Eng.* 4, 113-118 (1989)

Garcia-Ochoa, F, Santos, V.E., and Alcon, A. "Metabolic structure kinetic model for xanthan production", *Enzyme Microb. Technol.*, 23, 75-82 (1998)

Giannouli, P. and Morris, E. R. "Cryogelation of xanthan", *Food Hydrocoll.*, 17, 495-501 (2003)

Galindo E., Torrestiana B., and García-Rejón A. "Rheological characterization of xanthan fermentation broths and their reconstituted solutions." *Bioproc. Eng.* 4, 113-118 (1989)

Godfrey, J.C., Yuen, T.H. and Edwards, M.F. "Associative phenomena in galactomannan-deacetylated xanthan systems", *Int. J. Biol. Macromol.* 29, 181-192 (2001)

Goycoolea, F.M., Milas,M. and Rinaudo, M. "Associative phenomena in galactomannan-deacetylated xanthan systems", *Int. J. Biol. Macromol.* 29, 181-192 (2001)

Garcia-Ochoa, F and Casas, J.A., "Apparent yield stress in xanthan gum solutions at low concentrations", *The Chem. Eng. J.*, 53, B41-B46 (1994)

Harnby, N., Edwards, M.F. and Nienow, A.W. "Mixing in the process industries, second edition", *Reed Educational and Professional Publishing Ltd.*, (1997)

Havas, G., Sawinsky, J. and Deak, A. "Investigation of homogenization efficiency of the screw agitator, helical ribbon agitator, gate type anchor impeller and multi-paddle agitator in the mixing of high-viscosity Newtonian liquids", *Periodica polytechnic chem. Eng.*, 22, 317-330 (1978)

Hayes, R.E., Afcan, A., Boulanger, B. and Tanguy, P.A. "Experimental study of reactive mixing in a laminar flow batch reactor", *Trans. Instn. Chem. Engrs.*, 76, Part A, 73-81 (1998)

Harvey, A. D., Wood, S.P., Leng, D.E., "Experimental and computational study of multiple impeller flows", *Chem. Eng. Sci.*, 52(9), 1479-1491 (1997)

Heinlein, H.W. and Sandall, O.C. "Low Reynolds number heat transfer to non-Newtonian fluids in anchor-agitated vessels", *Ind. Eng. Chem. Process Des. Develop.*, 11(4), 490-495 (1972)

Herschel, W. E. and Bulkley, R. "Measurements of consistency as applied to rubber-benzene solutions." *Proc. Am. Soc. Test. Mat.*, 26 (part 2), 621-633 (1926)

Hiraoka, S., Yamada, I. and Mizoguchi, K., "Numerical analysis of flow behaviour of highly viscous fluid in agitated vessel", *J. Chem. Eng. Jpn.*, 11(6), 487-493 (1978)

Hoogendoorn, C.J. and Den Hartog, A.P. "Model studies on mixers in the viscous flow region", *Chem. Eng. Sci.*, 22, 1689-1699 (1967)

Hosuka, M. "Engineering aspects in rheololgy of thixotropic fluids", PhD thesis, CVUT, Prague (1981)

Ihejirika, I. and Ein-Mozaffari, F. "Using CFD and ultrasonic velocimetry to study the mixing of pseudoplastic fluids with a helical ribbon impeller", *Chem. Eng. Technol.*, 30(5), 606-614 (2007)

Iranshahi, A., Heniche, M., Bertrand, F. and Tanguy, P.A. "Numerical investigation of the mixing efficiency of the Ekato Paravisc impeller", *Chem. Eng. Sci.*, 61, 2609-2617 (2006)

Iranshahi, A., Devals, C., Heniche, M., Fradette, L., Tanguy, P.A. and Takenaka, K. "Hydrodynamics characterization of the Maxblend impeller", *Chem. Eng. Sci.*, 62, 3641-3653 (2007)

Issa, R.I. "Solution of the implicitly discretized fluid flow equations by operator-splitting", *J. Comp. Phys.*, 62, 40-65 (1986)

Kai, W. and Shengyao, Y. "Heat transfer and power consumption of non-Newtonian fluids in agitated vessels", *Chem. Eng. Sci.*, 44(1), 333-40 (1989)

Kaminoyama, M., Saito, F. and Kamiwano, M. "Flow analogy of pseudo-plastic liquid in geometrically similar stirred vessels based on numerical analysis", *J chem. Eng. Jpn.*, 23(2), 214-221 (1990)

Kaminoyam, M., Akabane, K., Arai, K., Saito, F. Kamiwano, M., "Numerical analysis of flow of a Bingham fluid in an anchor impeller", *Intl. Chem. Eng.*, 34(2), 263-269 (1994)

Kennedy, J. F. and Bradshaw, I. J. "Production, properties and applications of xanthan", *Prog. Ind. Microbiol.*, 19, 319–371 (1984)

Kang, K. S. and Pettit, D. J. "Xanthan, gellan, wellan, and rhamsan." In: Whistler, R.L and BeMiller, J.N, Editors, 1993. *Industrial gums, Academic Press, New York*, 341-398 (1993)

Katsuraya, K., Okuyama, K., Hatanaka, K., Oshima, R., Sato, T. and Matsuzaki, K. "Constitution of konjac glucomannan: chemical analysis and ^{13}C NMR spectroscopy", *Carbohydr. Polym.* 53, 183-189 (2001)

Kelly, W. and Gigas, B., "Using CFD to predict the behavior of power law fluids near axial- flow impellers operating in the transitional flow regime", *Chem. Eng. Sci.*,58, 2141-2152 (2003)

Kerdouss, F., Bannari, A. and Proulx, P. "CFD modeling of gas dispersion and bubble size in a double turbine stirred tank", Chem. Eng. Sci., 61(10), 3313-3322 (2006)

Khopkar, A.R., Mavros, P., Ranade, V.V., and Bertrand, J., "Simulation of flow generated by an axial flow impeller-bath and continuous operation", *Chem. Eng. Res Des.*, 82,737-751 (2004)

Kuriyama, M., Inomata, H., Arai, K. and Saito, S. "Numerical solutions for the flow of highly viscous fluid in agitated vessel with anchor impeller", *AIChE J.*, 28(3), 385-391 (1982)

Kukukova, A., Mostek, M., Jahoda, M., and Machon, V., "CFD prediction of flow and homogenization in a stirred Vessel: Part 1 vessel with one and two impellers", *Chem. Eng. Technol.* 28 (10), 1125-1133 (2005)

Lane, G.L., Schwarz, M.P., Evans, G.M., "Numerical modeling of gas-liquid flow in stirred tanks", *Chem. Eng. Sci.*, 60(8-9), 2203-2214 (2005)

Lee, R.E., Finch, C.R. and Wooledge, J.D. "Mixing of high viscosity Newtonian and non-Newtonian fluids", *Ind. Eng. Chem.*, 49(11), 1849-1854 (1957)

Lenonard, B.P. "A stable and accurate convective modeling procedure based on quadratic upstream interpolation", *Comput. Meth. Appl. Mech. Eng.*, 19, 59-98 (1979)

Leonard, B. P., Mokhtari, S., "Beyond first-order upwinding: The ultra-sharp alternative for non-oscillatory steady-state simulation of convection", *Int. J. Num. Meth. Eng.*, 30, 729-766 (1990)

Lobe, V. M. and White, J. L. "An experimental study of the influence of carbon black on rheological properties of a polystyrene melt", *Polymer Eng. Sci.*, 19, 617 (1979)

Luo, J.Y., Gosman, A.D., Issa, R.I., Middleton, J.C. and Fitzgerald, M.K., "Full flow filed computation of mixing in baffle stirred vessels", *Chem. Eng. Res. Des.*, 71, 342-344 (1993)

Luo, J.Y., Gosman, A.D. and Issa, R. I. "Prediction of impeller induced flows in mixing vessels using multiple frames of reference." *Inst. Chem. Eng. Symp.*, 136, 549-556 (1994)

Macosko, C.W "Rheology: Principles, measurements and appicaitons" *Wiley-VCH, New York*, (1994)

Marouche, M., Anne-Archard, D. and Boisson, H.C. "A numerical model of yield stress fluid dynamics in a mixing vessel", *Applied Rheology*, 12, 182-191 (2002)

Mavros, P. "Flow visualization in stirred vessels, a review of experimental techniques", *Chem. Eng. Res. Des.*, 75(A8), 729-736 (2001)

Metzner, A. B. and Otto, R. E. "Agitation of non-Newtonian fluids" *AIChE J.*, 3, 3-11 (1957)

Murakami, Y., Fujimoto, K., Simada, T., Yamada, A. and Asano, K. "Evaluation of performance of mixing apparatus for high viscosity fluids", *J chem. Eng. Jpn.*, 5(3), 297-303 (1972)

Montante, G., Moštěk M., Jahoda M., and Magelli F. "CFD simulation and experimental validation of homogenization curves and mixing time in stirred newtonian and pseudoplastic liquids." *Chem. Eng. Sci.*, 60, 2427-2437 (2005)

Morris E. R. "Molecular origin of xanthan solutions." *Extracellular Microbial Polysaccharides, ACS Symp.*, 45, 81-89 (1977)

Murthy S. S. and Jayanti S. "Mixing of Power-Law Fluids Using Anchors: Metzner-Otto Concept Revisited." *AIChE J.*, 49 (1), 30-40 (2003a)

Nagata, S. "Mixing principles and applications", *John Wiley & Sons Inc., New York* (1975)

Nagata, S., Nishikawa, M., Katsube, T., Takaish, K. "Mixing of highly viscous non-Newtonian liquids", *Intl. Chem. Eng.*, 12(1), 175-182 (1972)

Nienow, A.W., Wisdom, D.J., Solomon, J., Machon, V. and Vlcek, J. "The effect of rhgeological complexities on power consumption in an aerated and agitated vessel" *Chem. Eng. Comm.*, 19, 273-293 (2005)

Nomura, T., Yongfu, H. and Takahashi, K. "Development and mixing characteristics of folding impeller for round-bottomed flask", *J chem. Eng. Jpn.*, 29(1), 134-138 (1996)

Ohta, M., Kuriyama, M., Arai, K. and Saito, S. "A two-dimensional model for the secondary flow in an agitated vessel with anchor impeller", *J chem. Eng. Jpn.*, 18(1), 81-84 (1985)

Pakzad, L. "Using electrical resistance tomography and computational fluid dynamics to study the mixing of pseudoplastic fluids with a scaba 6SRGT impeller", *MASc Thesis, Ryerson University* (2007)

Pakzad, L., Ein-Mozaffari, F. and Chan, P. "Using electrical resistance tomography and computational fluid dynamics modeling to study the formation of cavern in the mixing of pseudoplastic fluids possessing yield stress", *Chem. Eng. Sci.*, 63, 2508-2522 (2008)

Patankar, S.V. "Num. Heat Transfer and Fluid Flow", *Hemisphere Publishing Corporation, Taylor & Francis Group, New York* (1980).

Patankar, S.V. and Spalding, D.B. "A Calculation Procedure for Heat, Mass, and Momentum Transfer in 3-D Parabolic Flows." *Int. J. Heat Mass Trans.*, 15, 1787-1806 (1972)

Paul E. L., Atiemo-Obeng, V. A., and Keresta, S. M. "Handbook of Industrial Mixing-Science and Practice" *John Wiley & Sons Inc.*, (2004)

Pakzad, L., Ein-Mozaffari, F. and Chan, P. "Using electrical resistance tomography and computational fluid dynamics modeling to study the formation of cavern in the mixing of pseudoplastic fluids possessing yield stress" *Chem. Eng. Sci.*, 63, 2508-2522 (2008)

Pedrosa, S.M.C.P., Nunhez, J.R. "The behaviour of stirred vessels with anchor type impellers", *Comp. and Chem. Eng.*, 24, 1745-1751 (2000)

Peixoto, S.M.C., Nunhez, J.R. and Durate C.G. "Characterizing the flow of stirred vessels with anchor type impellers", *Braz.J. Chem.. Eng.*, 179, 4-7 (2000)

Peters, D.C. and Smith, J.M. "Fluid flow in the region of anchor agitator blades", *Trans. Instn. Chem. Engrs.*, 45, T360-T366 (1967)

Podolsak, A.K., Tiu, C., Saeki. T., Usui, H., "Rheological properties and some applications for rhamsan and xanthan gum solutions", *Polymer Intl.*, 40, 155-167 (1996)

Pour, S.B., Fradette, L. and Tanguy, P.A. "Laminar and slurry blending characteristics of dual shaft impeller system" *Chem. Eng. Res. Des.,* 85(A9), 1305-1313 (2007)

Press, W.H., Flannery, B.P., Teukolsky, S.A. and Velterling, W.T., *Numerical recipes-the art of Scientific, Fortran version, Cambridge University Press, Cambridge* (1992)

Ranade, V.V."*Computational flow modeling for chemical reactor engineering*", *Academic Press, San Diego* (2002)

Renaud, M., Belgacem, M.N., Rinaudo, M. "Rheological behaviour of polysaccharide aqueous solutions", *Polymer*, 46, 12348–12358 (2005)

Rieger, F. and Novak, V. "Power consumption of agitators in highly viscous non-Newtonian liquids", *Trans. Instn. Chem. Eng.*, 51, 105-111 (1973)

Rocks, J.K., "Xanthan gum", *Food Technology*, 25, 476-484 (1971)

Rochefort, W. E. and Middleman , S. "Rheology of xanthan gum: salt, temperature, and strain effects in oscillatory and steady shear experiments." *J. Rheology*, 31 (4), 337-369 (1987)

Rubart, L. and Bohme, G. "Numerical simulation of shear-thinning flow problems in mixing vessels", *Theoretical Comp. Fluid Dynamics*, 3, 95-115 (1991)

Runchal, A. K. and Wolfshtein, M. "Numerical integration procedure for the steady state Navier-Stokes equations." *J. Mech. Eng. Sci.*, 11, 445-452 (1969)

Shamlou, P. A. and Edwards, M.F. "Power consumption of anchor impellers in Newtonian and non-Newtonian liquids", *Chem. Eng. Res. Des.*, 67, 537-543 (1989)

Shaw, C.T. "Using computational fluid dynamics", *Prentice Hall, New Jersey, USA* (1994)

Shyy,W., Thakur, S. S., Ouyang, H., Liu, J. and Blosch, E. "Computational Techniques for Complex Transport Phenomena" *Cambridge University Press, New York* (1997)

Silvester, R.S. "Mixing of non-Newtonian media, technical review", *BHRA*, vol.12, (1985)

Smith, J. H. and Pace, G. W. "Recovery of microbial polysaccharides." *J. Chem. Technol. Biotechnol.*, 32, 119–129 (1982)

Sommerfeld, M. and Decker, S., "State of the art and future trends in CFD simulation of stirred vessel hydrodynamics", *Chem. Eng. Technol.*, 27(3), 215-224 (2004)

Speers, R.A and Tung, M.A., "Concentration and temperature dependence of flow behavior of xanthan gum dispersions", *J. Food Sci.*, 51(9), 96-98 (1986)

Sweeney, E.T. "An introduction and literature guide to mixing", *BHRA*, vol.5 (1978)

Savreux, F., Jay, P. and Magnin, A. "Viscoplastic fluid mixing in a rotating tank", *Chem. Eng. Sci.*, 62, 2290-2301 (2007)

Sestak, J., Zinty, R. and Houska, M. "Anchor-agitated systems: Power input correlation for pseudo-plastic and thixotropic fluids in equilibrium", *AIChE J.*, 32(1), 155-158 (1986)

Takahashi, K., Arai, K. and Saito, S. "Power correlation for anchor and helical ribbon impellers in highly viscous liquids", *J Chem. Eng. Jpn.*, 13(2), 147-150 (1980)

Takahashi, K., Yokota, T., Furukawa, T. and Harada, K. "Mixing of highly viscous Newtonian liquids in a helical ribbon vessel at various liquid depths", *J chem. Eng. Jpn.*, 27(2), 244-247 (1994)

Tako, M. and Nakamura, S. "Rheological Properties of Deacetylated Xanthan in Aqueous Media", *Agric Biol. Chem.*, 12, 2987-2993 (1984)

Tanguy, P.A. and Bertrand, F. "Mixing of viscoplastic fluids with anchor impellers", *8th European conference on mixing, UK, Inst. Chem. Eng.*, 525-532 (1994)

Tanguy, P.A., Thibault, F. and Brito de la Fuente, E. "A new investigation of Metzner-Otto concept for anchor mixing impellers", *Can. J. Chem. Eng.*, 74, 222-228 (1996)

Tatterson, G.B. "Various ways to calculate power consumption for viscous creeping flow mixing of shear thinning fluids in stirred vessels", *AIChE, Annual meeting ,Miami Beach* 1-47 (1994)

Tatterson, G.B., "Scaleup and design of industrial mixing processes", *McGraw-Hill, Inc.* (1994)

Torres, L.G., Flores, F., and Galindo, E., "Apparent yield stress of xanthan solutions and broths", *Bioprocess Eng.*, 12, 41-46 (1995)

Van Doormaal, J.P. and Raithby, G.D. "Enhancements of the simple method for predicting incompressible fluid flows." *Num. Heat Trans.*, 7, 147-163 (1984)

Versteeg, H.K. and Malalasekara, W., "An Introduction to Computational Fluid Dynamics", *Longman Scientific and technical* (1995)

Versteeg, H.K. and Malalasekara, W., "An Introduction to Computational Fluid Dynamics – The Finite Volume Method", *Pearson education ltd.* (2007)

Whitcomb, P.J. and Macosko, C.W., "Rheology of Xanthan Gum", *J. Rheol.*, 22, 493-496 (1978)

Uhl, V.W. and Voznic, H.P. "The anchor agitator", *Chem. Eng. Prog.*, 56(3), 72-77 (1960)

Uhl, V.W. and Gray, J.B. "Mixing – theory and practice", *Academic Press, New York*, (1966)

Ulbrecht, J. J. and Patterson, G.K. "Mixing of liquid by mechanical agitation", *Gordon and Breach science publishers*, (1985)

Xu, Y. and McGrath, G., "CFD predictions of stirred tank flow", *Trans I Chem E.*, 74, part A, 471-475 (1996)

Xu, H. and Zhang, G. "Study of the effect of the non-orthogonality for non-staggered grids-the results." *Int. J. Numer. Math. Fluids*, 29, 625-644 (1999)

APPENDIX – I VELOCITY CONTOURS

CFD Velocity Contours for Two-blade Anchor (0.5% Xanthan Gum), m/s

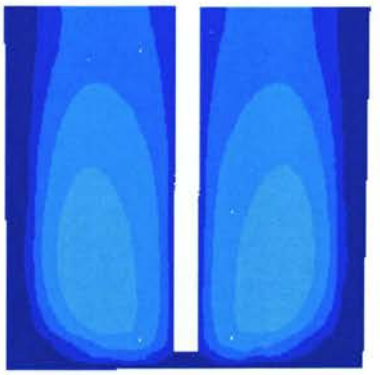

20 rpm

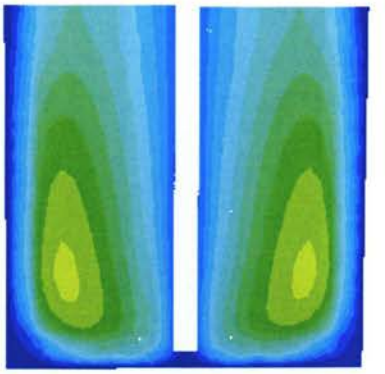

40 rpm

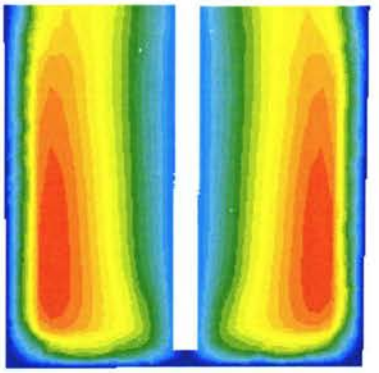

60 rpm

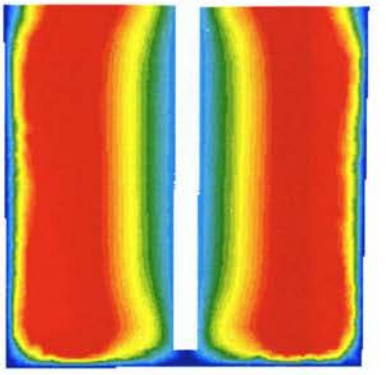

80 rpm

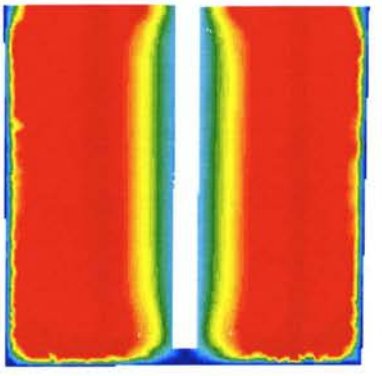

100 rpm

CFD Velocity Contours for Two-blade Anchor (1.0% Xanthan Gum), m/s

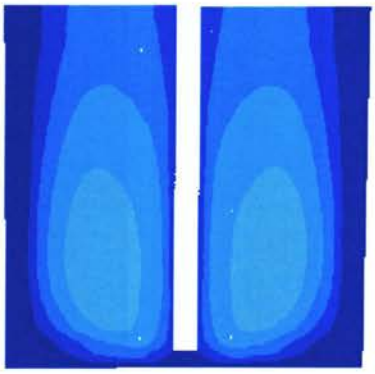

20 rpm

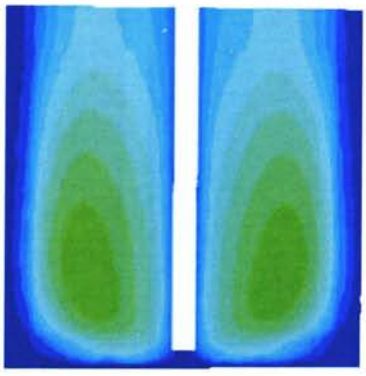

40 rpm

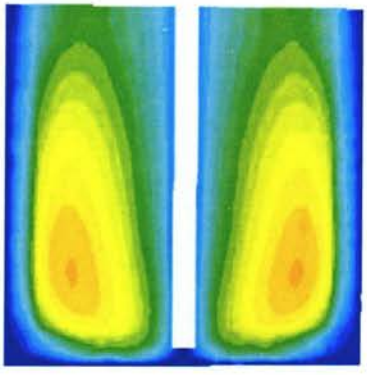

60 rpm

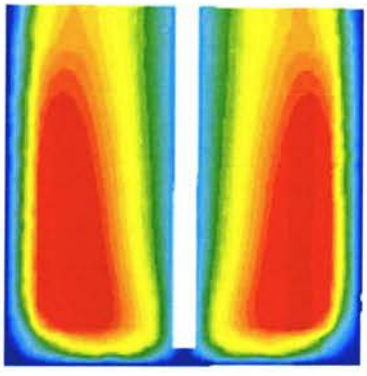

80 rpm

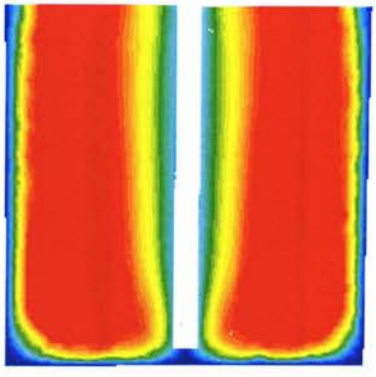

100 rpm

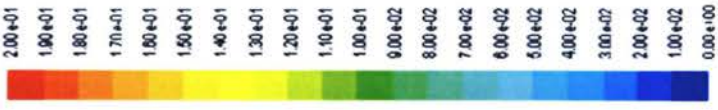

CFD Velocity Contours for Two-blade Anchor (1.5% Xanthan Gum), m/s

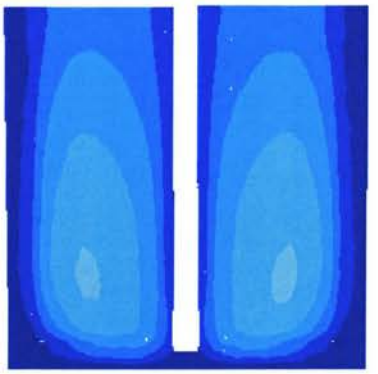

20 rpm

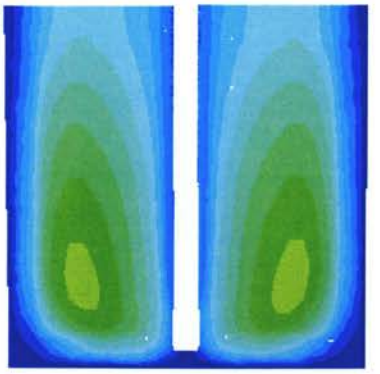

40 rpm

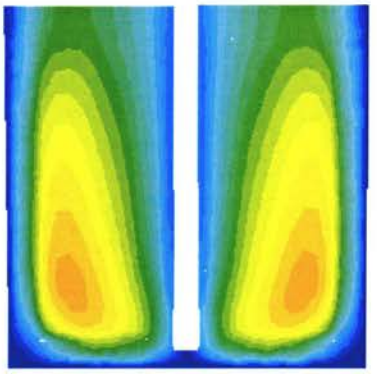

60 rpm

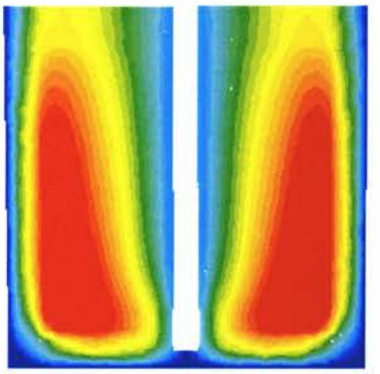

80 rpm

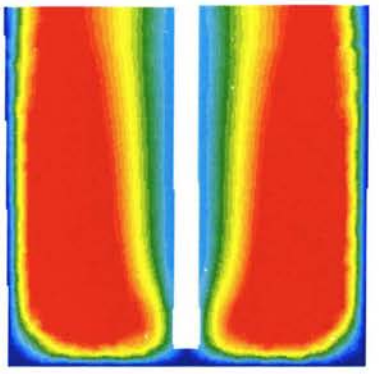

100 rpm

CFD Velocity Contours for Four-blade Anchor (0.5% Xanthan Gum), m/s

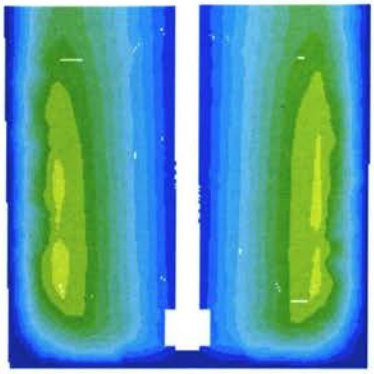

20 rpm

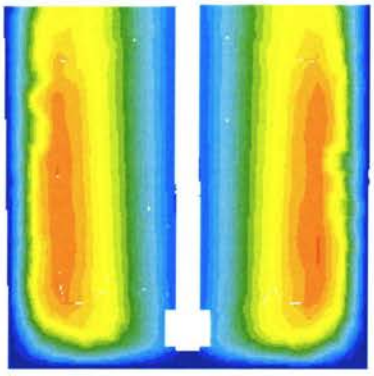

40 rpm

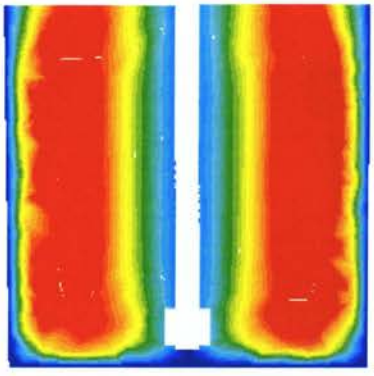

60 rpm

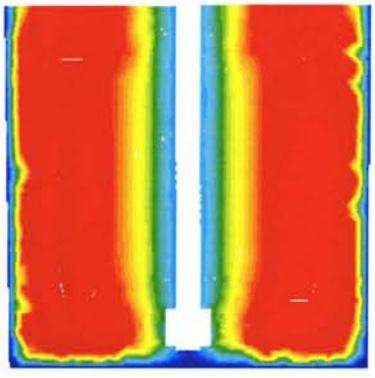

80 rpm

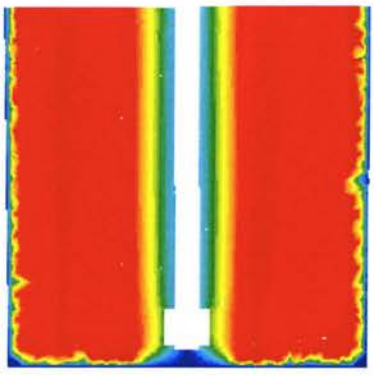

100 rpm

CFD Velocity Contours for Four-blade Anchor (1.0% Xanthan Gum), m/s

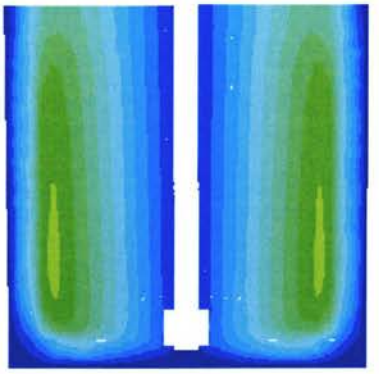

20 rpm

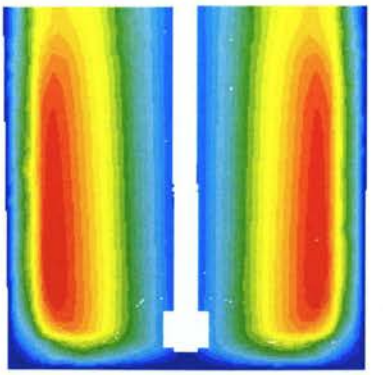

40 rpm

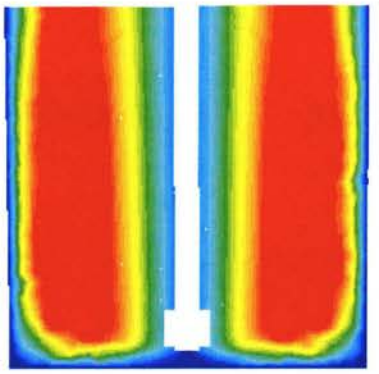

60 rpm

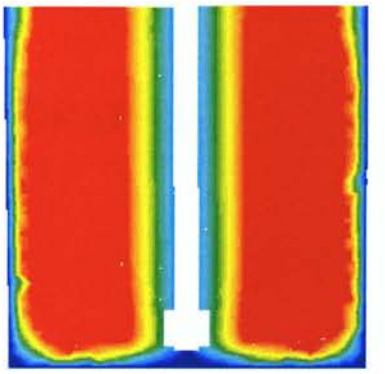

80 rpm

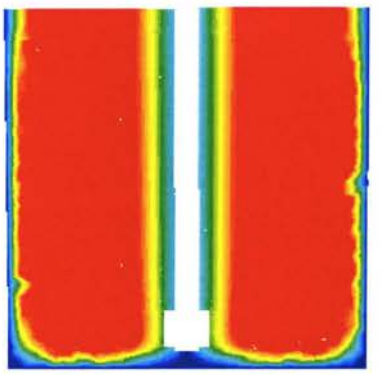

100 rpm

CFD Velocity Contours for Four-blade Anchor (1.5% Xanthan Gum), m/s

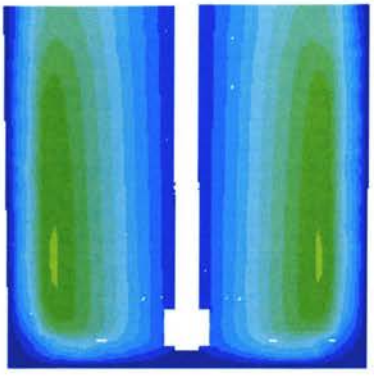

20 rpm

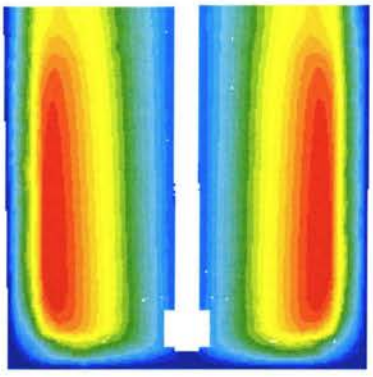

40 rpm

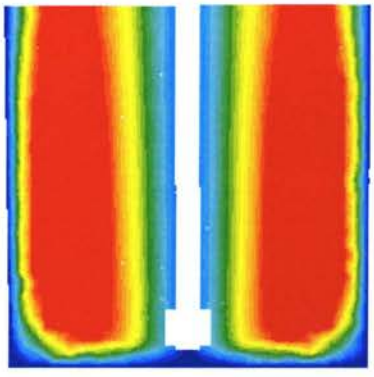

60 rpm

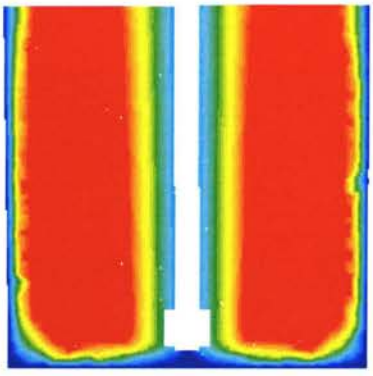

80 rpm

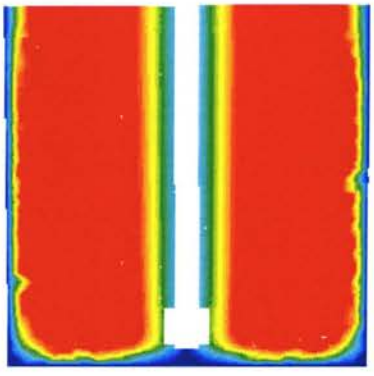

100 rpm

APPENDIX – II MIXING TIME GRAPHS

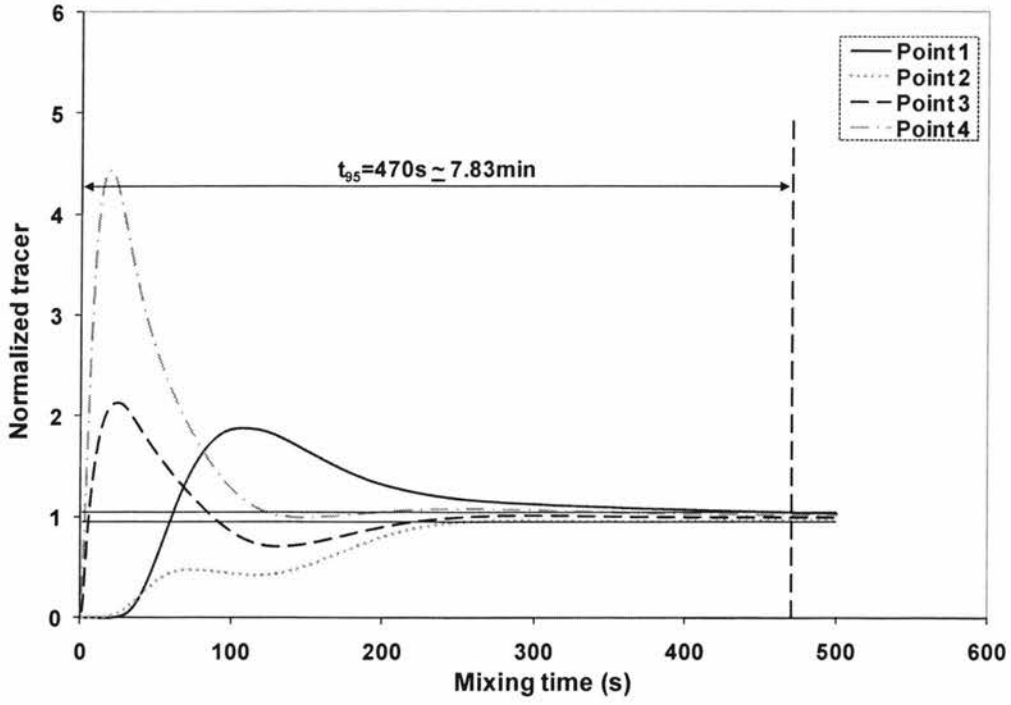

0.5% xanthan gum solution agitated at 30 rpm with two-blade anchor impeller

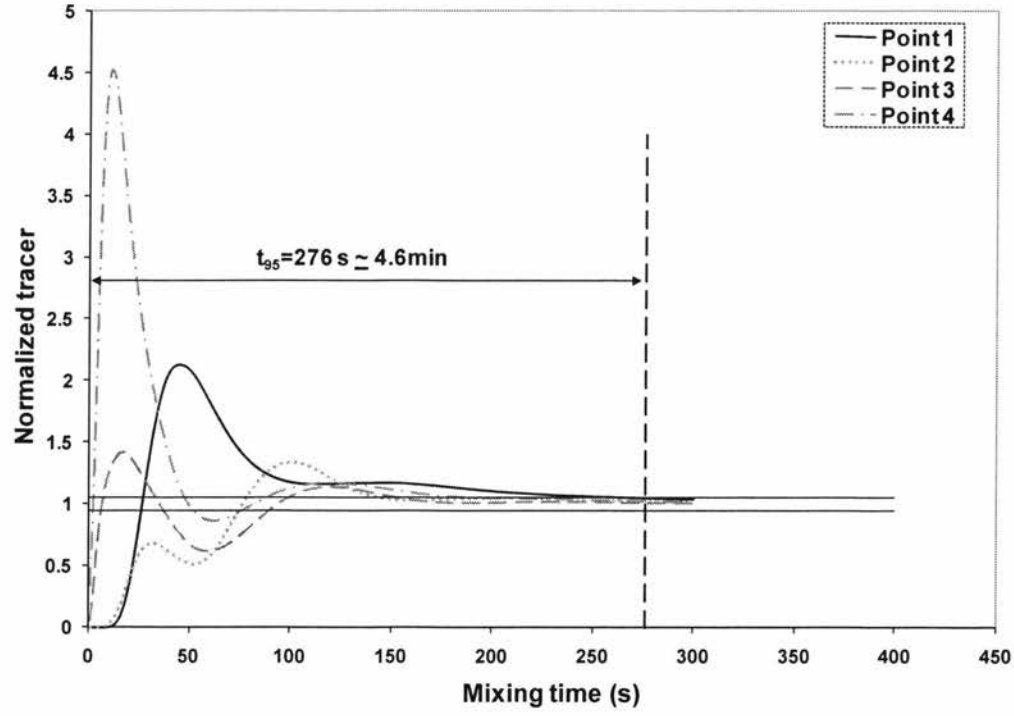

0.5% xanthan gum solution agitated at 40 rpm with two-blade anchor impeller

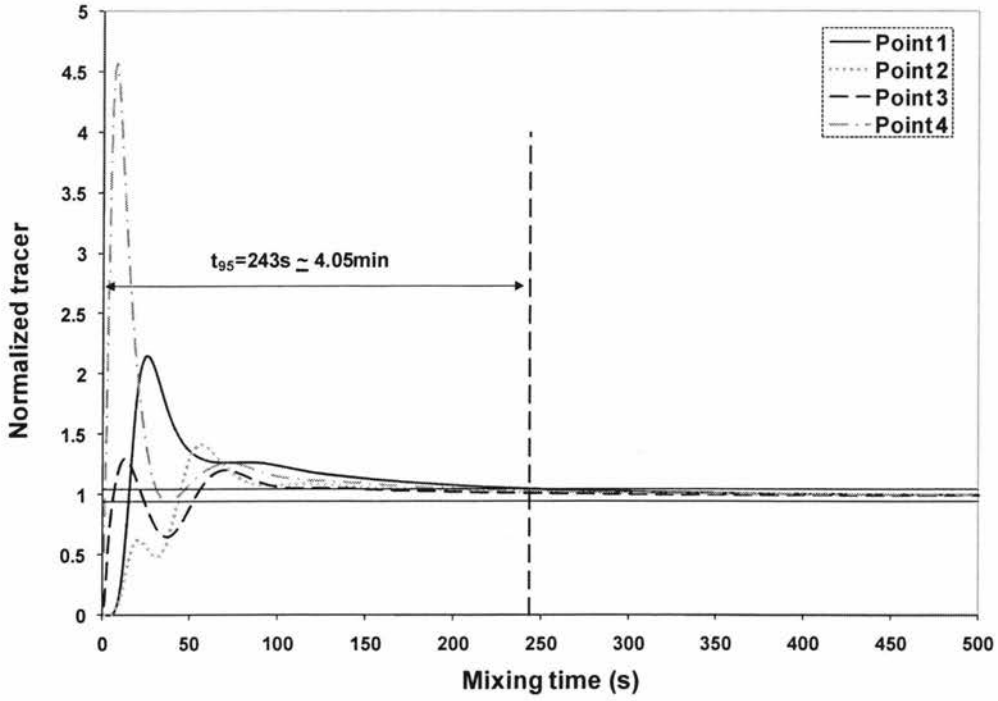

0.5% xanthan gum solution agitated at 50 rpm with two-blade anchor impeller

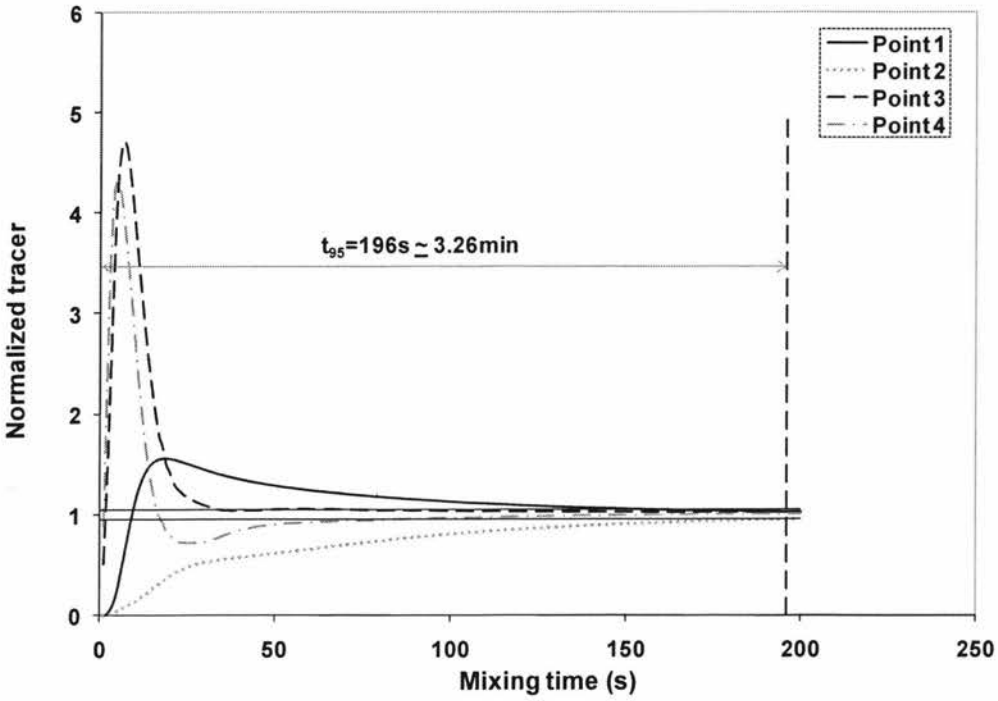

0.5% xanthan gum solution agitated at 80 rpm with two-blade anchor impeller

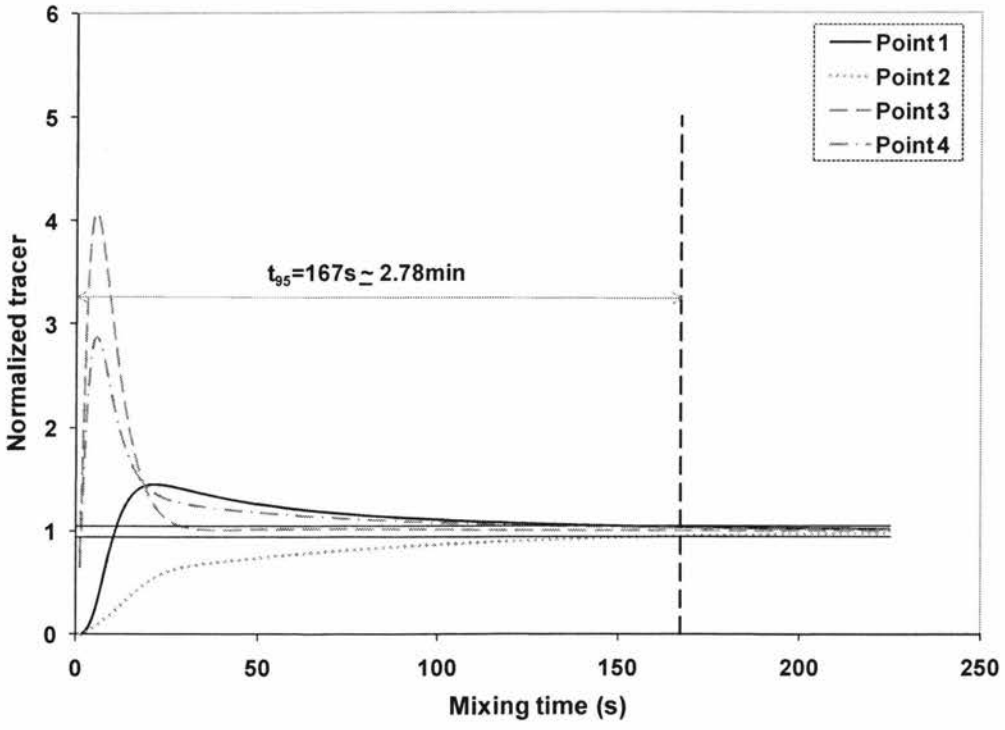

0.5% xanthan gum solution agitated at 100 rpm with two-blade anchor impeller

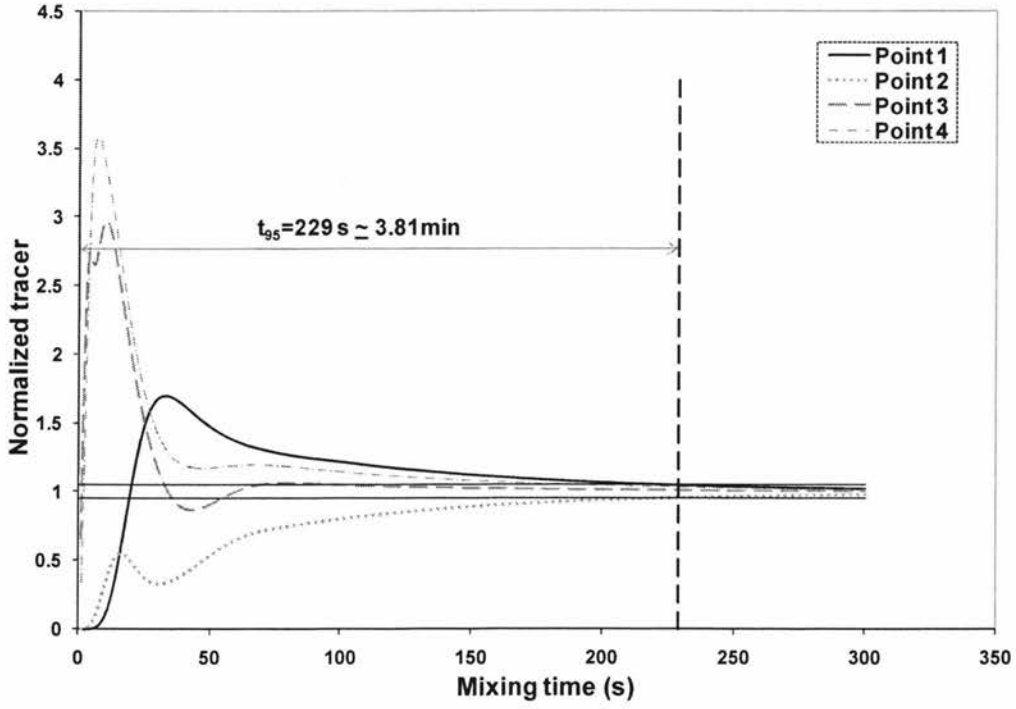

0.5% xanthan gum solution agitated at 40 rpm with four-blade anchor impeller

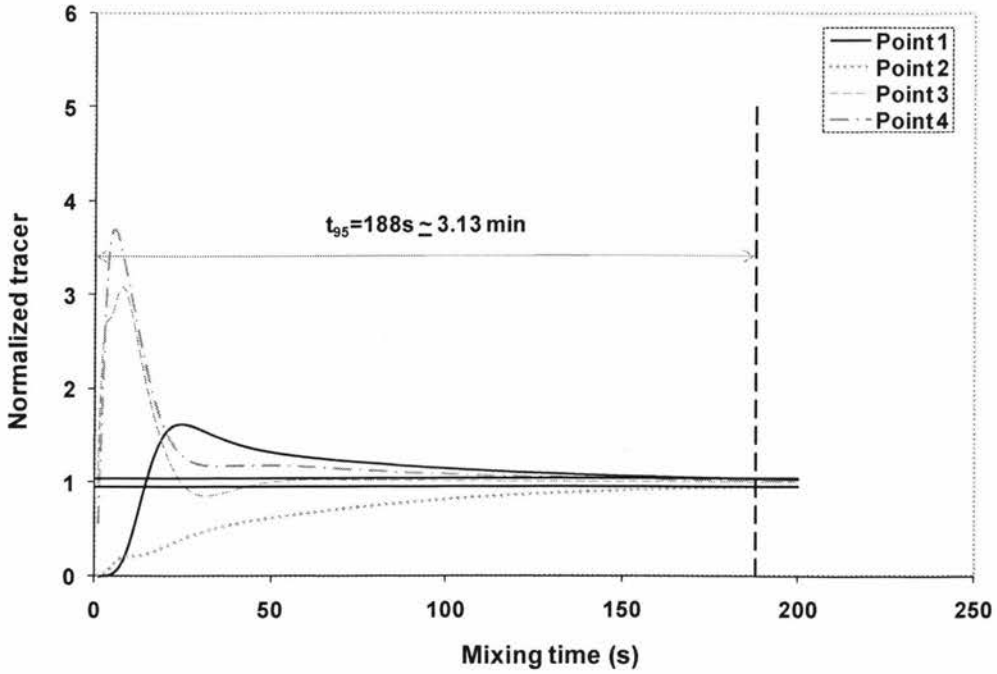

0.5% xanthan gum solution agitated at 50 rpm with four-blade anchor impeller

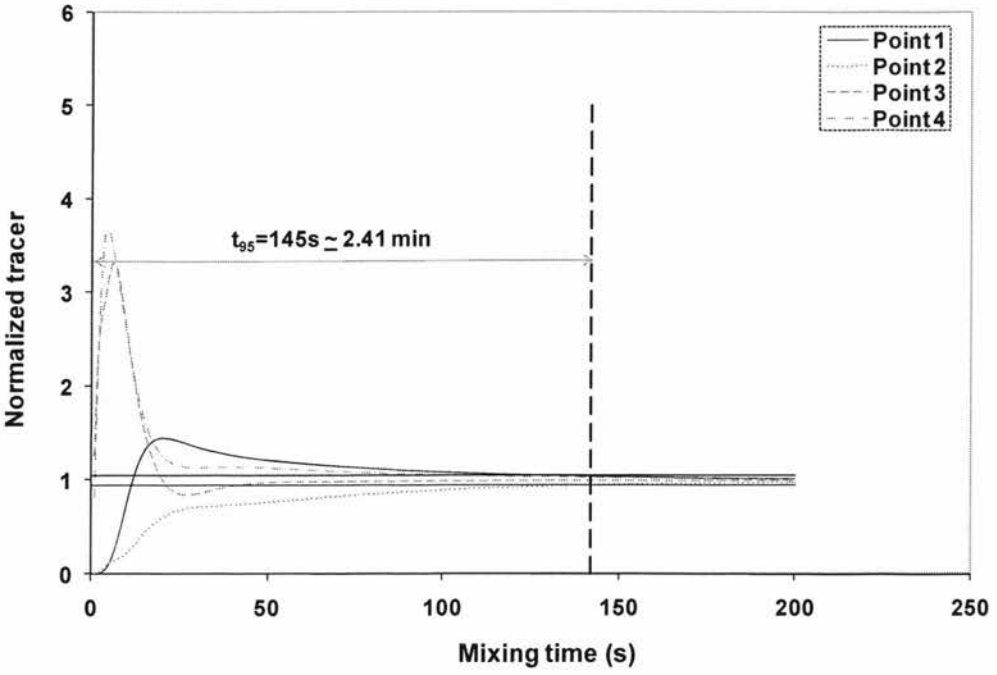

0.5% xanthan gum solution agitated at 60 rpm with four-blade anchor impeller

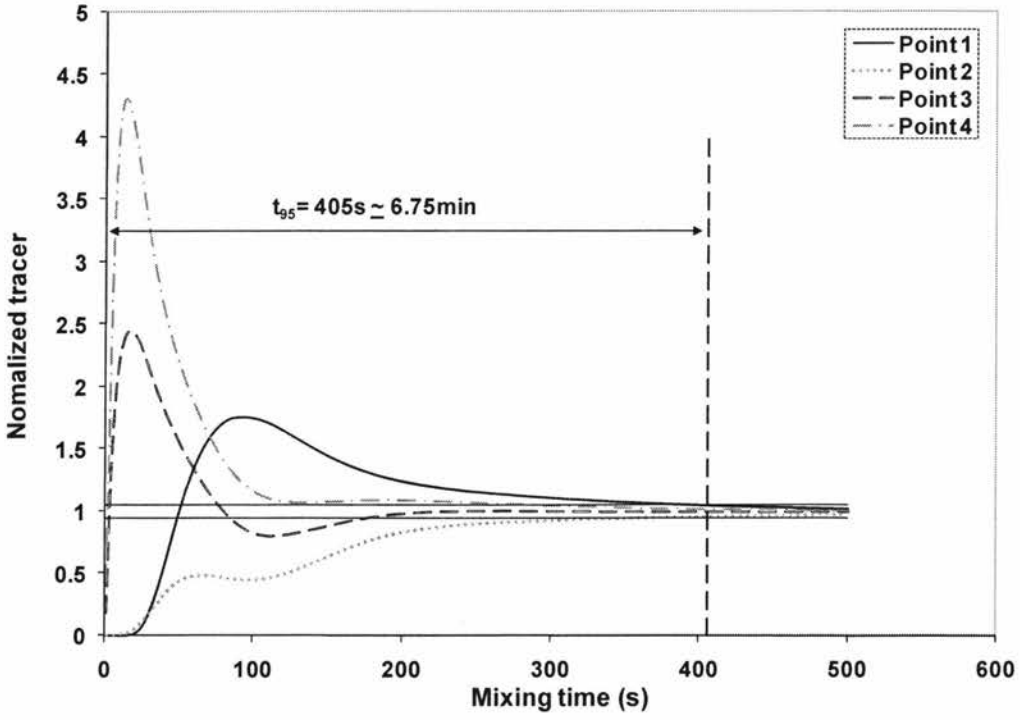

1.0% xanthan gum solution agitated at 45 rpm with two-blade anchor impeller

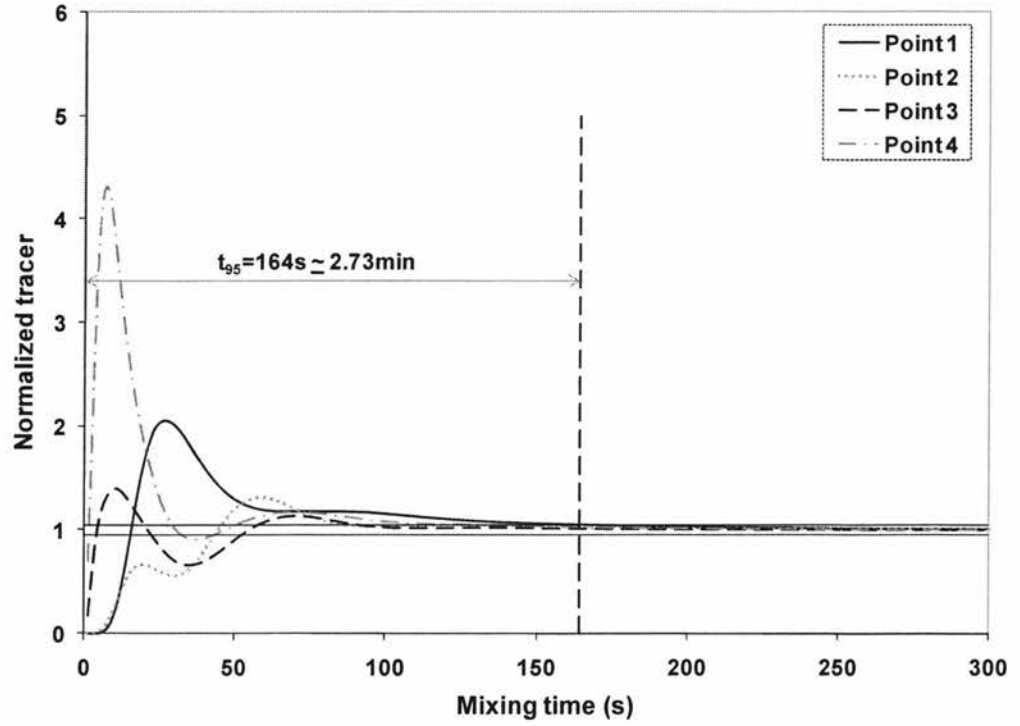

1.0% xanthan gum solution agitated at 70 rpm with two-blade anchor impeller

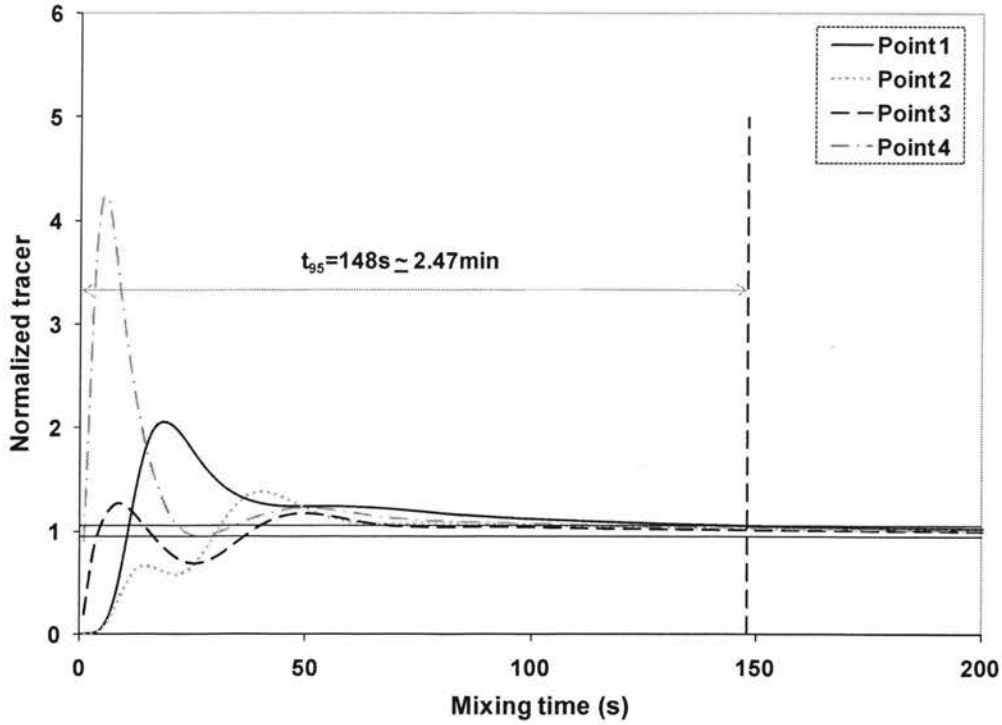

1.0% xanthan gum solution agitated at 80 rpm with two-blade anchor impeller

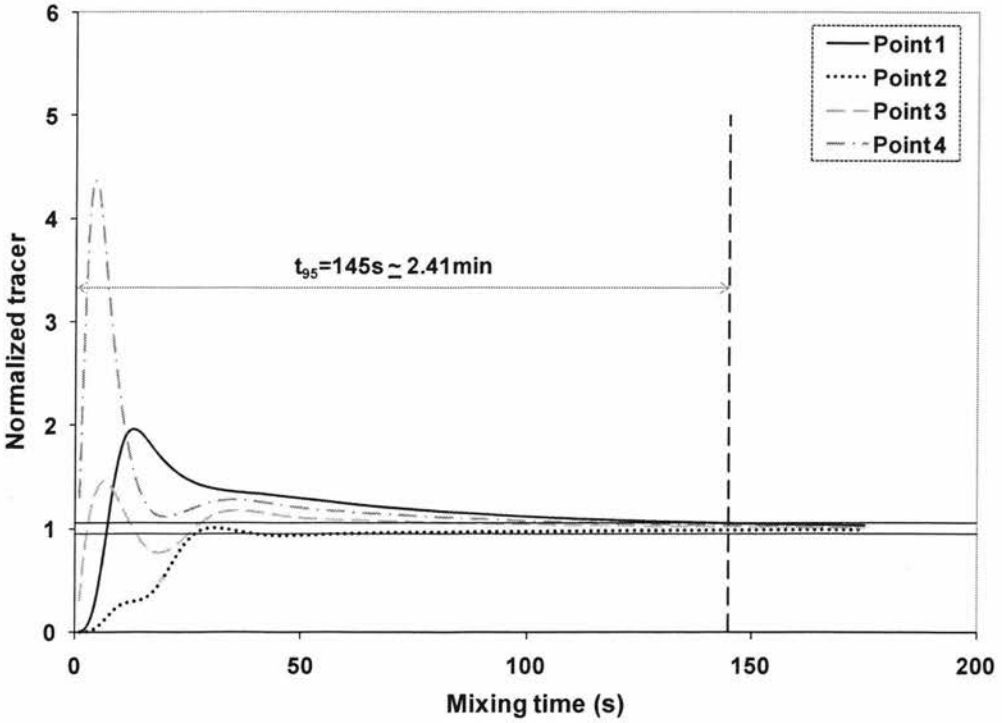

1.0% xanthan gum solution agitated at 90 rpm with two-blade anchor impeller

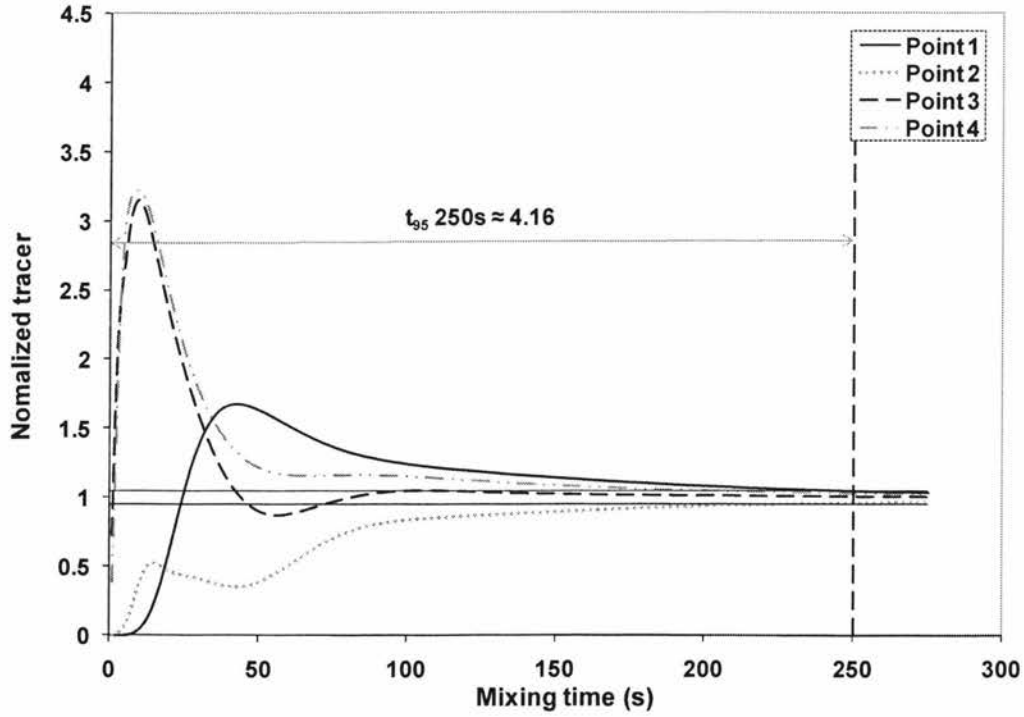

1.0% xanthan gum solution agitated at 50 rpm with four-blade anchor impeller

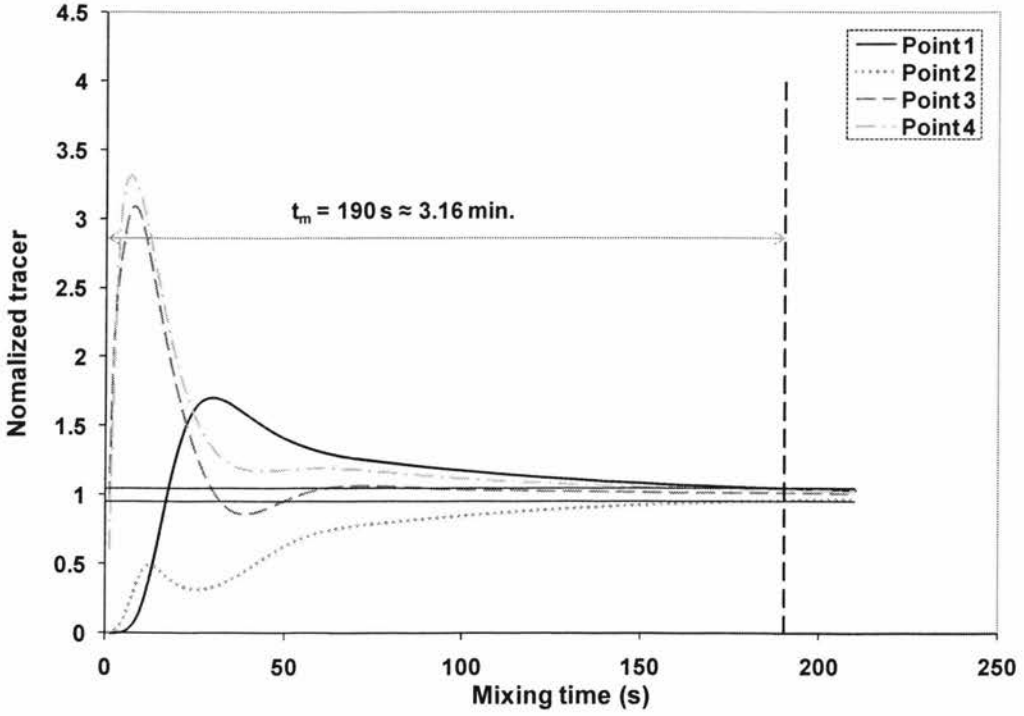

1.0% xanthan gum solution agitated at 60 rpm with four-blade anchor impeller

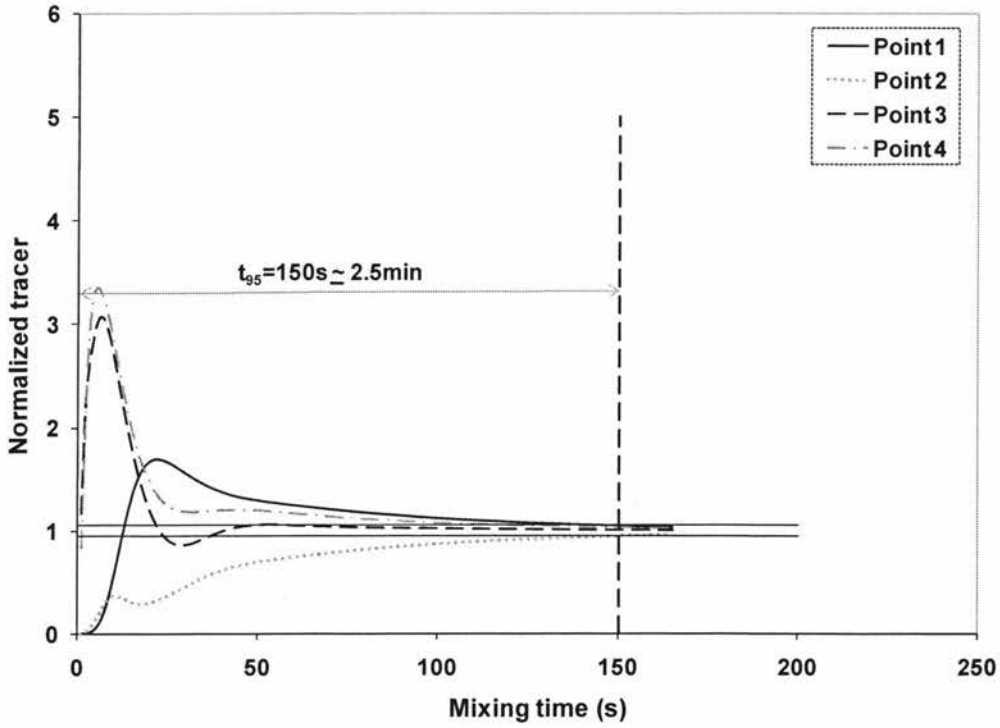

1.0% xanthan gum solution agitated at 70 rpm with four-blade anchor impeller

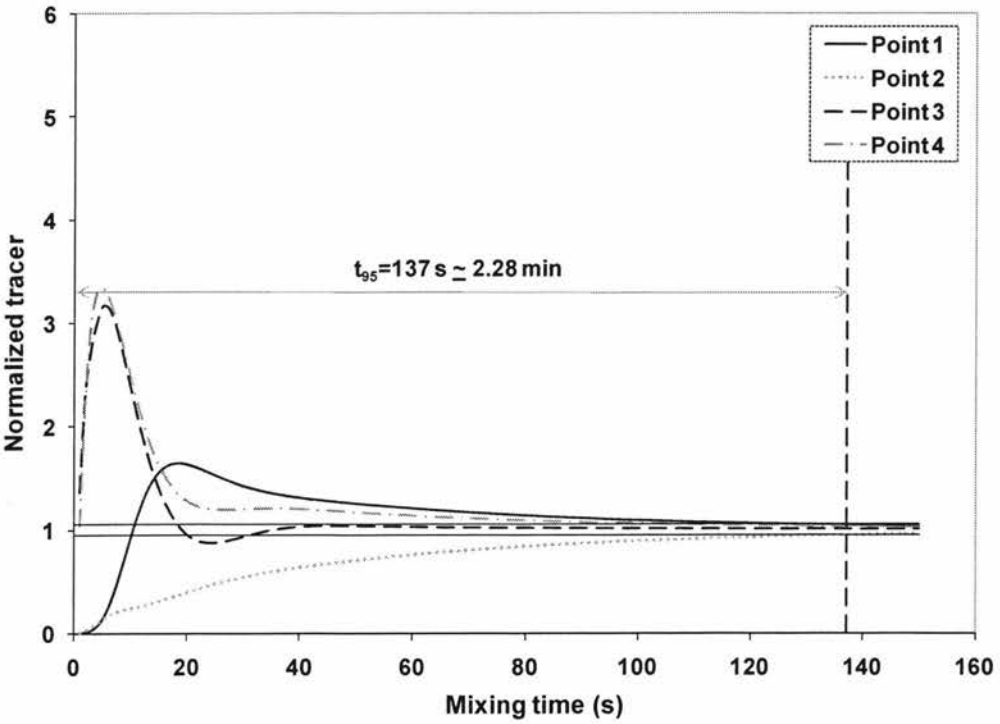

1.0% xanthan gum solution agitated at 80 rpm with four-blade anchor impeller

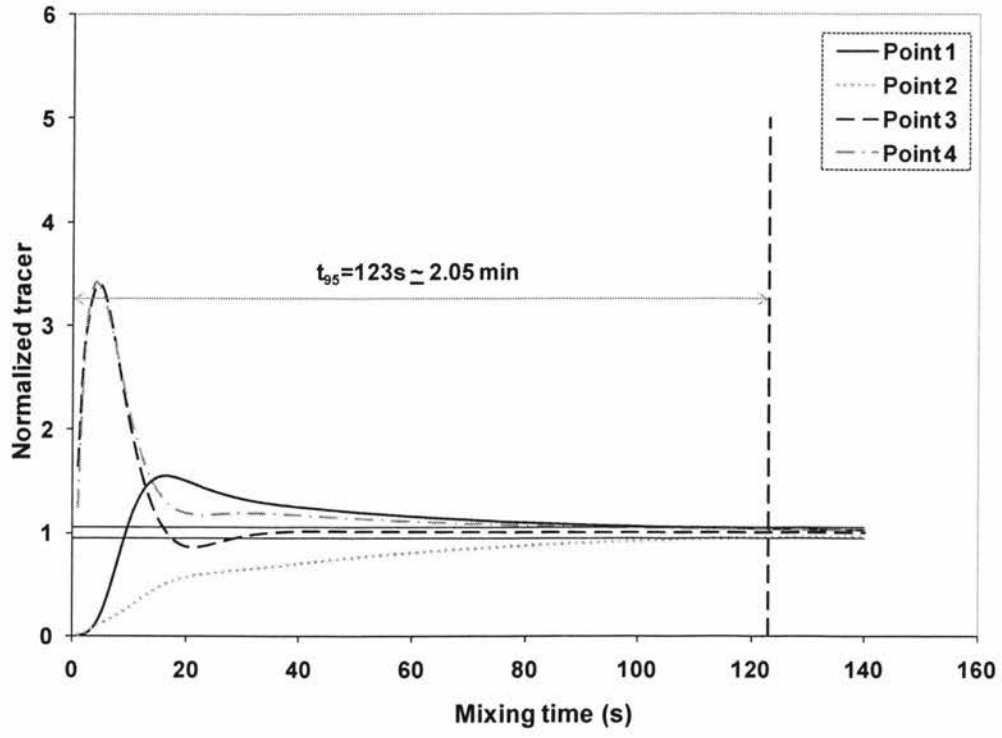

1.0% xanthan gum solution agitated at 100 rpm with four-blade anchor impeller

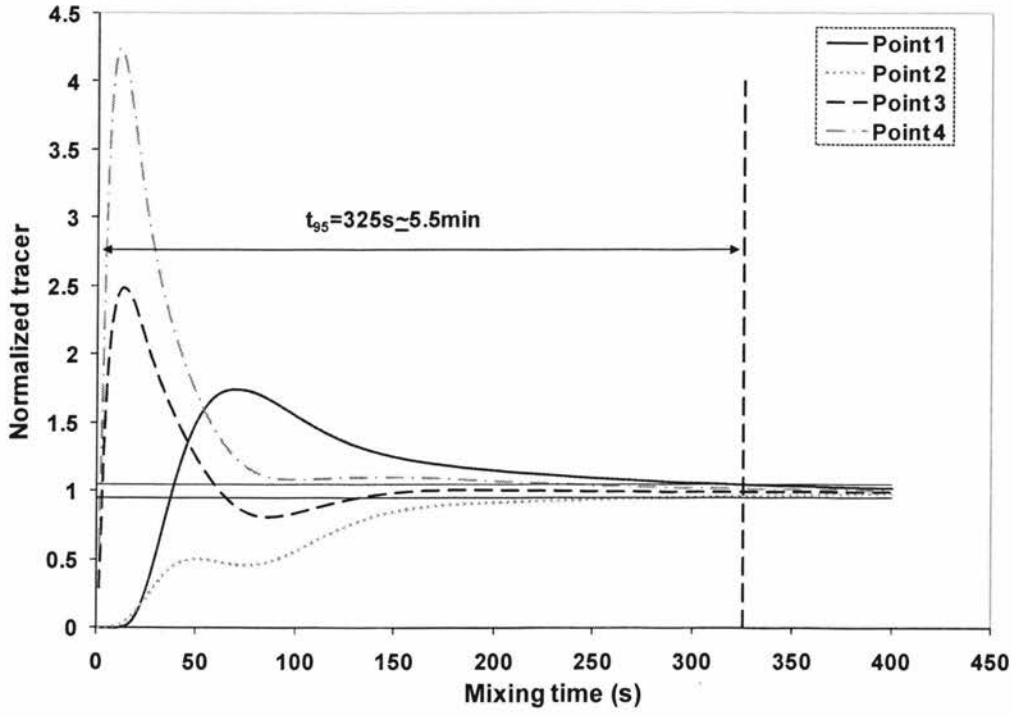

1.5% xanthan gum solution agitated at 60 rpm with two-blade anchor impeller

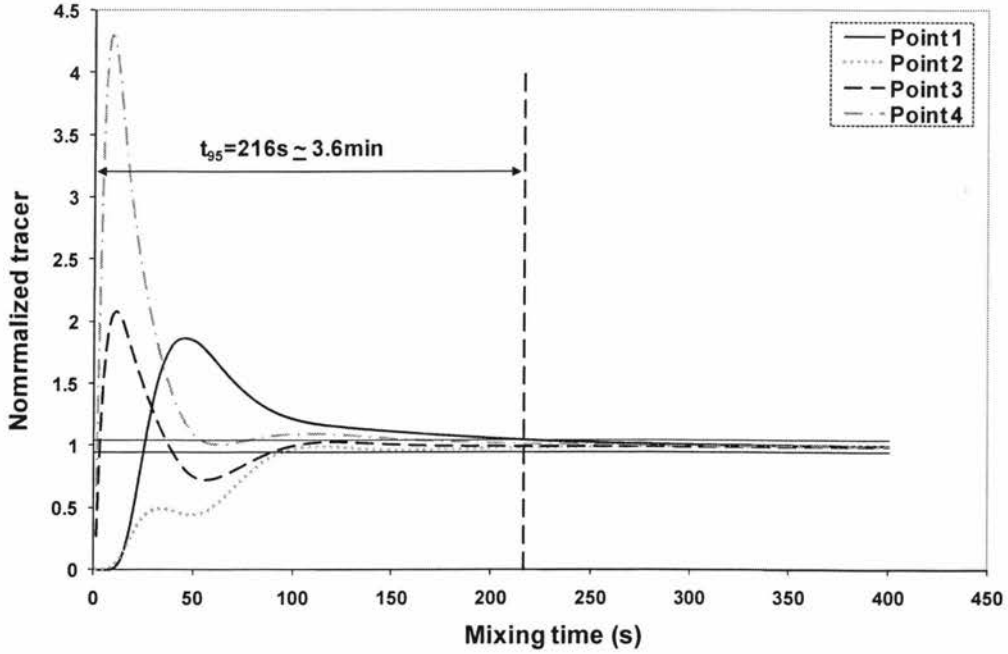

1.5% xanthan gum solution agitated at 70 rpm with two-blade anchor impeller

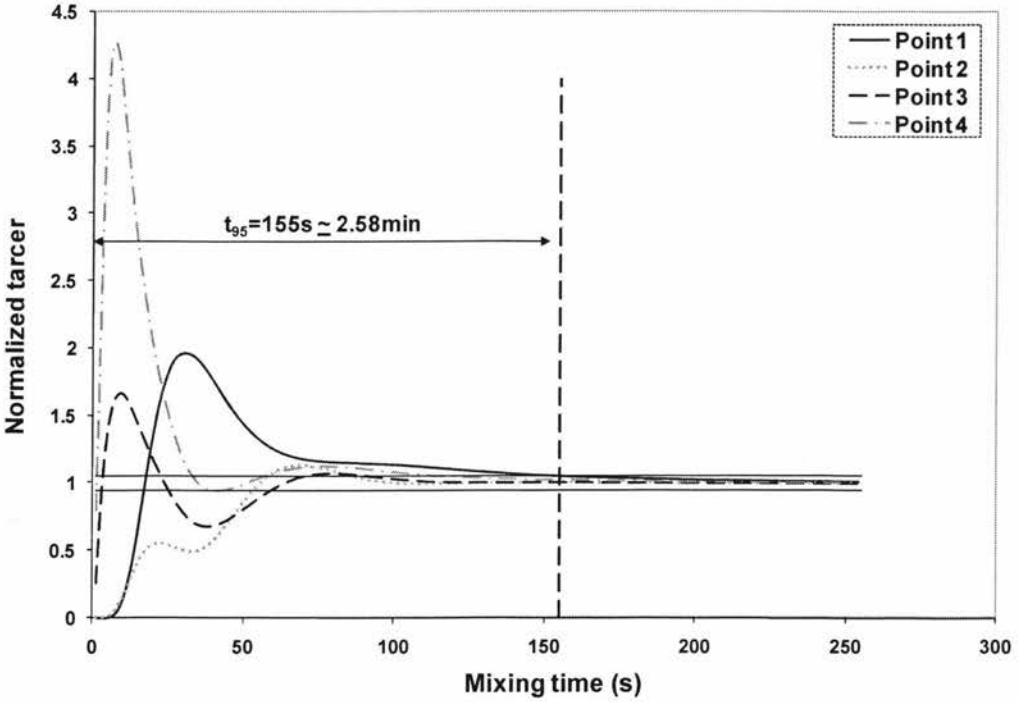

1.5% xanthan gum solution agitated at 80 rpm with two-blade anchor impeller

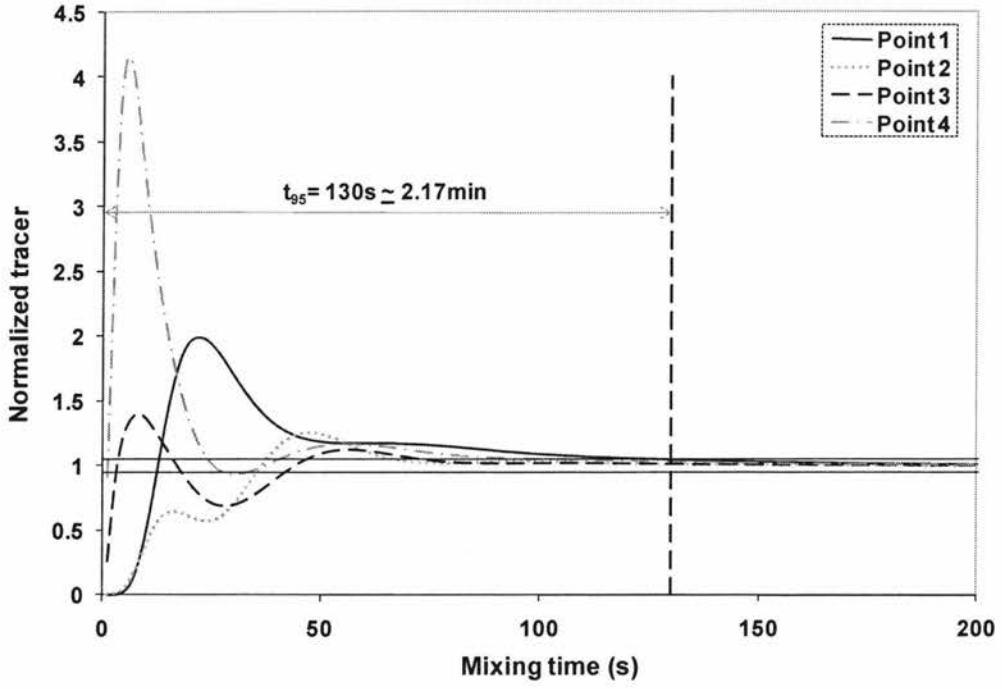

1.5% xanthan gum solution agitated at 90 rpm with two-blade anchor impeller

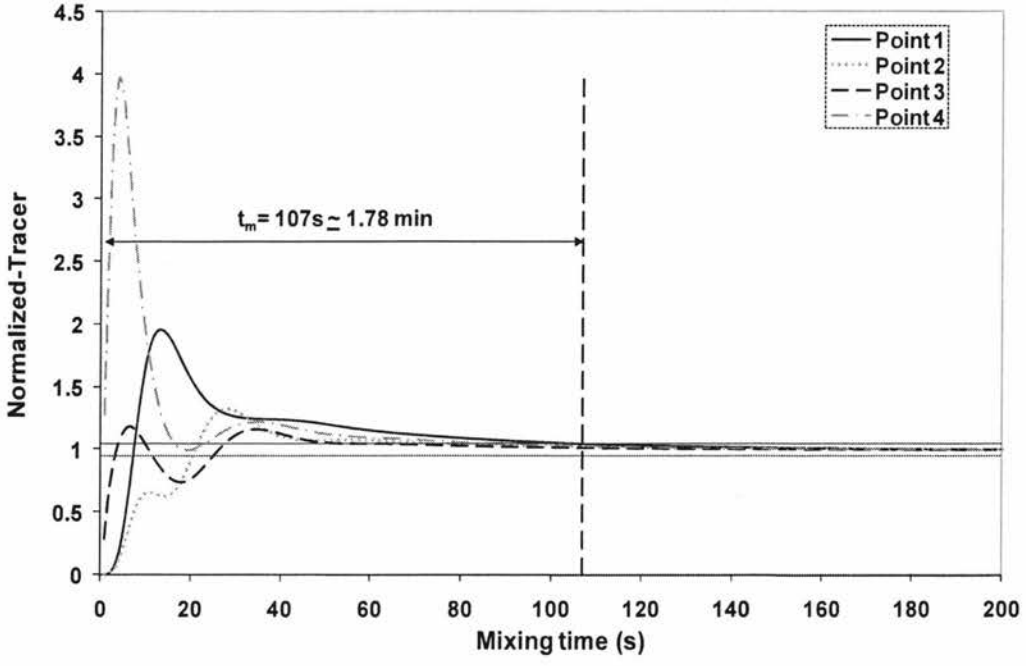

1.5% xanthan gum solution agitated at 110 rpm with two-blade anchor impeller

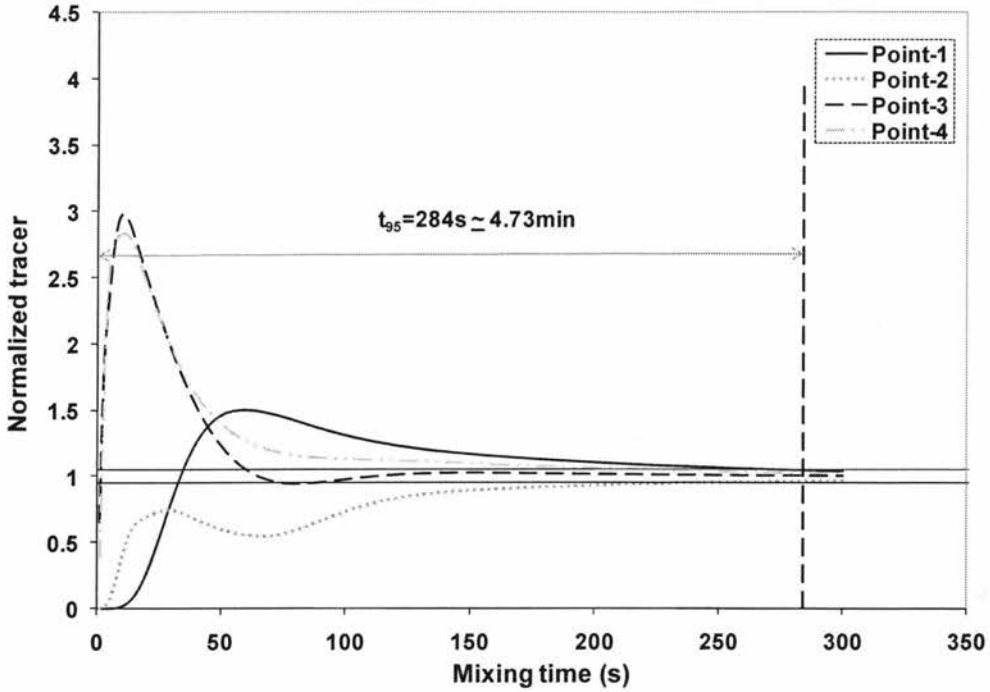

1.5% xanthan gum solution agitated at 50 rpm with four-blade anchor impeller

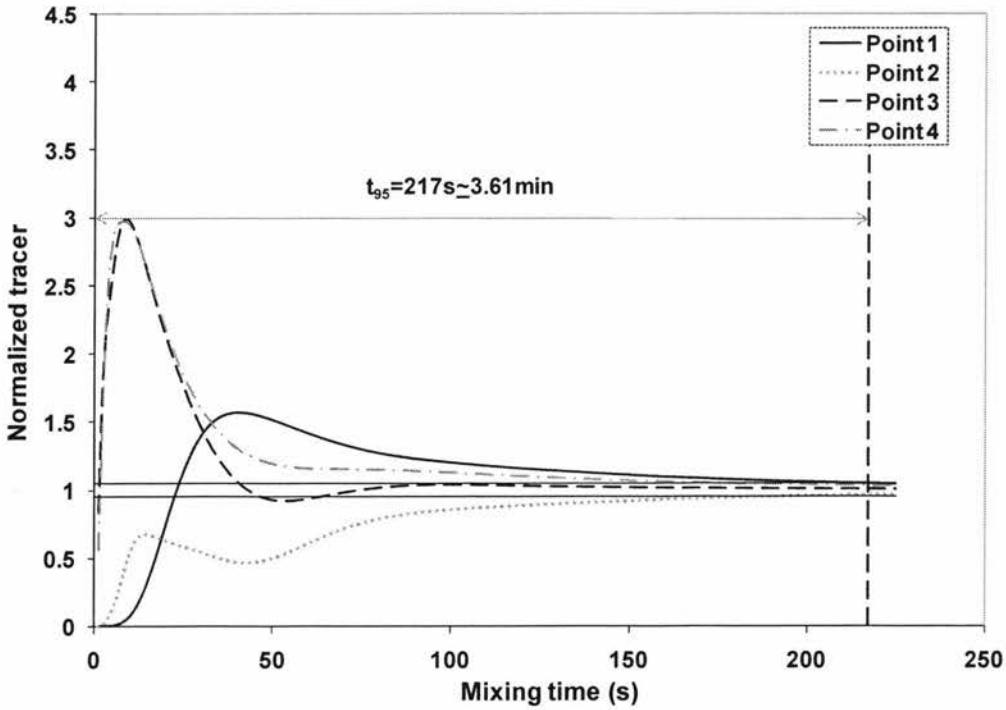

1.5% xanthan gum solution agitated at 60 rpm with four-blade anchor impeller

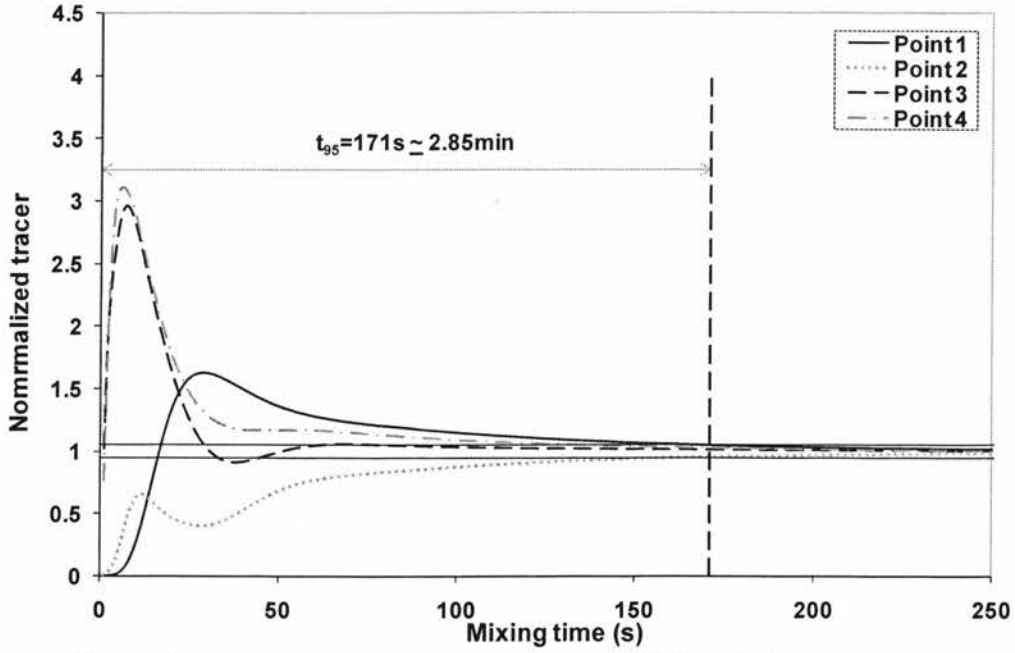

1.5% xanthan gum solution agitated at 70 rpm with four-blade anchor impeller

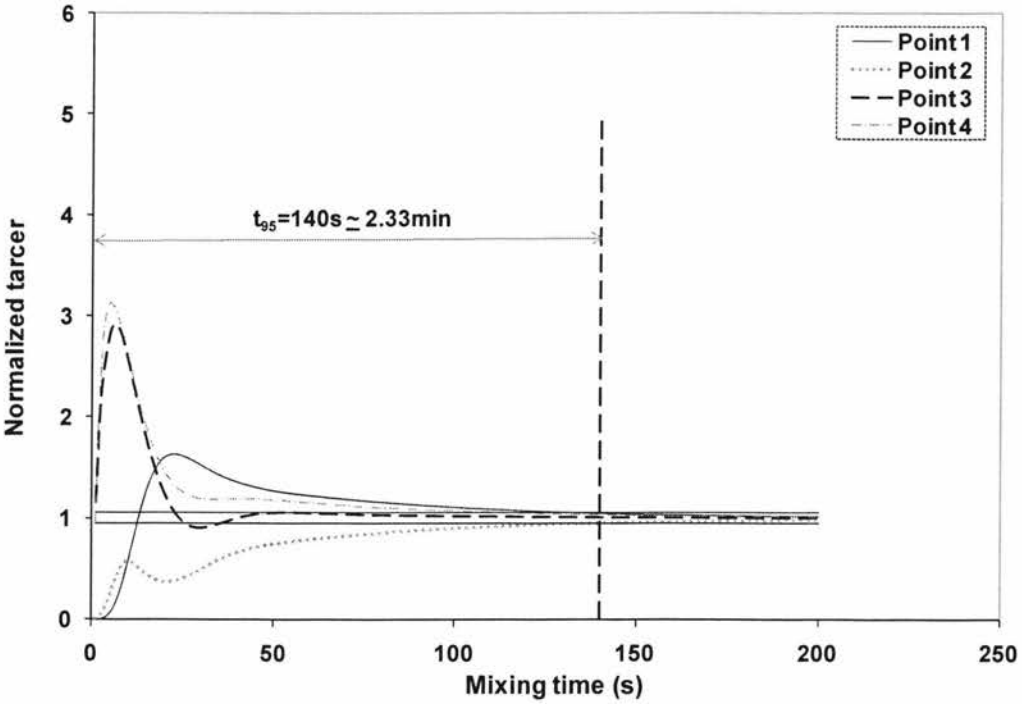

1.5% xanthan gum solution agitated at 80 rpm with four-blade anchor impeller

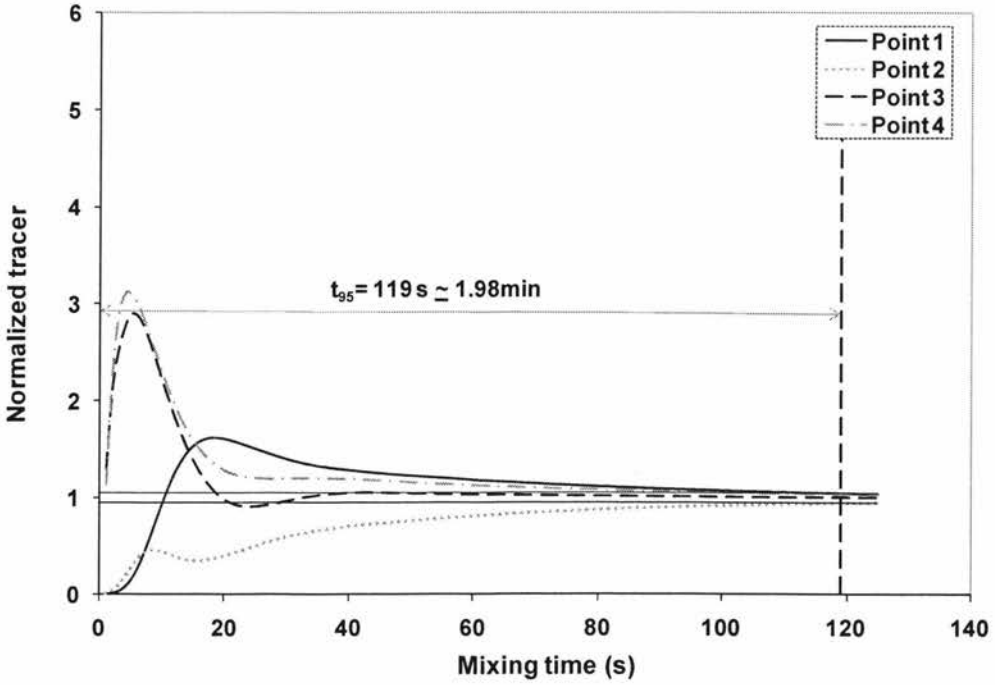

1.5% xanthan gum solution agitated at 90 rpm with four-blade anchor impeller

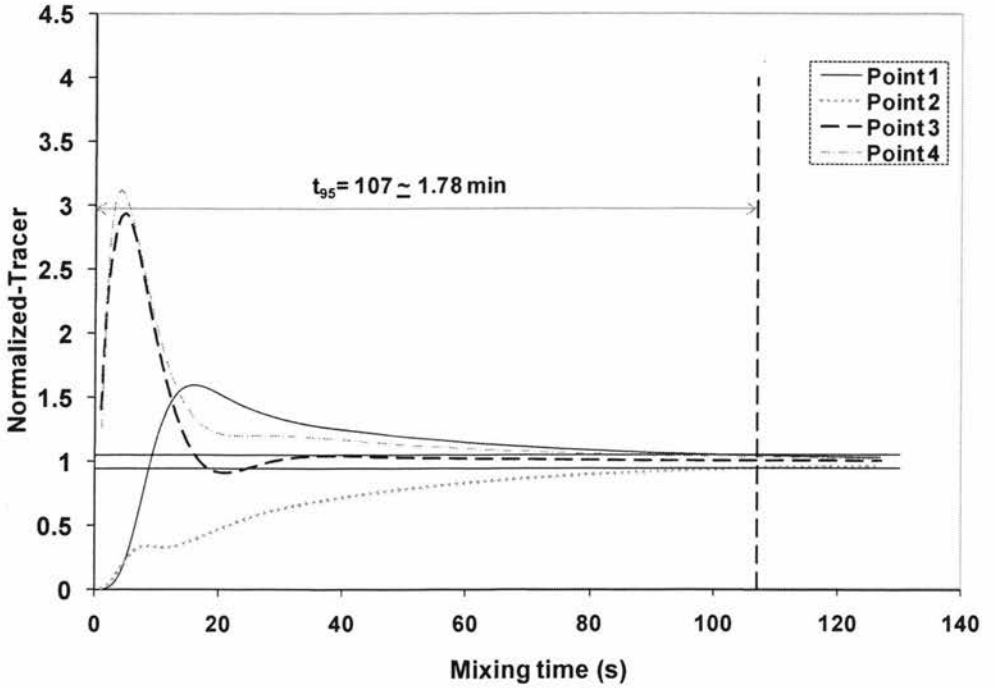

1.5% xanthan gum solution agitated at 100 rpm with four-blade anchor impeller

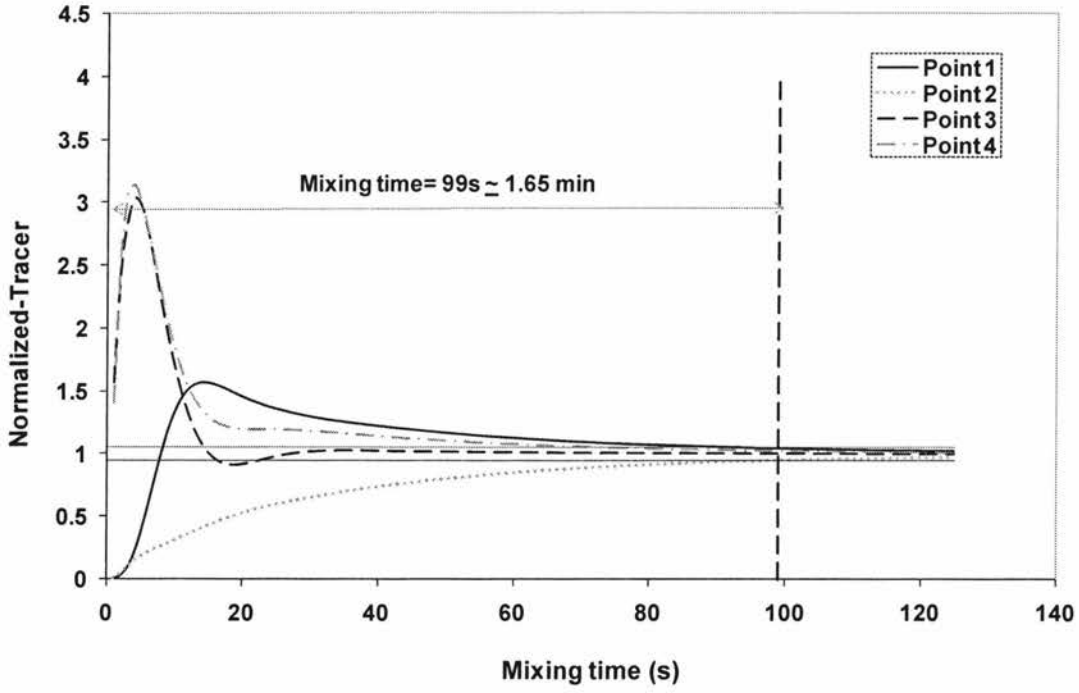

1.5% xanthan gum solution agitated at 110 rpm with four-blade anchor impeller

APPENDIX – III POWER CONSUMPTION DATA

1.5% Xanthan Gum Solution (Two-blade Impeller)

Impeller Speed (rpm)	Impeller Speed (rps)	Experimental Power Input (W)	Simulated Power Input (W)	Simulated Mixing Time (s)
20	0.333	0.084	0.096	325
30	0.500	0.157	0.155	216
40	0.667	0.210	0.220	171
50	0.833	0.288	0.293	155
60	1.000	0.377	0.373	140
70	1.167	0.477	0.458	130
80	1.333	0.545	0.552	119
90	1.500	0.660	0.653	110
100	1.667	0.765	0.760	107
110	1.833	0.864	0.874	99

1.0% Xanthan Gum Solution (Two-blade Impeller)

Impeller Speed (rpm)	Impeller Speed (rps)	Experimental Power Input (W)	Simulated Power Input (W)	Simulated Mixing Time (s)
20	0.333	0.063	0.057	405
30	0.500	0.094	0.093	250
40	0.667	0.126	0.133	190
50	0.833	0.183	0.178	164
60	1.000	0.220	0.229	150
70	1.167	0.293	0.283	148
80	1.333	0.352	0.301	145
90	1.500	0.424	0.407	137
100	1.667	0.482	0.478	123

0.5% Xanthan Gum Solution (Two-blade Anchor Impeller)

Impeller Speed (rpm)	Impeller Speed (rps)	Experimental Power Input (W)	Simulated Power Input (W)	Simulated Mixing Time (s)
20	0.333	0.021	0.021	-
30	0.500	0.031	0.036	470
40	0.667	0.054	0.053	276
50	0.833	0.078	0.073	243
60	1.000	0.094	0.096	196
70	1.167	0.132	0.124	188
80	1.333	0.159	0.156	167
90	1.500	0.198	0.193	196
100	1.667	0.230	0.231	145

1.5% Xanthan Gum Solution (CFD Results)

Impeller Speed (rpm)	Impeller Speed (rps)	Two-blade Anchor Power Input (W)	Four-blade Anchor Power Input (W)
10	0.167	0.042	0.055
20	0.333	0.096	0.124
30	0.500	0.155	0.201
40	0.667	0.220	0.282
50	0.833	0.293	0.369
60	1.000	0.373	0.460
70	1.167	0.458	0.556
80	1.333	0.552	0.658
90	1.500	0.653	0.767
100	1.667	0.760	0.883
110	1.833	0.874	1.010

1.0% Xanthan Gum Solution (CFD Results)

Impeller Speed (rpm)	Impeller Speed (rps)	Two-blade Anchor Power Input (W)	Four-blade Anchor Power Input (W)
10	0.167	0.025	0.033
20	0.333	0.057	0.073
30	0.500	0.093	0.117
40	0.667	0.133	0.163
50	0.833	0.178	0.213
60	1.000	0.229	0.268
70	1.167	0.283	0.326
80	1.333	0.301	0.410
90	1.500	0.407	0.462
100	1.833	0.478	0.541

0.5% Xanthan Gum Solution (CFD Results)

Impeller Speed (rpm)	Impeller Speed (rps)	Two-blade Anchor Power Input (W)	Four-blade Anchor Power Input (W)
20	0.333	0.021	0.035
30	0.500	0.036	0.042
40	0.667	0.053	0.062
50	0.833	0.073	0.083
60	1.000	0.096	0.109
70	1.167	0.124	0.140
80	1.333	0.156	0.175
90	1.500	0.193	0.213
100	1.833	0.231	0.247

APPENDIX – IV MRF AND SM COMPARISIONS

POWER CONSUMPTION AND MIXING TIME

Power consumption and mixing time for the xanthan gum solution with the concentration of 1.5% agitated at 60 rpm was measured using MRF and SM methods:

Impeller Modeling Technique	Power (W)	Mixing Time (min)
Multiple Rotating frame (MRF)	0.373	5.5
Sliding Mesh (SM)	0.379	5.8

It was found that there was no much difference in power consumption and mixing time for both the methods but the simulation time required for sliding mesh method was much higher (≈28 h) than multiple reference frame method (≈8 h). The MRF method was successfully used for modeling of stirred vessels to simulate the impeller rotation by a number of researchers (Harvey et al., 1997; Kelly & Gigas, 2003; Aubin et al. 2004; Khopkar et al., 2004; Sommerfeld and Decker, 2004; Kukukova et al., 2005; Lane et al., 2005; Deglon & Meyer, 2006; Buwa et al., 2006; Khopkar et al., 2006; Kerdouss et al., 2006; Yue-Lan et al., 2007). A complete analysis of the different modeling approaches for different types of mixing systems conducted by Brucato et al. (1998) showed that the MRF method provides reasonable results compared with the full unsteady computations and measurements. Therefore, MRF method was employed in this study to simulate the impeller rotation.